UNIVERSITÀ DELLA CALABRIA

Scuola di Dottorato di Ricerca

"SCIENZE E INGEGNERIA DELL'AMBIENTE, DELLE COSTRUZIONI E DELL'ENERGIA"

Tesi

MODELING OF BIOLOGICAL PERMEABLE REACTIVE BARRIERS

Settore Scientifico-Disciplinare

ICAR-02

Coordinatore del Dottorato.

Prof. Pietro Pantano.

Tutor

Prof. Salvatore Straface. PhD.

Co-tutore

Prof. Raffaele Molinari.

Dottorando

Dott. Fabian Ernesto Arias Arias

A.A 2016/2017   Ciclo XXIX

This work is dedicated to my beloved wife Maritza and my beautiful son Yoshua, thank you for endless love, sacrifices, prayers, supports and advice.

Introduction

The protection of groundwater sources in recent times has been growing, due to the populations great demand of fresh water and the increase of the pollution of the environment. The pollution detected in the groundwater contains dangerous organic and inorganic substances for the human health, in concentrations considerably higher than their natural level. The primary causes of this type of pollution are anthropogenic sources, such as industrial wastes and leachates produced in solid waste landfills. Common chemical present in groundwater are of various types including organic compounds such as pesticides (insecticides, fungicides, nematicides, herbicides), polychlorinated biphenyls (PCBs), dioxins, furans and inorganic compounds. Among the main ones are halogens and heavy metals.

Especially the zones where a high mining activity exists there are indications of polluted water sources, for the lack of control of the chemical waste, which are produced during the mining exploitation, principally in the artisanal extraction of the gold, where the utilization of Mercury is very regular. During the gold separation process with mercury the amalgam was burned and the gold was easily separated. The incorrect manipulation of the Mercury and the lack of regulation of the industrial waste caused the poisoning of the population living in these zones.

The World Health Organization has declared Hg as one of the most dangerous pollutants for human health (WHO, 1991). It primarily affects the central and peripheral nervous system as well as respiratory and renal systems.

Due to mercury's chemical-physical characteristics it is very important for the industrials process such as, pharmaceutical, oil refinery, electroplating, battery manufacturing. (Manohar et al., 2002).

Specifically, gold extraction processes are responsible for the emission of about 730 tons of mercury per year into the environment. According to the estimates of the United Nations Environment Program (UNEP), this amount is 35% of the global amount of mercury released in the environment (UNEP, 2013).

Organomercury compounds, such as methylmercury and ethylmercury, are readily absorbed by human organism causing damage of the central nervous system and, in

severe cases, blindness, deafness or even coma (Al-Damluji, 1976; Ratcliffe et al., 1996).

Therefore, there are considerable efforts to develop cost-effective methodologies for the removal of Hg from superficial water and groundwater to prevent sea pollution, fish contamination and hence man poisoning through the food chain.

The developed techniques used for heavy metals removal from aqueous solutions are electrochemical reduction and precipitation (Esalah et al., 2000; Lin S.H. et al., 1994; Cantrell K.J. et al., 1995), electrodialysis, coagulation (Mrozowski and Zielinski., 1983; Kumar et al., 2004; Adhoum et al., 2009), flotation, adsorption on surfaces and pores (Naiya et al., 2009; Zhang et al., 2005; Rao et al., 2009), ion-exchange (Visa, 2016 ; Alyüz and Veli 2009).

Adsorption through chemical-physical mechanisms using materials based on zero valent iron (Cantrell et al., 1995; Weisener et al., 2005; Liu et al., 2014; Wilkin and Neil, 2003), zeolites (Visa, 2016, Murthy et al., 2013; Alver and Metin, 2012; Wang and Peng, 2010), active carbons (Zhang et al., 2005; Rao et al., 2009, Zabihi et al., 2010; Juang et al., 2002) and ion exchange resins (Chiarle et al., 2000) have shown good efficacy in the removal of various heavy metals including Hg(II) (Gupta et al., 2015; Zhang et al., 2005; Rao et al., 2009; Liu et al., 2014; Murthy et al., 2013; Zabihi et al., 2010, Namasivayam and Kadirvelu, 1999). Synthetic porous organic polymers-based mercury nano-traps, have also been shown to have high efficiency and efficacy in the removal of Hg(II) from water (Li et al., 2014). However, all of these methods require the preliminary activation or the synthesis of the adsorbent materials through several steps, leading to rather costly and/or poor green technologies. Therefore, attention has been focused on several potentially low-cost sorbents (Bailey et al., 1999) among which lignocellulosic materials derived from plants as by-products or as waste from other production chains (agroindustry, paper, sugar production, etc.) (Namasivayam and Kadirvelu, 1999; Ho and Wang, 2008; Mahajan and Sud, 2013; Khoramzadeh et al., 2013) seem very promising. Lignocellulose is the most abundant raw material on Earth and is composed of cellulose, lignin, hemicellulose and pectin (Khachatourians and Arora, 2001) thus containing either carboxyl or hydroxyl functional groups at its surface (Henriksonn, 2009), which are in principle able to bind various heavy metals through chemical-physical adsorption (Lv et al., 2012).

The advantage of obtaining an adsorbent material, with a considerable yield for the reduction of concentrations of heavy metals is that it can be exploited in technologies for the treatment of contaminated water.

Perhaps no remedial technology has generated as much interest as the use of subsurface permeable reactive barriers (PRBs). This is due to the perceived PRB cost/benefit ratio and the potential of PRBs to mitigate the spread of contaminants that have proven difficult and expensive to manage with other cleanup methods. The concept of a PRB is relatively simple. Reactive material (adsorbent) is placed in the subsurface where a plume of contaminated ground water must move through it as it flows, typically under its natural gradient (creating a passive treatment system) and a ratio of water comes out the other side. The PRB is not a barrier to the water, but it is a barrier to the contaminant. When properly designed and implemented, PRBs are capable of remediating a number of contaminants to regulatory concentration goals. It is currently believed that these systems, once installed, will have extremely low, if any, maintenance costs for at least five to ten years. There should be no operational costs other than routine compliance and performance monitoring.

This thesis has achieved an original contribution to process of the heavy metal removal from the underground waters through the study the performances of the plant Spanish Broom as adsorbent lignocellulosic material for mercury removal from water. The common broom, also called fragrant broom or Spanish broom (Spartium junceum) is a plant belonging to the Febacaea family. It is a native species of the Mediterranean area, which goes from South Europe to North Africa, up to the Middle East zones, also reaching some areas of the central and South America. It grows in sunny areas up to an altitude of 1200 m asl, characterized by arid and sandy soils. It is a shrubby (from half to three meters high) and perennial plant with long stems. The stems are green and cylindrically shaped, straight, highly branched and compressible, but tensile resistant. The sporadic foliage is almost absent, while the bright yellow flowers are often located in the terminal part of the branches. Historically, the Spanish broom was a highly exploited plant and even nowadays it is used for several purposes: traditionally used in the ornamental trade, for yellow dye extraction, for cellulose fibers production (Gabriele et al., 2010), reforestation of degraded areas, consolidation of high slope terrains, extraction of essences from flowers for perfume creation, extraction of fibers for fabric production and reinforcement of building materials. (Chidichimo et al., 2015).

In spite of the multiple uses for which this plant was employed, this study focuses on the investigation of the broom adsorption properties with respect to mercury (II) through different laboratory tests.

In order to evaluate and characterize the physical and chemical properties of this material the study of this thesis is divided into different stages.

The first phase details the physical characterization of the Spanish broom, through instrumental methods.

In the second phase, the adsorption capabilities of the Spanish broom onto Hg, were performed using several batch tests in order to determine their adsorption capabilities as a function of pH, contact time, Hg initial concentration, adsorbent mass, reaction kinetics, isotherm and thermodynamic parameters.

The third phase is characterized by the performance of the dynamic tests in column, for the determination of the hydrodispersive properties, its dynamics of adsorption and the calculation of its isotherm. The final phase, is the Spanish Broom adsorption maximum capacity calculation.

Spanish Broom has many practical advantages as raw adsorbent material, due to its widespread diffusion, the very easy as well as economic pretreatment steps for its operation and the exceptional mechanical properties needed for setting up filters such as permeable reactive barriers. In addition, it served us to thoroughly investigate the adsorption performances of Hg(II) on a typical raw lignocellulosic material under either static or dynamic experimental set-ups and using Hg(II) polluted aqueous solutions under conditions typically found in groundwater.

For the case study of the gold mining region "Ponce Enriquez" located in Ecuador, where groundwater mercury contamination was detected, a Permeability Reactive Barrier (PRB) has been design for mercury removal. It was carried out through the 3D codes as GMS 7.1 it was possible to simulate the groundwater flow (Modflow), the transport of the contaminant inside the aquifer (MT3DMS), and the tracking particle (MODPATH), and through the Double Thomas Model equation calculate the thickness of the filter suitable for a real case study, ensuring that mercury's concentrations within the aquifer are below the maximum permissible limits fixed by law.

Introduzione

La protezione delle fonti sotterranee in tempi recenti è in crescita, a causa dell'elevata richiesta della popolazione d´acqua dolce e l'aumento dell'inquinamento ambientale.

L'inquinamento rilevato nelle acque sotterranee è costituito da sostanze organiche e inorganiche pericolose per la salute umana, in concentrazioni notevolmente superiori al loro livello naturale.

Le cause principali di questo tipo di inquinamento sono fonti antropiche, come i rifiuti industriali e percolati prodotti dalle discariche di rifiuti solidi. Le sostanze chimiche comune nelle acque sotterranee sono vari tipi di composti organici: come pesticidi (insetticidi, fungicidi, nematocidi, erbicidi), policlorobifenili (PCB), diossine, furani e composti inorganici. Tra cui i principali sono alogeni e metalli pesanti.

Soprattutto le zone in cui esiste un'attività estrattiva, vi sono indicazioni di fonti di acqua inquinata, dovuto alla mancanza di controllo dei rifiuti chimici, che sono prodotti durante lo sfruttamento minerario, principalmente nell'estrazione artigianale dell'oro, dove l'utilizzo di mercurio è molto abituale. Durante il processo di separazione dell'oro con mercurio, l'amalgama viene bruciata e l'oro è separato facilmente. La manipolazione errata del mercurio e la mancanza di controllo dei rifiuti industriali ha causato l'avvelenamento della popolazione che abita in queste zone.

L'Organizzazione Mondiale della Sanità ha dichiarato il Hg come uno degli inquinanti più pericolosi per la salute umana (OMS, 1991). In primo luogo esso colpisce il sistema nervoso centrale e periferico, nonché i sistemi respiratorio e renale.

A causa delle caratteristiche chimico-fisiche il mercurio è molto importante per i processi industriali: ad esempio, industria farmaceutica, raffinerie di petrolio, galvanica, produzione di batterie (Manohar et al., 2002).

In particolare, i processi di estrazione dell'oro sono responsabili dell'emissione di circa 730 tonnellate di mercurio all'anno nell'ambiente. Secondo le stime del Programma delle Nazioni Unite per l'Ambiente (UNEP), tale importo è il 35% della quantità globale di mercurio rilasciato nell'ambiente (UNEP, 2013).

I composti organomercurio , come metilmercurio e etilmercurio, sono facilmente assorbiti dall'organismo umano che provoca danni al sistema nervoso centrale e, in alcuni gravi casi, cecità, sordità o anche coma (Al-Damluji, 1976; Ratcliffe et al., 1996).

Pertanto, ci sono considerevoli sforzi per sviluppare metodologie di basso costo per la rimozione di Hg da acqua superficiale e acque sotterranee per prevenire l'inquinamento del mare, la contaminazione del pesce e quindi l'avvelenamento da parte dell'uomo attraverso la catena alimentare.

Le tecniche sviluppate per la rimozione dei metalli pesanti da soluzioni acquose sono la riduzione e la precipitazione elettrochimica (Esalah et al., 2000; Lin SH et al., 1994; Cantrell KJ et al., 1995); elettrodialisi, coagulazione (Mrozowski e Zielinski, Naiya et al., 2009; Zhang et al., 2005; Rao et al., 2009), ioni-scambio (Visa, 2016, Alyüz e Veli 2009).

Adsorbimento attraverso meccanismi fisici-chimici utilizzando materiali basati su Ferro Zero Valente (Cantrell et al., 1995; Weisener et al., 2005; Liu et al., 2014; Wilkin e Neil, 2003); Zeoliti (Visa, 2016, Murthy, Zhang et al., 2005; Rao et al., 2009, Zabihi et al., 2010; Juang et al., 2002; e Chiarle et al., 2000) hanno mostrato una buona efficacia nella rimozione di vari metalli pesanti tra cui Hg (II) (Gupta et al., 2015; Zhang et al., 2005; Rao et al., 2009; Liu et al., 2014; Murthy et al., 2013; Zabihi et al., 2010; Namasivayam e Kadirvelu, 1999). Anche le nano-trappole di mercurio a base di polimeri organici porosi sintetici hanno dimostrato di avere elevata efficienza ed efficacia nella rimozione di Hg (II) dall'acqua (Li et al., 2014).

Tuttavia, tutti questi metodi richiedono l'attivazione preliminare o la sintesi dei materiali adsorbenti attraverso diversi passaggi, diventando tecnologie verdi piuttosto costose.

Pertanto, l'attenzione è stata focalizzata su diversi sorbenti potenzialmente di basso costo (Bailey et al., 1999) tra i quali i materiali lignocellulosici, che derivano da piante come sottoprodotti o come rifiuti provenienti da diverse catene di produzione agroindustria, carta, produzione di zucchero, (Namasivayam e Kadirvelu, 1999; Ho e Wang, 2008; Mahajan e Sud, 2013; Khoramzadeh et al., 2013) sembrano molto promettenti. Lignocellulosica è la materia prima più abbondante della Terra ed è composta da cellulosa, lignina, emicellulosa e pectina (Khachatourians e Arora, 2001) contenenti così gruppi carbossilici o idrossilici nella sua superficie (Henriksonn, 2009), i quali in principio sono capaci di legare vari metalli pesanti attraverso adsorbimento chimico-fisico (Lv et al., 2012).

Il vantaggio è quello di ottenere un materiale adsorbente, con una notevole capacità per la riduzione delle concentrazioni di metalli pesanti, e che può essere sfruttato con diverse tecnologie per il trattamento dell'acqua contaminata.

Forse nessuna tecnologia di recupero ha generato tanto interesse quanto l'uso di barriere reattive permeabili (PRBs) sotterranee. Ciò è dovuto al rapporto costi-benefici e al potenziale delle PRBs di mitigare la diffusione dei contaminanti, che hanno dimostrato grande difficoltà e un elevato costo per gestirla con altri metodi di bonifica. Il concetto di PRB è relativamente semplice.

Il materiale reattivo (adsorbente) è posto nella superficie sottostante, in cui il plume contaminante dell´acqua sotterranea deve muoversi attraverso di essa mentre scorre, tipicamente sotto la sua pendenza naturale, creando così un sistema di trattamento passivo. La PRB non è una barriera all'acqua, ma è una barriera al contaminante. Se sono correttamente progettati e implementati, le PRBs sono in grado di rimediare un certo numero di contaminanti agli obiettivi di concentrazione di normativa legale. Attualmente, si ritiene che questi sistemi, una volta installati, avranno costi di manutenzione estremamente bassi, per almeno cinque o dieci anni. Non ci dovrebbero essere i costi operativi, soltanto il monitoraggio di routine dei livelli fisico-chimici e il monitoraggio delle prestazioni.

Questa tesi ha dato un contributo originale al processo di rimozione di metalli pesanti nelle acque sotterranee attraverso lo studio delle prestazioni lignocellulosici della ginestra come materiale assorbente per rimuovere il mercurio da soluzioni acquose. La ginestra comune, chiamata anche aromatica o Ginestra Spagnola (Spartium junceum) è una pianta appartenente alla famiglia delle Febacaea. Si tratta di una specie nativa dell'area mediterranea, che va dal sud dell'Europa, nord dell'Africa e anche parti del Medio Oriente, si trova anche in varie parti del continente americano. Cresce in zone soleggiate con un'altitudine fino a 1200 m.s.l.m, caratterizzata da terreni aridi e sabbiosi. È un arbusto (da uno a tre metri), una pianta perenne molto ramificata e comprimibile con lunghi steli, verdi e cilindrici, diritti ma con resistenza a trazione. Il fogliame è sporadico quasi assente, mentre i fiori di colore giallo brillante trovano spesso nella parte terminale dei rami. Storicamente, la Ginestra Spagnola era una pianta altamente utilizzata e ancora oggi viene usata per diversi scopi: tradizionalmente utilizzati nel commercio ornamentali, per l'estrazione di colorante giallo, per la produzione di fibre di cellulosa (Gabriel et al., 2010), riforestazione di aree degradate, consolidamento terreno ripido, estrazione di essenze floreali per la creazione di profumo, l'estrazione delle fibre per la produzione di materiali tessuti e costruzione rinforzo (Chidichimo et al., 2015).

Nonostante i molti usi di questa pianta, questo studio si è concentrato sulla ricerca delle proprietà di assorbimento della Ginestra sul Hg (II) attraverso vari test di laboratorio.

Al fine di valutare e caratterizzare le proprietà fisiche e chimiche di questo materiale, lo studio di questa tesi è diviso in diverse fasi. La prima fase riguarda la caratterizzazione fisica della Spanish Broom attraverso metodi strumentali.

Nella seconda fase, sono state valutate le capacità di adsorbimento della ginestra sul Hg, utilizzando vari Test di Batch, al fine di determinare la sua capacità di assorbimento, in funzione del pH, tempo di contatto, della concentrazione iniziale di Hg, della massa di adsorbente, della cinetica di reazione, della termodinamica e dei parametri isotermici.

La terza fase è caratterizzata dalla realizzazione delle prove dinamiche in colonna, per determinare le proprietà dinamiche idrodispersive, la dinamica d'adsorbimento e il calcolo dell'isoterma. La fase finale è il calcolo della capacità massima di adsorbimento della Spanish Broom.

La Spanish Broom ha molti vantaggi pratici come materia prima adsorbente, dovuto alla sua ampia diffusione, anche per il pretrattamento del materiale che si realizza per il suo funzionamento il quale è facile e poco costoso. Inoltre grazie alle sue eccellenti proprietà meccaniche può essere utilizzata per l'installazione di filtri, come le barriere permeabili reattive.

Questo materiale ha aiutato ad investigare ulteriormente le prestazioni di adsorbimento di Hg (II) in una tipica materia prima lignocellulosica, utilizzando soluzioni acquose contaminate con Hg (II) in condizioni tipiche trovati nelle acque sotterranee, eseguendo una prova sperimentale statica e dinamica.

Nella regione mineraria del distretto "Camilo Ponce Enríquez" in Ecuador dove è stata rilevata una contaminazione di Hg nelle acque sotterranee, dovuto all'estrazione dell'oro per amalgamazione di Hg, si è effettuata la progettazione di una barriera permeabile reattiva (PRB) per la rimozione del mercurio, che è stata condotta tramite codici 3D come GMS 7.1, con cui è possibile simulare il flusso delle acque sotterranee (Modflow), il trasporto del contaminante nella falda (MT3DMS) e il percorso della particella (Modpath). Tramite l'equazione del modello doppio di Thomas, è stata calcolata la quantità necessaria di materiale sorbente e lo spessore del filtro, per questo caso studio, assicurando che le concentrazioni di mercurio nella falda sono inferiori ai limiti stabiliti dalla legge.

Contents

List of figures

xiii

List of Tables

List of Images

CHAPTER 1

1   MERCURY   AND   THE ENVIRONMENT.

1.1   WATER RESOURCES AND THEIR POLLUTION.

The environmental problems originated by the current economic, political and social system have been increasing since the industrial revolution, and thanks to the advances in the area of communication, this industrialization has become Global. The commercial process has granted a diversification of goods and services around the world, and a growing demand, which leads to a greater exploitation of natural resources (raw materials) to improve industrial production and meet the needs of the market. The overexploitation of our non-renewable resources such as oil natural gas, the extraction of precious metals such as silver, platinum and mainly gold, the production of energy through coal plants, have become a real threat for the planet, causing a growing contamination of our vital resources, such as air, soil and especially water.

The water reserve of the hydrosphere corresponds to 1,390,000,000 km^3, which are distributed in large reserves of decreasing size (Castany 1984). The water contained in these large reservoirs plays an important role for the planet's climatic stability, which acts as physical, hydrodynamic, chemical and biological regulators. Of all the water that exists on the planet, only 16,000,000 km^3 correspond to fresh water, 60% of which is in the form of glaciers, eternal snow, ice and the rest 40% is distributed in underground sources, which constitute one of the main sources of drinking water for humans (Straface, 2015), wells and springs provide 50% of drinking water for cities, also used for agriculture and industry.

Due to climate change, in recent years the impact on water resources has been observed, such as droughts of large lakes like the Poopó, the second largest lake in Bolivia, which was officially declared dried in December of 2015, threatening the livelihoods of communities living in the area and a large number of species of flora and fauna or the Aral Sea in Kasajistan, furthermore global warming and political problems has caused the fourth largest lake in the world to lose 80% of its original volume.

The melting in the Arctic and Antarctica, due to the rising temperature of the oceans, from 1979 to the end of summer 2014, has reduced the area covered by ice by 40%.

In Antarctica, the data extracted is not very encouraging, either. It has recently been known that its largest glacier, Totten, 130 km long and 30 km wide, is melting, another of its large glaciers, the Smith, has been declining at a rate of 2 km^2 per year, losing 35 Km^2 of its surface. All this impact would have serious consequences in the world, according to the Environmental Protection Agency (EPA) the sea level has risen 15 to 20 cm in the last 100 years, affecting sensitive ecosystems, their flora and fauna, etc.

However not only surface water sources are threatened, one of the main sources of water for domestic use, groundwater, is not far from this effect either.

Groundwater is water that is located below the earth's surface. Over time, water from rain and rivers migrates through the ground and is stored in porous soils and rocks. Groundwater is found in vast quantities filling the spaces between grains of soil or rock; it slowly flows through aquifers, which are typically made up of gravel, sand, sandstone, or fractured rock, such as limestone. The water can move through these materials because they have large connected spaces that make them permeable. The speed at which groundwater flows is dependent upon on the size of the spaces in the soil

or rock and how well the spaces are connected. Therefore it is an important component of the planet's hydrological cycle. When it rains, some of the water trickles into soil and soaks underground into the aquifer. Over centuries, the aquifer gradually releases the water to the surface, and eventually to the sea.

Groundwater plays a number of important roles in our environment and in our economies. In the environment it supports rivers, lakes and wetlands, especially through drier months when there is little direct input from rainfall; the flow of groundwater into rivers through the river bed, known as baseflow, can be essential to the health of wildlife and plants that live in the water.
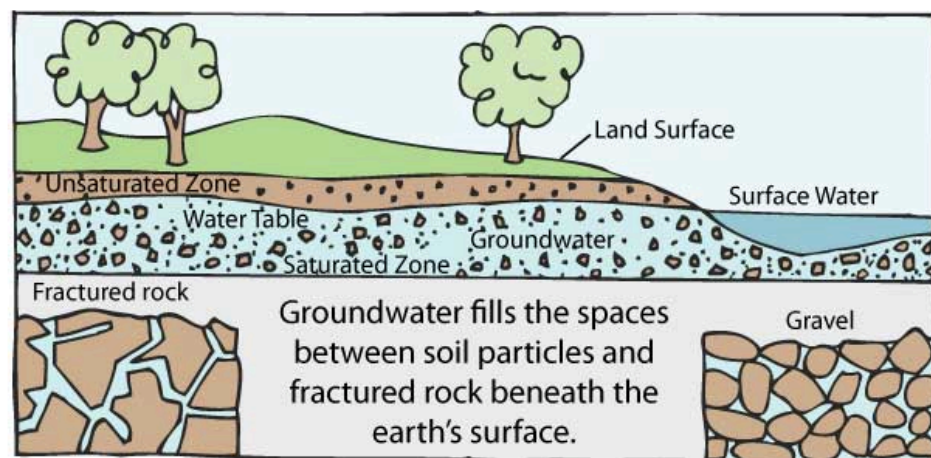
Figure 1.1 Graphic descriptive, groundwater formation

Groundwater is present in areas where there are limited sources of surface water, it is often of very good quality, the soil and rocks through which groundwater flows help to eliminate contaminants therefore respond slowly to changes in rainfall, and so it stays available during the summer and during droughts when rivers and streams have dried up.

By this reason groundwater is the primary source of drinking water for between 1.5 and 2 billion people world- wide, some of the largest cities in the developing world including Jakarta, Dhaka, Lima, and Mexico City depend on aquifers for almost all their water. And in rural areas, where centralized supply systems are undeveloped, groundwater is typically the sole source of water. **Table 1.1**

Table. 1.1. Groundwater used as Drinking Water.		
Region	Share of Drinking Water from Groundwater (percent)	People Served (million)
Australia	15	3
Asia-Pacific	32	1 000 to 1 200
Latin America	29	150
United States	51	135
Europe	75	200 to 500
Africa	Not available	Not available
World		1 500 to 2 000

U.S Geological Survey's (USGS) Water Science School, 2017

Groundwater are contaminated when chemical pollutants, such as pesticides, fertilizers used in agriculture, the industrial wastewater or chemical leaking from a storage tank or landfill, are widely spread on the land surface, and through processes of infiltration they reach the groundwater.

Moreover the excessive exploitation of the aquifers, have provoked the saline waters to invade the fresh waters, increasing considerably the salts concentration. Once a pollutant reaches an aquifer its impact will depend on its chemistry, nature of the aquifer and the distance between the source of pollution and the point at which groundwater reaches the surface again, either in a river or by being pumped. Some pollutants will naturally degrade, or will be filtered out of the water as it flows through the aquifer. Others will be persistent and need to be removed before the water can be used. It is best to prevent groundwater pollution because it is not always possible to remove pollution and clean-up operations are expensive. (Worldwatch Institute, 2000)

The assessment of the degree of pollution is very important, several towns and cities around the world have had to seek out alternate supplies of water because their groundwater has become unusable. e.g. Bangkok, Thailand, the excessive pumping of groundwater caused sea- water to enter the aquifer. Chloride levels increased 60-fold; many wells have been abandoned. In recent years, half of all wells in Santa Monica, California, have been shut down because of dangerously high levels of the gasoline additive MTBE. In Shenyang, China overpumping and Nitrate pollution, ammonium, oils, phenol, and other industrial pollutants, have forced authorities to replace

groundwater with more expensive surface water supplies. A chemical spill at a storage tank at a pharmaceutical factory in Barceloneta, Puerto Rico led to carbon tetrachloride and other chlorinated solvents to be present at levels of 100 times the guidelines. Costs of supplying alternate sources were $10 million. (Worldwatch Institute, 2000)

1.2 Groundwater contamination by heavy metals.

Heavy metals are most dangerous pollutants present in sources of water contaminated with metals. This contamination is observed mainly in the countries where the mining is one of the main sources of economic incomes.

Mining is the selective procurement of minerals and other materials from the earth's crust and is referred to as a primary economic activity: the extraction of elements from which an economic benefit can be obtained. Depending on the type of material to be extracted, mining is divided into metal and not metal.

The methods of exploitation can be open pit or underground mines. The factors that will determine the method, among others, are the geology and geometry of the deposit and the geomechanical characteristic of the mineral.

The main mining countries of the world are shown in table (1.2).

Table .1.2. List of countries by mineral production.						
Sn	Li	Ag	Au	Zn	Cu	Various metals
China	Bolivia	Poland	South Africa	Australia	Chile	China
Malaysia	Chile	Mexico	Australia	China	China	Russia
Indonesia	China	Peru	Peru	USA	Peru	Bolivia
Peru	Brazil	Australia	Russia	Kazakhstan	USA	USA
Brazil	USA	China	USA	Peru	Congo	Tajikistan
Bolivia	Canada	USA	Indonesia	Canada	Australia	South Africa
Russia	Australia	Canada	Canada	Mexico	Russia	Peru

T J Brown, et al. 2017 World mineral production 2011-15

Years of heavy metal mining has led to the contamination of groundwater and surface water in many areas of the world, by the discharge of mining waste or by leachate from landfills, for example in the United States, the United States Geological Survey's Toxic Substances Hydrology Program, conducted a study on the incidence of abandoned Zn

and Pb mines in Oklahoma and Kansas, finding high levels of heavy metals, and in India (Amin, S., et al, 2011), Bangladesh (Smith AH., et al 2000), Iran (Amin, S., et al 2011), Ethiopia (Haileslassie T., and Gebremedhin,K., 2015), Finland and Slovakia (Backman, B., et al. 1998), China (Rodríguez-Lado L., et al, 2013), Ecuador (INIGEM 2013), etc. Heavy metals as, As^{2+}, Cd^{2+}, Cr^{2+}, Fe^{2+}, Hg^{2+}, and Pb^{2+} have been reported as potential pollutants of both surface and groundwaters.

Among the heavy metals present in groundwater, Mercury has become one of the metals which has caused greater concern to the scientific community due to its toxicity that is preserved over time in the aqueous medium, and also for its characteristic of bioaccumulation and biomagnification, within the food chain. (Valls M., and Lorenzo, V., 2002).

The mercury is present in surface and groundwater, at concentrations generally below 0.5g/L, although higher concentrations may occur in groundwater due to the presence of mercury mine sites in the area. The WHO (World Health Organization) has declared Mercury as one of the most dangerous heavy metals for human health, it is related to problems to the central nervous system and also to the renal and respiratory system.

To better understand the importance of the removal of mercury in groundwater, we must understand the origin and possible sources of released mercury into the environment and its effects on human health.

Below is a brief overview on the aspects mentioned above. It also summarizes the current procedures for the removal of contaminants in aquifers, and thus be able to focus on the objective of the research, which is to propose a low cost alternative material for the removal of Hg from groundwater.

1.3   Chemistry of Mercury.

Mercury is a chemical element popularly known as liquid silver, its name comes from the Greek "hydrargyrum" which is a compound word that means "water" and "silver" and is represented by the acronym Hg. It takes the name mercury in honor to A Roman God who was known for his speed and mobility and was also associated with the first planet in the solar system whereby the alchemists represented him with the astrological symbol of the planet Mercury. Within the distribution of the updated Periodic Table of the Elements by IUPAC, it is classified within the D-block of transition metals, in group

12, period 6, atomic number 80, with an atomic mass of 200,59 amu, a melting point of -38,83 ºC (234,32 K, - 37,89 ºF), Its boiling point of 356,73 ºC (629,88 K, 674,11º F) , density 13,456 g/cm^3, oxidation state of 2-1 (Lew K, Mercury, 2009). It is the only metal that is liquid under normal conditions of temperature and pressure. Despite being a transition metal Hg's ability to transmit heat is low compared to other metals, but it is a good conductor of electricity, its electronic configuration is unique $1s^2$ $2s^2p^6$ $3s^2p^6d^{10}$ $4s^2p^6d^{10}f^{14}$ $5s^2p^6d^{10}$ $6s^2$, because its electrons fill all available orbitals in the energy sub-levels. Its behavior is similar to that of noble gases, resisting the removal of electrons by their strong configuration, forming weak bonds that allow the fusion of solid particles with ease.
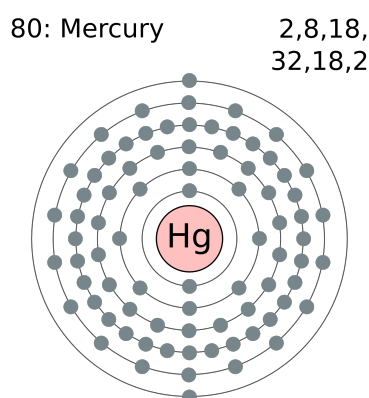
Figure. 1.2. Electronic configuration (Hg).

Mercury is moderately reactive, the reactivity of Hg is analogous to the other metals of group D, it can form conventional salts with the oxidation state +1, +2, or it can also react with organic compounds forming organomercurial compounds.

Hg can react with oxygen in the presence of heat (350 °C) forming Mercury (II) oxide.

$$2Hg + O_2 \rightarrow 2HgO$$
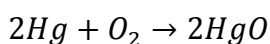
It can be decomposed by raising the temperature to over 400 ° C. (Patniak P., 2003).

Mercury also reacts with Halogens to obtain Mercury (II) salts, known as mercury halides.

$$Hg + X_2 \rightarrow HgX_2$$
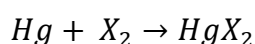
These halides, when reacted with metallic mercury, form Hg (I) halides, the best known of these compounds, is the Calomel.

23

$$HgCl_2 + Hg \rightarrow Hg_2Cl_2$$
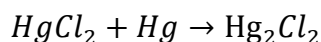
Mercury does not react with most acids, such as dilute sulfuric acid, but reacts with concentrated oxidizing acids, such as nitric acid and sulfuric acid, or with acqua regia to form sulphate, nitrate and chloride salts.

$$2Hg + 2HNO_3 \rightarrow Hg_2(NO_3) + H_2$$
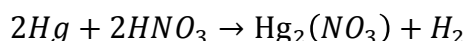
Mercury forms alloys with most of the heavy metals, which dissolve in the Hg, for example, gold, zinc, in addition, can form an amalgam with sodium, producing a powerful reducing agent. Among the metals which it can not form amalgams with are: Iron, Tantalum, Tungsten and Platinum.

The organomercurial compounds are formed, from the reaction, of amalgam of sodium with alkyl halides, wherein, R, is an organic group and X is a halide:

$$2Hg + 2RX \rightarrow HgR_2 + HgX_2$$
$$HgX_2 + 2Na \rightarrow Hg + 2NaX$$
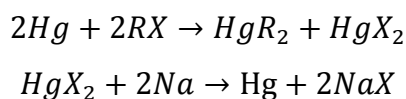
Organomercurial compounds are of great importance due to their high toxicity, where Methylmercury is the compound that has the greatest presence within this group and is one of the most toxic compounds in water sources and streams contaminated by mercury. (WHO)

Through laboratory chemical synthesis, it has been possible for Hg to react with high oxidation states, forming (HgF4), Mercury Fluoride (IV) by means of matrix isolation techniques. (Wang et al.,2007) And also, by means of electric discharges, applied to noble gases and combining with Mercury vapor, it has been possible, thanks to the forces of Van der Waals, to form bonds, giving compounds like: Hg.Ne, Hg.Xe, Hg.Ar, and Hg.Kr. (Nabi, S., 2014).

1.3.1   Environmental Mercury Emission Sources.

Hg is present naturally throughout the planet, through natural sources such as minerals, for example Cinnabar a bright red mineral of volcanic origin, which has in its chemical composition 85% mercury as HgS, being one of the main sources for the extraction of mercury throughout the history, also we can find Hg in nonferrous minerals, in the coal, in deposits of petroleum like impurities.

The release of mercury into the atmosphere occurs naturally through the constant wear of rocks, volcanic explosions, geothermal activity of the earth releasing the underground mercury, through the oceans to the different atmospheric receptors, such as air, water and earth, these represent 10% of the total Hg released into the atmosphere annually, of approximately 5 500 - 8 900 tons of Hg. (UNEP 2013).

Thirty percent of this total is anthropogenic pollution, which, thanks to increasing industrialization and the constant increase in energy requirement, has led the increasing of Hg concentration in recent years, it is known that Hg has been used by man for many centuries ago, as a bright red pigment (Cinnabar) in the Neolithic times, painting various images or walls in caves, its use over time was expanded, also used as a cosmetic dye by the Romans, to give color to the wood or for use as a seal to close documents. Mercury was also used for a long time in the pharmaceutical area, due to its antiseptic and laxative characteristics, as a component of antidepressant drugs, against syphilis and in the area of dentistry. (EPA 2013).

Mercury emissions can be classified into two categories: 1) unintentional discharges, in which Mercury is a by-product of an industrial process; As in the burning of coal, mining in the cement industry, in the production of raw materials where Mercury is present in small quantities as an impurity, and 2) direct discharges in which mercury is intentionally used, due to its chemical-physical characteristics its applications in the industry is very broad as: in the industries that manufacture or use measurement equipment of pressure, temperature and electrical, e.g. thermometers, manometers, electric navigation equipment, seals, valves, barometers, etc.

Industry uses mercury metal as a liquid electrode in the manufacture of chlorine and sodium hydroxide by electrolysis of brine. Mercury is still used in some electrical gear, such as switches and rectifiers, which need to be reliable, and for industrial catalysts. Much less mercury is now used in consumer batteries and fluorescent lighting, but it has

not been entirely eliminated, due to its ease of forming amalgam with gold it is widely used in the extraction of this precious metal through mining, analysis and research laboratories. In addition mercury compounds such as mercury chloride (Hg_2Cl_2) is used as a standard in electrochemical measurements and in medicine as a purgative. Mercury chloride ($HgCl_2$) is used as a disinfectant, rat poison and insecticide, etc. (Lenntech Ltd. 2016).

According to different studies by various agencies such as the UNEP, EPA, WHO, on the emission of Hg to the environment, they have determined, that among the main mercury emission sources are the fossil fuel power stations. These power stations provide electric energy to large cities in the world; it convert the heat energy that comes from the combustion of coal, natural gas or petroleum, into mechanical energy, which feeds the electric generators producing electrical energy, which is controlled by large generators, this type of energy production has low economic cost but at great environmental cost.

Coal is one of the most abundant fossil fuels on the planet, as of December 31, 2011, the world total of proved recoverable coal reserves were estimated at 979.8 million tons (EIA. Gov. June 17, 2016) so, it has become the main material used in this industries-type, although the mercury presence in fossil fuels is not very high, its excessive use causes the becoming one of the main anthropogenic sources of mercury unintentional discharge.

Moreover, by-products of industrial processes, as the petroleum refinery processes, cement production, mining, smelting, the production of iron and non-ferrous metals produce by-products containing Hg, but the inadequate disposal of solid waste in large landfills can become sources of environment pollution.

Applying control measures to the discharges of each process can reduce unintentional mercury emissions from these sectors. In which the mercury that can be recovered is refined and entered into the commercial supply chain, however, not all the waste can be recovered, such as fly ash or refinery waste, so, they have to be disposed. (UNEP, 2013).

The Hg that is used as a primary or intentional material, can be released into the environment in many ways, for example when a thermometer is broken, or through the industrial waste of fluorescent bulbs, batteries, manometers, cleaning solutions, switches, transmitters, sensors, paints, electrical and electronic devices, pesticides, fungicides, medicine, etc. Some of these wastes are discharged directly into sewers

entering the water stream and others are deposited in landfills and that through slow filtration they move toward the environment, further the uncontrolled incineration of these wastes causes a significant source of environmental pollution.

However, within this category one of the industries, which have increased the incidence of Hg contamination by direct discharge, is gold mining. Gold dissolves in mercury to form an amalgam with strong and stable bonds, the gold recovery is viable through several methods. The process of distillation or burning of the amalgam, it is one of the main recovery methods, it consists of distilling the mercury from the amalgam by means of a retort of cast iron or steel retort, consisting of a vessel with a fixed lid to avoid the loss of vapor during the boiling that passes through of the condenser. The vapor is conveyed to a vessel containing water where the mercury vapor condenses to a metallic state. The distillation is carried out at low temperature and rising slowly to reach 810 ° C and maintaining it for 2 hours.

The large-scale industrial mining uses technology innovative and efficient to avoid gold losses and to recover mercury. However, these procedures have not been transferred or adapted to small-scale artisanal gold mining (ASGM), which accounts for 20% of all gold produced in the world. (EPA "Reducing Mercury Pollution from Artisanal and Small-Scale" http//www.epa.gov).

ASGM is an extraction operation that may be legal or illegal and may involve the extraction of primary or secondary minerals. In addition, ASGM activities are not defined by the magnitude of their operation; most of them are characterized by the lack of planning and control of the mine in the long term and for the use of rudimentary techniques. (J.J. Hinton et al. 2003)
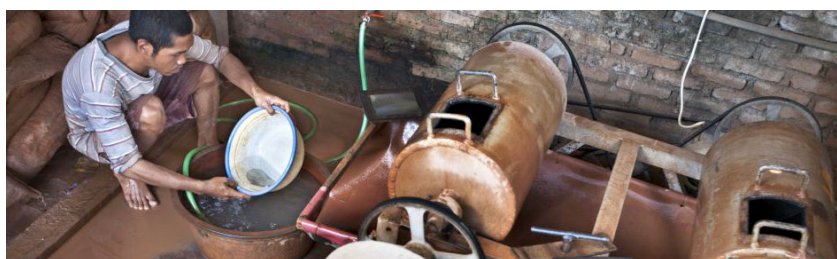
Figure 1.3 Gold extraction process in small-scale artisanal gold mining from UNEP Minamata Convention on Mercury: ASGM

Most of the ASGM miners are not legalized and work clandestinely, making it difficult to control personal and environmental safety; taking into consideration these specific conditions and the lack of economic resources, the information and awareness about the

environmental impacts, the artisanal miners prefer to use techniques that are economically more profitable, and of easy application so, the outdoor burning of Hg-Au amalgams has become a very common practice in ASGM, causing direct Hg emissions to the environment which can not be quantified in their totality by the illegality that exists in this industry, in spite of this difficulty the UNEP has determined that until 2010 the emissions of Hg to the environment were of 700 tons per year. (UNEP, 2013), the Gold industry has become one of the main anthropogenic sources of mercury emission to the environment.
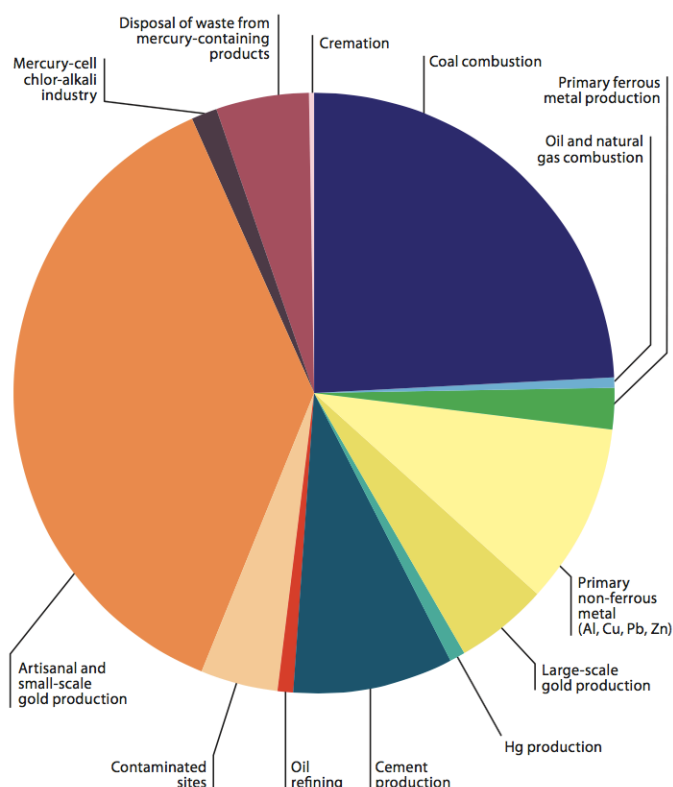
Figure 1.4 Relative contributions to estimated emissions to air from anthropogenic sources in 2010. (UNEP 2013).

1.3.2   Re-emission and re-mobilization of mercury.

This is a source of Hg emission that has not been taken into account in previous years, recent studies have considered the importance of the re-emission and re-mobilization of Hg, released from natural and anthropogenic sources, which are deposited in the air, soil, vegetation and the aquifer system, can be re-emitted into the environment by action of nature (rain, eruptions, erosion, forest fires), global warming, which cause organic and inorganic mercury to transform into its elemental form Hg^{2+}, which is readily

volatile and provoking its release in the air again, this process can not be considered anthropogenic or natural because the origin of the re-emitted Hg can not be determined specifically, however this process represents 60% of the total Hg that is released into the environment.

At present the natural mercury cycle is altered, because each year the amount of mercury released into the environment increases, despite the existence control and reduction of industrial discharges, the re-emission and remobilization process, will keep mercury levels high in the environment Fig (1.5).
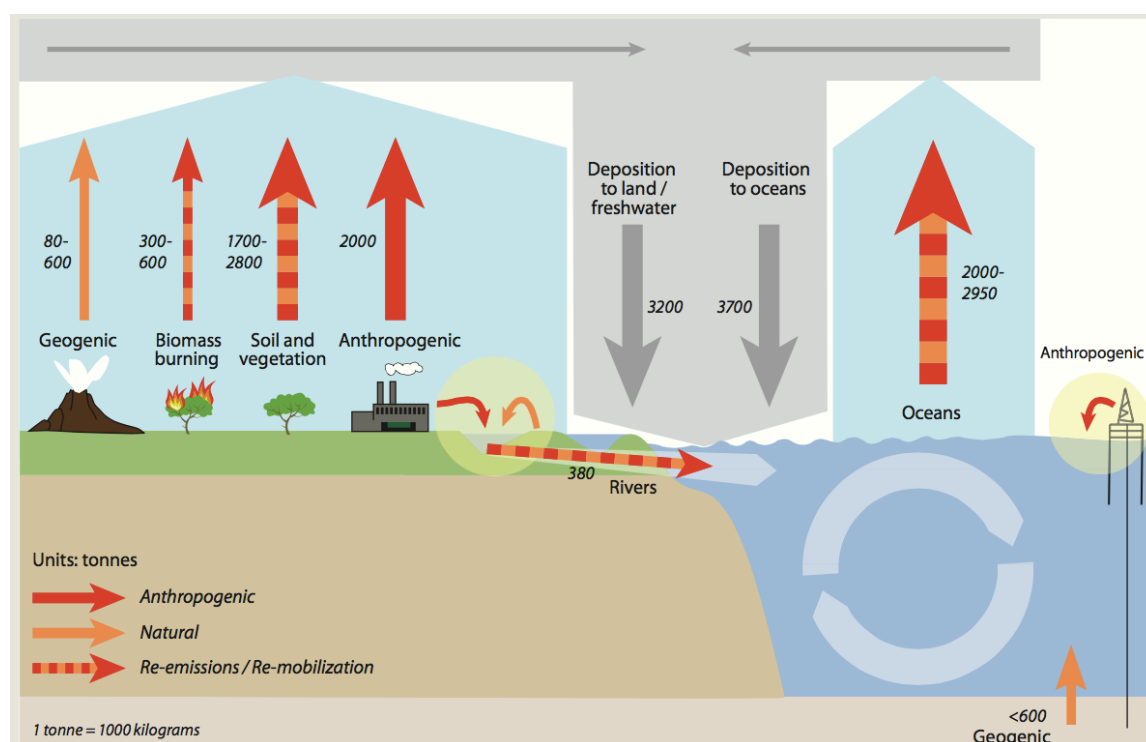
Figure 1.5. The global mercury cycle. From UNEP 2013

As we can see the levels of mercury are alarming, so it is necessary to make great efforts to mitigate their emission, at least the sources of release that man can control: the anthropogenic sources. Nowadays the release of Hg according to UNEP, 2010, estimates that releases are 1 960 tons of Mercury per year directly by human activity.

1.3.3   Exposure to mercury and its consequences on human health.

The events raised in Japan (Minamata Bay) in 1950, for the wastewater discharges (Methyl-mercury Me-Hg), discarded from the chemical plants of Acetaldehyde and Vinyl Chloride, in the bay and in the rivers of Minamata, for more than 10 years, contaminated a large part of the fish and shellfish that consumed the population of Bahia and its surroundings. Those who had an acute exposure to Me-Hg for more than 20 years presented severe clinical symptoms, now known as Minamata's disease, consisting of patients with neurological signs including sensory loss, ataxia, visual loss, dysarthria and hearing problems and a significant number of newborn infants from the exposed areas presented with cerebral palsy. (Kitamura et al., 1959).

On the other hand, in 1971 also an important case of Hg poisoning was presented in Iraq, where the population consumed grains of wheat and barley that were destined for the planting and were not fit for its consumption, they were treated with fungicides that contained methylmercury and phenylmercury acetate, about 73,210 tons of wheat and 22,262 tons of contaminated barley were distributed around the country. Some months after, its distribution around 6,530 cases of people with symptoms of poisoning were hospitalized in the country, causing 459 deaths, the clinical symptoms presented by the patients were similar to Minamata's disease. (F. Bakir, et al, 1980).

The main problems caused by mercury on human health are:

- Nervous system, Memory loss, including Alzheimer like dementia, deficit in attention, hypoesthesia, ataxia, dysarthrea, subclinical finger tremor impairment of hearing and vision, sensory disturbances, increased fatigue in adults. In children and infants, it presents as deficit in language (late talking) and memory deficit in attention (autism).

- Motor system: Disruption of fine motor function, decreased muscular strength, increased tiredness in adults and late walking in children and infants.

- Renal system: Increases plasma creatinine level.

- Cardiovascular system: Alters normal cardiovascular homoeostasis.

- Immune system: Decreases overall immunity of the body, exacerbates lupus like autoimmunity, multiple sclerosis, autoimmune thyroiditis or atopic eczema

- Reproductive system: Decreases rate of fertility in both males and females, birth of abnormal offsprings.

These serious clinical disorders have caused many of the people who are constantly exposed to mercury emissions; their quality of life decreased and even caused death.

The human being comes into contact with the mercury by different ways:

Through direct exposure to elemental Hg gases, by processes of incineration (coal, amalgams), there have been reported cases of presence of Hg in the blood in the workers of the coal plants and in the artisanal miners, by the direct contact to these gases.

Through water, which thanks to the wind, acid rain (mercury in the air) it can be deposited into rivers, lakes, oceans and the direct discharge of wastes into the water system has contaminated even the groundwater sources. This occurred in India where research conducted by The Hindustan Times showed that groundwater from 8 different sites: Punjab, Haryana, Andhra Pradesh, Gujarat and Kanpu showed levels of mercury concentrations up to 268 times higher than the legal limit. (Polluting India's groundwater. The Hindustan Times, September 2-1999. www.hindustantimes.com).

Mercury in the aquatic environment may be present as elemental Hg^0 which is insoluble, mercury ions (Hg^+, Hg^{2+}) in the form of salts which are poorly soluble and methylated mercury [CH_3Hg^+, $(CH_3)_2Hg$], which are readily soluble. The mercury in the water begins to have several biogeochemical transformations through biotic and abiotic processes, which are presented both in fresh water and sea water, where transformations are produced through various mechanisms as (Barkay et al., 2003):

- Hg(II) methylation
- CH3Hg(I) demethylation
- Hg(II) reduction
- Hg(0) oxidation

Of these processes the Hg (II) methylation is one of the most important since the monomethylated species are neurotoxic (CH3 Hg) (Halbach, 1995), (M. Ravichandran (2004).
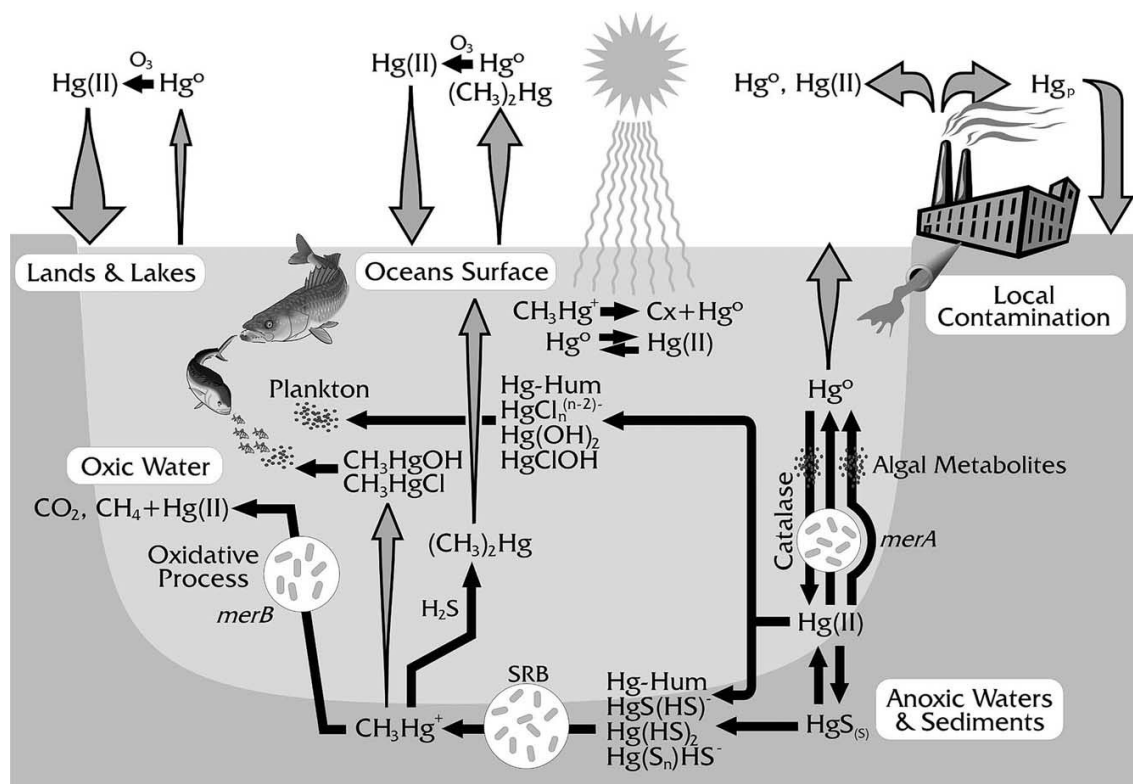
Figure 1.6 Mercury Biogeochemical Cycle (T. Barkay et al. 2003)

Contamination through food is one of the main means of human intoxication. Mercury is found as methylated compounds, which have great affinity with fatty tissues and are more susceptible to biomagnification and bioaccumulation as the cases exposed previously from Japan and Iraq.

Mercury within the marine food chain is determined by bacteriological processes, oxidation-reduction reactions and by the presence of dissolved organic material, which affect the speciation, solubility, mobility, and toxicity of Hg in the aquatic environment. The methylated mercury accumulates in plankton; which is the main source of nutrition of marine species. These are ingested and bioaccumulate within their fatty tissues then enter the human food chain when the polluted species are ingested (T. Barkay et al., 2003).

The danger level from consuming fish depends on species and size. Size is the best predictor of increased levels of accumulated mercury. Sharks, such as the mako shark, have very high levels of mercury. A study on costal fish in New Jersey indicated that one third of the sampled fish had levels of mercury above 0.5 ppm, a level that could pose a human health concern for consumers who regularly eat this fish. Another study of marketplace fish caught in waters surrounding Southern Italy showed that,

undoubtedly, greater fish weight leads to additional mercury found in fish body tissues. Moreover, the concentration measured in milligrams of mercury per kilogram of fish steadily increases with the size of the fish. Anglerfish off the coast of Italy were found with concentrations as high as 2.2 milligrams of mercury per kilogram, higher than the recommended limit of 1 milligram of mercury per kilogram. Annually, Italy catches approximately a third of its fish from the Adriatic Sea, where these anglerfish were found. (Storelli, M. M. 2000)

As described above, there are different forms of man exposure to mercury and in order to reduce the risk of poisoning, regulatory laws have been enacted for the use of mercury as the Mercury Export Ban Act of 2008, Mercury-Containing, Rechargeable Battery Management Act of 1996, Clean Air Act, Clean Water Act, Emergency Planning and Community Right-to-Know Act (EPCRA) Drinking Water Act (SDWA) among others.

Awareness of this great environmental and sanitary problem led several researchers to investigate techniques for the recovery of sites contaminated by heavy metals, which has led to the development of various methods and techniques using various chemical and physical processes and the use of different types of materials.

1.4   Treatments and techniques for heavy metals removal in aquatic systems.

The human being has always felt the need to acquire and drink healthy water, thus, so that centuries ago, Hippocrates "The father of Medicine", designed his own filter to purify raw water and used it with his patients, known later as the "Hippocratic sleeve," this filter eliminated sediments from the water that caused unpleasant taste and odor.

With the advancement of time and thanks to the development of science, processes of water purification were making great progress, so in the middle of the XIX century, the city of London, issued a regulatory decree for the drinking water quality in the city by the presence of an epidemic of cholera in London. This decree served as a precedent for other cities and municipalities to control their water supply systems. Hence in 1804, the city Paisley Scotland (the first city) built and installed a water treatment plant, which provided drinking water to homes within the city limits.

The industrial progress of the XXI century and the growing population in cities led other metropolitan areas of the world to find the need to install treatment plants to

provide healthy water to its inhabitants, meeting minimum quality requirements. The guidelines for drinking-water quality describe the minimum requirements of safety and consumer protection, in order to define mandatory limits; it is preferable to consider the guidelines in the context of the local or national, social, economic and cultural environment. (WHO, 1991)

The Guidelines contain maximum permissible limit values of different parameters, such as heavy metals, for example the WHO, has determined a maximum level of 0.006 mg L^{-1} in drinking water, 0.05 mg L^{-1} water for agricultural use, 0.05 mg L^{-1} and for groundwater 0.001 mg L^{-1} of Mercury (TULSMA, 2012). Higher concentrations to the permissible levels can be considered as potentially contaminated waters. Several researchers have used various methods of heavy metal removal in water resources; among the various techniques that have been used include chemical precipitation, ion exchange, adsorption, membrane filtration, coagulation, flocculation, flotation, and electrochemical methods. (Fu and Wang, 2011).

1.4.1   Heavy metal wastewater treatment techniques

Among the most important techniques for heavy metals removal from water are:

1.4.2   Chemical Precipitation.

This is a method that, due to its simplicity and low operating costs, is one of the most widely used techniques in industrial processes, this process is based on the precipitation of heavy metals, when reacting with various chemicals, forming insoluble compounds, the precipitates that form are separated from the aqueous phase through filtration or sedimentation. A highlighted process of chemical precipitation: Hydroxide precipitation, this process is based on the control of the pH value of the aqueous solution, through several bases, such as NaOH or Ca $(OH)_2$, which raise the pH of the solution within a range of 8.00 - 11.00, where the solubility of the Hydrolyzed Metals is low. This technique has some disadvantages such as the generation of large volumes of low-density sediments.

Sulfide precipitation is also an effective process for the treatment of toxic heavy metals ions. The advantages of using sulfides are that the solubility of the metallic sulfide precipitates are lower, than hydroxide precipitates and sulfide precipitates are not amphoteric. And hence, the sulfide precipitation process can achieve a high degree of

metal removal over a broad pH range compared with hydroxide precipitation. Metal sulfide sludge also exhibit better thickening and dewatering characteristics than the corresponding metal hydroxide sludge. However, there are potential dangers in the use of sulfide precipitation process. As we know, heavy metal ions often in acid conditions and sulfide precipitants in acidic conditions can result in the evolution of toxic H_2S fumes. It is essential that this precipitation process be performed in a neutral or basic medium. (Fu and Wang, 2011).

Species	Precipitant	Removal efficiency (%)
$Cu^{+2}, Zn^{+2}, Cr^{+3}, Pb^{+2}$,	CaO	$99.37 - 99.6$
$Cu^{+2}, Zn^{+2}, Pb^{+2}$,	H_2S	$100, > 94, > 92$
Hg^{+2}	1,3-benzenediamidoethanethiolate	> 99.9
CuEDTA	1.3.5-hexahydrotriazinedithiocarbamate	$99.0, 99.3, 99,6$

Table 1.3. Heavy metal removal using chemical precipitation from Fu and Wang., 2011.

Heavy metal chelating precipitation is a technique where through chemical reagents called chelators form complexes with heavy metal ions, the commercial chelants most used are trimercaptotriazine, potassium / sodium thiocarbonate and sodium dimethyldithiocarbamate, this technique is still under development to avoid environmental risks it causes.

1.4.3   Ion exchange

Ion exchange consists of interchange ions between two phases. The ion-exchange resins cross-linked polymer network is the insoluble phase, where an ion is electrostatically bound; when contacted with a solution containing ions of the same charge, an exchange could take place. The exchange depends on the concentration of the ion(s) in the solution and the affinity of the ion(s) for the insoluble phase relative to the solution phase. In other words the ions in solutions are replaced by different ions originally present in the solid.

Ion exchange is a chemical process that can be represented by a stoichiometric equation, for example, when ion A in solution replaces ion B in the solid phase:

$$A(solution) \; + \; B(solid) \; \rightleftharpoons \; A(solid) \; + \; B(solution)$$
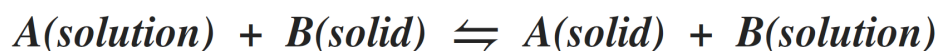
The most common cation exchangers are the strong acidic resins with sulfonic acid groups (eSO3H) and weak acid resins are those with carboxylic acid groups (eCOOH). Hydrogen ions in the sulfonic group or carboxylic group of the resin can serve as exchangeable ions with metal cations. The uptake of heavy metal ions by ion-exchange resins is further affected by certain variables such as pH, temperature, initial metal concentration and contact time. Ionic charge also plays an important role in ion-exchange process. (Fun and Wang, 2011).

Due to their various advantages, such as high treatment capacity, high removal efficiency and fast kinetics, ion-exchange processes have been widely used to remove heavy metals from wastewater. Among the materials used in ion-exchange processes, are synthetic resins. They are generally preferred as they are effective and practical in removing the heavy metals from the solution, and for not removing the natural zeolites, and naturally occurring silicate minerals. They are also used widely due to their low cost and high abundance. Many researchers have demonstrated that zeolites exhibit good cation-exchange capacities for heavy metal ions in different experimental conditions (Motsi et al., 2009; Ostroski et al., 2009; Taffarel and Rubio, 2009).
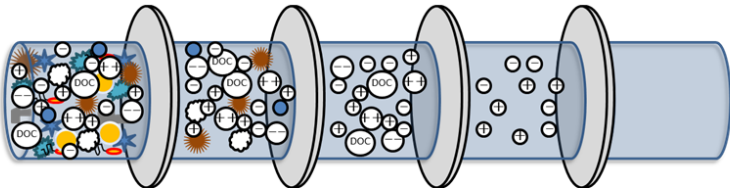
Despite the high performance of these materials for the removal of heavy metals their usage is on laboratory experiments scale. Hence, their use in industrial scale is limited.

1.4.4   Membrane filtration

A membrane is a thin layer of semi-permeable material that separates substances, when a driving force is applied across the membrane. Membrane processes are increasingly used for the removal of heavy metals, for their high efficiency, easy operational use and space saving. Membrane filtration can be divided up between Micro and Ultra-filtration on the one hand and Nano Filtration and Reverse Osmosis (RO or hyper filtration) on the other hand. Ultra-filtration (UF) is a membrane technique, works at low transmembrane pressures for the removal of dissolved and colloidal material. Since, the pore sizes of UF membranes are larger than dissolved metal ions in the form of hydrated ions or as low molecular weight complexes, these ions will pass easily through UF membranes. To obtain high removal of metal ions efficiently is through the use of the

micellar enhanced ultrafiltration (MEUF). This separation technique is based on the addition of surfactants to wastewater and polymer enhanced ultrafiltration (PEUF), that uses water-soluble polymer to complex metallic ions and form a macromolecular. Recently, they have been used for the removal of heavy metals in aqueous solutions. (Fu and Wang, 2011)

Nano filtration and RO membranes do not work according to the principle of pores; separation takes place by diffusion through the membrane. The pressure that is required to perform nano filtration and Reverse Osmosis is much higher than the pressure required for micro and ultra filtration, while productivity is much lower.

Membrane Technology:	Microfiltration > 0,2 mm	Ultrafiltration 0,1 – 0,01 mm	Nanofiltration 0,01 – 0,001 mm	Reverse Osmosis < 0,001 mm
Retained Water ingredents:	zooplankton / algae / turbidity / bacteria / Suspended particles	macromolekules / viruses / colloids	Organic compounds / Multi valent ions	Monovalent ions
Needed pressure difference:	0,2 – 3 bar	0,5 – 5 bar	5 – 10 bar	10 – 150

Figure. 1.7.Types of filtration and contaminants that removed.© 2016 Chriwa Wasseraufbereitungstechnik GmbH

Zambrano et al, investigated separation of Hg from aqueous solutions by complexation-ultrafiltration, used polyethylenimine as polymeric complexing agent. They have obtained mercury retention values closed to 100% for neutral solutions. Depletion of mercury from 100 to 20 mg/L, was achieved, when the current density was 1.09 mA.g$^{-1.}$ Zambrano et al. 2002. Bessbousse et al. 2008, investigated removal of Hg(II) from aqueous solutions by sorption and filtration with a membrane containing poly(ethyleneimine) as a complexing polymer. The maximum retention capacity of the membrane was 311 mg . g^{-1} . The elimination ratio of Hg(II) was close to 99%

Filtration type	Pollutant name	Range Hg Concentration	Removal efficiency (%)
Complexation-Ultrafiltration (Polyethylenimine)	$HgCl_2$	5 to 10 mg L^{-1}	> 99
Ultrafiltration (Polyethylenimine, PEI)	$HgCl_2$	> 30 mg L^{-1}	100
Containing poly (ethyleimine) as a complexing polymer	$HgCl_2$	100 mg L^{-1}	99
Poly (vinylalcohol)/poly(vinylimidazole) complexing membrane	$HgCl_2$	91.6 mg L^{-1}	99.4
UF membrane (Poly vinyalcohol modified)	$HgCl_2$	-	> 98

Table 1.4. Heavy metal removal by membrane separation. From Sharma et al. 2015.

1.5   Adsorption

Adsorption is the phenomenon of accumulation of large number of molecular species at the surface of liquid or solid phase in comparison to the bulk. The process of adsorption arises due to presence of unbalanced or residual forces at the surface of liquid or solid phase. These unbalanced residual forces have tendency to attract and retain the molecular species when it comes into contact with the surface. Adsorption is essentially a surface phenomenon.

Nevertheless, we should not confusing adsorption with absorption, because absorption means uniform distribution of the substance throughout the bulk, and adsorption is the link-up of atoms, ions, or molecules from a gas, liquid, or dissolved solid to a surface. When, both the adsorption and absorption phenomenon are concomitant phenomenon become in Sorption.

Adsorption process involves two components Adsorbent and Adsorbate. Adsorbent is the substance on the surface of which adsorption takes place. Adsorbate is the substance, which is being adsorbed on the surface of adsorbent.
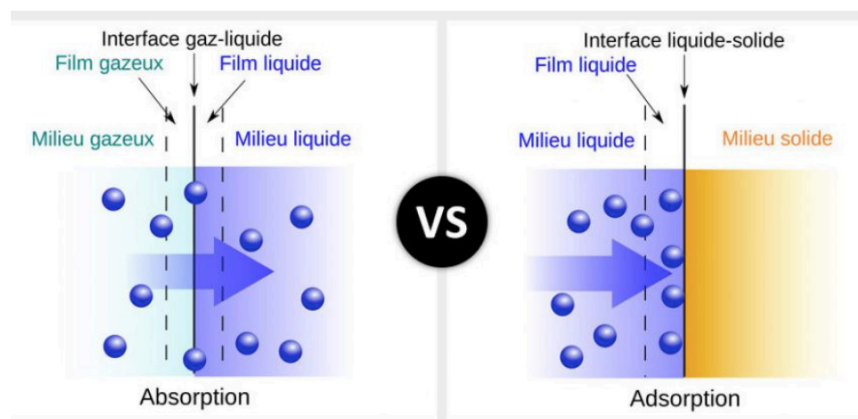
Figure 1.8 Difference between Absorption vs Adsorption

Nowadays the adsorption is recognized as an effective and economic method for the use of heavy metal wastewater treatment. The adsorption process offers flexibility in designing, operating and in many cases produces high-quality treated effluent. In addition, because adsorption is sometimes reversible, adsorbents can be regenerated by suitable desorption process.

The search for materials that can used as adsorbent for contaminants removal from aqueous source, have led several researchers to use different materials and technics for obtaining high adsorption capacity. (Zabihi, 2009, Gupta, 2015).

1.5.1   Types of adsorbents to heavy metals removal

Currently, there is a wide variety of adsorbent materials that are used in the industry for various uses including: glass masks, clarification of sugar, paint industry, chromatographic analysis, catalysis and softening of hard water as well as metal removal.

The following are the details of the variety of adsorbents that can be used for the elimination of heavy metals through adsorption.

1.5.2   Low-cost adsorbents

In recent years, the search for low-cost adsorbents that have metal-binding capacities has intensified. Materials locally available in large quantities such as natural materials, agricultural waste or industrial by- products can be utilized as low-cost adsorbents. Some of these materials can be used as adsorbents with little processing. Conversion of these materials into activated carbon, can be used as an adsorbent for water purification,

which would improve economic value and help industries to reduce the cost of waste disposal and providing a potential alternative to activated carbon. Currently, a large number of studies have been published on the use of low-cost adsorbents (Kurniawan et al 2006, Gupta 2015).

1.5.2.1   Activated carbons adsorbents.

Activated carbon (AC) adsorbents are widely used in the removal of heavy metal contamination. Its usefulness derives mainly from its large micropore and mesopore volumes and the resulting high surface area.

Activated Carbons (AC) were the first adsorbents to be developed. The AC are produced from a solid carbonaceous based material, which is non-graphitic and non-graphitizable, and has an initial isotropic structure.

Since an activated carbon is structurally a non-graphitic carbonaceous material, almost any carbonaceous solid material can be converted into activated carbon. There are, therefore, plenty of possible raw materials in practice for example, wood, coconut shells, fruit stones, coals, lignite, petroleum coke, lignocellulosic biomass, peat and etc. they can all be used to make activated carbon, since they are all inexpensive materials with a high carbon content and a low inorganic content, and consequently, are suitable for use as an activated carbon precursor. The precursor is transformed or activated by means of medium to high temperature treatments, which removes solid mass, and at the same time, create pores, where the removed mass was previously located. The common properties of activated carbons and other kinds of carbon adsorbents, is a good developed pore network, and the similar ways of production. (J. A. Menéndez-Díaz and I. Martín-Gullón, 2006).
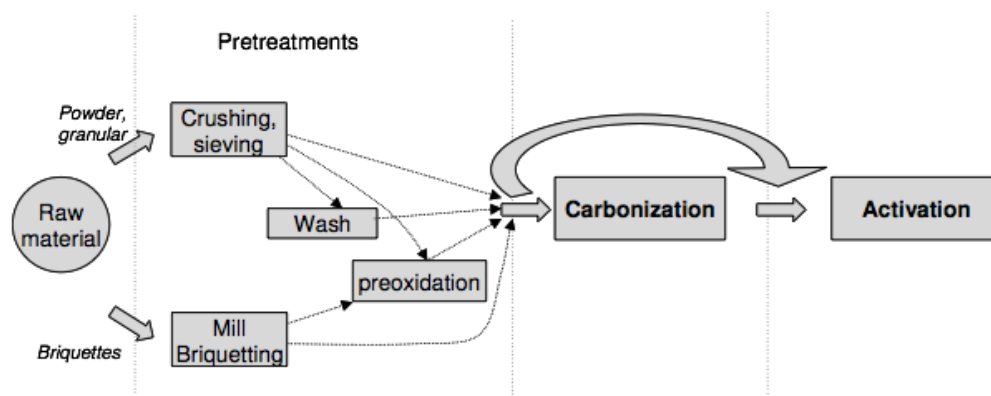
Figure 1.9. Process for obtaining carbon and its activation

The efficiency of heavy metal removal depends on the preparation conditions of active carbon.   There are two basic methods for the preparation of popular adsorbents i.e. activated carbons: physical and chemical activation. The physical activation method involves carbonization of raw material followed by activation of carbon dioxide at a high temperature in steam or water vapor atmosphere. Chemical activation, which is a well-known method in the preparation of activated carbon, involves one-step heat treatment at lower temperature than physical activation in the presence of some chemical agents. (Zabihi et al, 2009.)

Numerous researchers are studying the use of AC for removing heavy metals and improving its adsorption capacity through physical and chemicals modifications, achieving high results of performance in the of removal of Cd, Cu, Pb, Cr, Ni, (Wang et al., 2007). For aqueous solution, even for mercury removal, there are Active Carbons modificated with high adsorption capacity, such as MERSORB activated carbon 230.00 mg g^{-1} (NUCON International, Inc), etc. However all these adsorbents required complicated activation processes, therefore the cost of production is expensive. Moreover, the activated carbon also requires complexing agents to improve its removal performance for inorganic matters. Therefore, this characteristic makes it no longer attractive to be widely used in small-scale industries because of its cost inefficiency.

Due to the problems mentioned previously above, research interest into the production of alternative adsorbents to replace the costly activated carbon has intensified in recent years. The focused has been on the various adsorbents, which have metal-binding capacities and are able to remove unwanted heavy metals from contaminated water at a low cost. (S. Babel, 2003).

1.5.2.2 Agricultural waste

Agricultural waste is one of the rich sources for low- cost adsorbents besides industrial by-product or natural material. Due to abundant availability, agricultural waste such as orange peel, hazelnut shell, rice husk, coir pith, almond husk, pecan shells, jackfruit and etc, has little economic value. Moreover, it creates serious disposal issues. The material wastes can be used as an adsorbent for heavy-metal uptake after chemical modification or as conversion by heating into activated carbon. Several reviews are available that discuss the use of agricultural waste for the treatment of heavy metals wastewater. (Kurniawan et al 2006, ; S.Babel 2003, ; Gupta 2015.)

The adsorption capacity of these adsorbents depends on the pH, and the working temperature, the initial concentration of metal, the dosage of the adsorbent and mainly on the conditions of the production treatment. Therefore, these processes can be costly due to energy and chemicals consumption. However, if adsorption capacity improved after additional processing may compensate the cost for such a process. For example, coconut shell charcoal (CSC) is an agricultural waste from coconut industry the applicability of CSC modified with oxidizing agents for Cr (VI) removal was investigated by Babel and Kurniawan, (2004) they obtained adsorption capacity from 3,65 mg/g to 10,88 mg/g. Zabihi et al, (2007) used the walnut shell active carbon with ZnCl2 modification for improve the uptake of Hg achieving values of 151,50 mg/g. The rice husk with sulphuric acid treatment have an adsorption capacity of 384,62 mg/g, for Hg removal (El-Shafey, 2010) these modification onto the adsorbents suggest that surface modification with a strong oxidizing agent generated more adsorption sites on its solid surface for metal adsorption.

1.5.2.3 Industrial by-products.

An industrial by-product (IBP) is a residual material resulting from industrial, commercial, mining, and agricultural operations that are not primary products and are not produced separately in the process. IBP is technically classified as solid waste, and are the result of processes such as food and beverage processing, livestock vehicle washing, ethanol production, generation of electricity, and treatment of drinking water, they are inexpensive and are available abundantly. IBP can be chemically modified and used for others processes. In several industries there are projects for the utilization of IBP to reduce the cost of disposable spending.

An alternative to these IBP is the use as adsorbents, there are various studies, where by-products have been used such as lignin (Betancur et al., 2009; Reyes et al., 2009), diatomite (Sheng et al., 2009), clino-pyrrhotite (Lu et al., 2006), lignite (Mohan and Chander, 2006), aragonite shells (Kohler et al., 2007), peat (Liu et al., 2008), red mud, a solid by- product from alumina production Zouboulis and Kydros (1993), blast-furnace slag Dimitrova, 1996, Activated slag (Gupta 1998), bagasse fly ash, a solid waste from sugar industry (Gupta, 2003), they were studied for heavy metals removal, obtained larger results for metals as Cu, Ni, Zn, Pb.

1.5.2.4 Natura Materials.

Natural materials are widely used as adsorbents, the more widely used are the:

- Zeolite, basically zeolites are a naturally occurring crystalline aluminosilicates consisting of a framework of tetrahedral molecules, linked with each other by shared oxygen atoms. The natural zeolites gained a significant interest among scientists, due to their ion-exchange capability in removing unwanted heavy metals such as strontium and cesium, (Babel S, 2003). Zeolites consist of a wide variety of species such as clinoptilolite and chabazite. Clinoptilolite is most abundant in nature and is readily available from more than 40 natural zeolites species (M. Vaca-Mier, et al., 2001). Clinoptilolite have received extensive attention due to its selectivity for heavy metals. Table 4. shows the efficiency of clinoptilolite for removing heavy metal ions, such as Pb^{2+}, Cd^{2+}, Zn^{2+} and Cu^{2+}.

Material	Cd^{2+}	Co^{2+}	Ni^{2+}	Zn^{2+}	Cu^{2+}	Pb^{2+}
Clinoptilolite	2.40	1.42	0.48	0.50	1.64	1.60
	1.20					1.40
	70.00					62.00
	3.70	1.50	0.90	2.70	3.80	6.00
Chabazite	6.70	5.80	4.50	5.50	5.10	6.00
Chabazite-phillipsite			0.56	0.04	0.37	

Table.1.5 Adsorption capacities (mg g^{-1}) of zeolites for some heavy metals. (Babel 2003).

Clay, is widely known and there are three basic species of clay: smectites (such as montmorillonite), kaolinite, and micas; amongst them montmorillonite has the highest cation exchange capacity. Therefore, a number of studies have been conducted using clays. Manohar et al. 2002, prepared 2-mercaptobenzimidazole loaded natural clay was prepared for the removal of Hg (II) from aqueous media. They have found increment in the maximum adsorption with change in pH from 4 pH onwards and reach the plateau at 8 pH. The Hg (II) removal was more than 99% at an intial concentration of 50 mg L^{-1}. Idris et al. 2011, prepared Silica sorbents, based on mesoporous crystalline material, functionalized using mercaptopropyl or diethylenetriamine to extract mercury (II) ions from water. It a maximum adsorption capacity of 1245 mol/g. Oubagaranadin et al. 2007, used Fuller's earth as an adsorbent to remove mercury from aqueous solutions. The monolayer adsorption capacity was 1.145 mg/g of fuller's earth. Viraraghavan and

Kapoor 1994, we studied the potential of bentonite for adsorbing mercury from wastewater, having a adsorption capacity was in the range of 0.01 to 0.04 mg.g^{-1} of bentonite.

Adsorbent	Pollutant name	Adsorption capacity	Range Hg Concentration	Removal efficiency (%)
Chlor-alkali industry wastewater using 2-mercaptobenzimideazole-clay	HgCl$_2$	23.3 mg L^{-1}	50 mg L$^-$	99
2-Mercaptothiazoline modified mesoporous silica	HgCl$_2$	13 mg L^{-1}	0.1 M	-
Novel organo-clay minerals	HgCl$_2$	46.6 mg L^{-1}	140 mg L$^-$	98
Mercapto functionalized-MCM-41.	HgCl$_2$	1.45 μmol g^{-1}	25 ug L^{-1}	97

Table. 1.6 Adsorption capacities of clay for different heavy metals. From Sharma et al. 2015

Natural oxide, are a class of minerals that consist of naturally occurring chemical compounds in which elements are combined with oxygen, a hydroxyl group, or both O and OH. A natural oxide may include as many as 40 cationic elements, most of which are lithophile, for example, Si, Ti, Nb, Ta, Mn, Al, Mg, Sn, and Zr; many natural oxides, however, are formed from chalcophile and siderophile elements. The removal of Pb^{+2} and Cd^{2+} from aqueous solutions using aluminium oxide and goethite, an iron oxide was explored (Babel S., et al. 2003). It was found that goethite exhibits a better adsorption capacity for both ions than alumunium oxide and that the uptake of Pb^{2+} is higher than that of Cd^{2+}. Furthermore, there are several studies, about the development of new types of activation of naturals oxides, improving its ion exchange power and to obtain a better yield for heavy metals removal.

Material	Cd^{2+}	Pb^{2+}	Cr^{2+}
Aluminium oxide	31	33	
Ferric oxide	72	230	

Table.1.7 Adsorption capacities (mg g^{-1}) of natural oxides for some metals Babel S., et al. 2003

1.5.2.5 Bioadsorbents.

Typical biosorbents can be derived from three sources as in the following: (1) non-living biomass such as bark, lignin, shrimp, krill, squid and crab shell, etc; (2) algal biomass; (3) microbial biomass, e.g. bacteria, fungi and yeast (Apiratikul and Pavasant, 2008). The agricultural by-products are also considered as bioadsorbentes.

The major advantages of bio-sorption are its high effectiveness in reducing the heavy metal ions and the use of inexpensive biosorbents. There are a large number of research studies on the metal biosorption using biomass: type bacteria, fungi and algae, shown Table 1.8.

Due to the complex nature of the cell wall of the microbial biomass, the mechanism of the biosorption process is not well understood. The process can take place via many mechanisms depending on the speciation of the metal ion, the source of biomass and its processing to biosorbent (Gupta, 2015).

Material (Biomass)	Cd^{2+}	Zn^{2+}	Ni^{2+}	Hg^{2+}	Pb^{2+}
[a]*Cystoseira baccata*				329	
[a]*Ulva onoi (NaOH pre-tratament*	90.7				
[b] *Tolypocladium sp.*				161.1	
[b] *Saccharomyces cerevisiae*	15.4				204
[b] *Baker's yeast (lab cultured)*	11.63				
[b] *Phomopsis sp. (lab cultured)*	29				
[c] *Thiobacillus ferrodoxins*		172.4			443.0
[c] *Bacillus thuringiensis*			45.9		
[d] Rice husk (acid treated)		19.38			108.0
[d] Rice husk (sulphuric acid treatment)				384.62	
[d] Walnut shell (ZnCl2 mod)				151.50	
[d] Wheat bran (chem mod)				70.00	
[d] Coconut chem mod coir pith (PGCP)				13.73	

Table. 1.8 Biosorption Capacities (mg g^{-1}) of Various Biomass for Removal of Toxic Metal Ions from Waste Water. [a]Algae, [b]Fungi, [c] Bacteria, [d] Agricultural by-products. (Gupta, 2015).

We can determine that there are various types of adsorbents that can be classified by their nature, mechanism of adsorption, composition and form of production. Many of them have a great performance in the reduction of diverse heavy metals in aqueous

solutions. Various researchers have developed different processes for potentiation the adsorption capacity, modifying the adsorbent's surface structure, through physical and chemical processes, combining mechanisms as: filtration, precipitation, coagulation, adsorption, flotation. They obtain a wide variety of materials for the treatment of contaminated water, such as membranes, filters, gel, active carbon, zeolites, clays and modified oxides.

A detailed study of the literature allows us to know, that low cost adsorbents have a large future in the treatment of polluted water. However, despite of all the advantages in the use of low cost adsorbents, a lot of these materials need additional process to improve its performance to achieve higher values of remotion. Therefore, the cost of production increases and it should be emphasized that many modified adsorbent materials, only have a high performance on a laboratory scale and cannot be used in the industry.

1.6   Remediation Technology for Groundwater Sources.

One of the most pervasive problems afflicting people throughout the world is inadequate access to clean water and sanitation. Problems with water are expected to grow worse in the coming decades, with water scarcity occurring globally, even in regions currently considered water-rich. Addressing these problems calls out for a tremendous amount of research to be conducted to identify robust new methods of purifying water at lower cost and with less energy, while at the same time minimizing the use of chemicals and impact on the environment. Before proceeding to detailed description of the possible technologies usable for remediation of contaminated sites, it is important to evaluate certain aspects of the site in order to identify the most efficient technique for cleaning; these include:

• Properties of the pollutants present on areas of interest, its chemical and physical characteristics, concentrations, its spatial distribution on the study area;

• Properties of polluted matrices, paying particular attention to the size of the medium, its hydraulic properties, moisture and pH;

• Characteristics of the site, its intended use, extension of the area of interest, contaminated volumes;

Once described, as comprehensively as possible, the polluted site, we can proceed in search of a better remediation technique.

The design of a remediation process begins with the selection of the technologies available in the market that can be applied to the contaminated site. In fact there is no applicable technique for all cases of contamination in general, because each technique has its properties, characteristics and special limitations.

In the case of contamination of aquifers there are several technologies for in situ remediation some traditional and other more innovative, which are applicable according to the type of pollutant and goals of treatment. Among the main technologies available for usage are:

- Aeration:
    1. Air sparging;
    2. Air Stripping.

- Containment:
    1. Perimeter Barriers;
    2. Permeable Reactive Barriers.

- Extraction:
    3. Pump & Treat;
    4. Dual-phase extraction;
    5. Method electrokinetic.

- Chemical Oxidation:
    6. Fenton
    7. Ozone
    8. Potassium permanganate and sodium;

- Flushing;

- Fracturing;

- Bioremediation (biological treatment):
    9. Intrinsic (natural attenuation);
    10. Induced (biosparging).

Amongst these techniques the method of containment with the application of reactive barriers is one of the techniques that has produced a great interest for the groundwater remediations during the last years. Since, it can be used in the design of different types

of adsorbents, among which are the adsorbent materials of low cost. Therefore, their application to eliminate different types of pollutants is very broad, for example type of radioactive pollutants as the Uranium (Simon F.-G,. et al. 2002.), organic components and heavy metals.

1.6.1   Containment.

Containment is a method of groundwater remediation in which the movement of contaminated groundwater is retarded; the contained groundwater system can be defined as being either active or passive, in the case of perimeter barriers the flow is stopped. While in the case of permeable reactive barriers the flow does not stop, but the aquifer flux lines are forced to pass through a reactive barrier, where the abatement of contaminants occurs.

1.6.1.1 Perimeter Barriers.

The Perimeter barriers are impermeable barriers that are intended to isolate the contaminant source in situ, in order to prevent the spread within the aquifer. They are used to contain the contaminated groundwater, deflecting the areas of drinking water pumping or to isolate part of aquifer, in order to effectively manage the water.
These can be made with plastic diaphragms (cement-bentonite), composite diaphragms with tarpaulins, concrete diaphragms and cell diaphragms.
In cases where the waterproof substrate on which rests the aquifer is too deep it may be convenient to add to the perimeter barriers a bottom barrier. Attention must be paid to the fact that specific types of contaminants can degrade the barrier components in the long-term term and reduce its performance.

1.6.1.2 Permeable Reactive Barriers (PRB).

Permeable Reactive Barriers (PRB) are an emerging alternative to pump-and-treat systems for treating groundwater contamination. PRB technology is a novel groundwater remediation method, which enables physical, chemical or biological in situ treatment of contaminated groundwater by means of reactive materials. The most commonly used processes/reactions are: redox reactions, precipitation, adsorption, ion

exchange and biodegradation. Environmental Protection Agency (EPA) defines PRB as an installation of reactive material in the subsurface to intercept a plume of contaminated groundwater, which must move through it as flows, typically under its natural gradient. Thereby, creating a passive treatment system and as the contaminant moves through reactive materials, reactions occurs transforming it to be less harmful (nontoxic) or immobile species.

The reactive materials are placed in underground trenches downstream of the contamination plume. By doing so, the contaminants are treated without soil excavation or water pumping (Smyth et al., 1997). Generally, this cost-effective clean-up technology impairs the environment much less than other methods.

The main advantages of using a permeable reactive barrier include the following:

- Passive operation

- Relatively low costs of operation and monitoring

- Most PRB designs do not include aboveground structures

Nevertheless, the use of permeable reactive barrier may have the following limitations:

- Barrier system may not be a stand-alone technology.

- Remediation time frame may require a long treatment period, depending on the size of the contaminated area.

- Disposal issues could develop in the PRB treatment media after the contaminants are concentrated within the barrier system. This is most important in PRB systems that retain the contaminants (e.g., metals and radionuclides), as opposed to PRB systems, which degrade the contaminants as they flow through the system (e.g., hydrocarbons and chlorinated organics).

- Biofouling and mineral precipitation may limit the permeability of the wall system if not managed properly.

1.6.1.3 PRB Operating modes.

Among the aspects to be considered within the design of a PRB, is the selection of the reactive material, which is the key in order for it to function correctly. The material must be compatible with the surface environmental, that does not produce adverse reactions or byproducts with the compounds of contaminant plume. (EPA, 1998). The material used should not alter or limit the natural groundwater flow, thereby the size of the material is important. Since if it possess a reduced permeability, it could block the

barrier, wherefore, it is advisable to be unimodal with respect to grain size, its availability, moreover its manipulation must be considered and mainly, this material must persist over long periods of time, ie, it should not be readily soluble or depleted in reactivity. Therefore, a correct physical and chemical characterization of the reagent medium, through laboratory such as test batch, columns studies are very important.

Treatable Contaminants and design of PRB.

The following list shows the most common components, which have been successfully treated, with different reactive materials.

Groups	Pollutans
Organic compounds	
Methane	Tetrachlomethane, trichloromethane, dichloromethane.
Ethanes	Hexachloroethane, 1.1.1-trichloroehtane.
Ethenes	Tetrachloroethene, trichloroethene, cis-dichloroethene
Propanes	1,2,3-Trichloropropane, 1-2-dichloropropane.
Aromatics	Benzene, Toluene, ethylbenzene
Others	Hexachlorobutadiene, 1,2-dibromoethane, Freon 113
Inorganic compounds	
Trace metals/heavy metals	Cr, Ni,Pb, U, Fe, Mn, Se, Cu, Co, Cd, Zn
Anion contaminants	Sulphate, nitrate, phosphate, arsenic

Table. 1.9 Some of the common contaminants in groundwater for remediation from Thiruvenkatachari, 2008.

The interaction processes involved in the removal of pollutants are mainly:

- Reductive degradation of organic pollutants.

- Oxidative degradation of organic pollutants.

- Retardation and biodegradation of organic pollutants.

- Sorption of organic or inorganic pollutants.

- Reduction and/or precipitation of heavy metal compounds.

In accordance with operational principles, we can identify different categories of permeable reactive barriers, such as:

1. Absorbent barriers: The most representative of absorbent materials, usable for such barriers, is activated carbon, which is particularly effective for non-organic compounds. Polar contaminants, such as metals, however, are usually treated on the basis of adsorption systems with electrostatic attraction or the formation of surface complexes. Special attention is paid to the natural zeolites, for the characteristic wide cavity structure and the high exchange capacity. Zeolites are improved through chemical modifications to enable their use also with non-polar compounds. The success of the absorbent material in PRB is mainly due to the advantage of not releasing any chemical in the water table, but its main limitation is the lack of specificity.

2. Chemical barriers: they are based on transformations of the pollutants into less harmful compounds. The transformation within the reactive barrier is commonly a redox reaction in which the contaminant is reduced or oxidized. The reactive medium may provide electrons for reduction as in the case of a metal iron barrier. To ensure the completion of the decontamination reactions, it is necessary to increase the thickness of the barrier (ensuring a residence time of up to 4-5 days), however having higher costs. Among the metal construction of the barriers include iron, tin and zinc. Fe potent reducing agent, has aroused more attention especially among researcheres by the opportunity to study the removal of   organochlorines and heavy metals such as chromium and uranium VI.

3. Biological barriers: Biological technologies are particularly attractive since the destruction of pollutants takes place naturally without leaving potentially toxic compounds in groundwater. The "bioremediation", as widely seen in the previous paragraphs, is based essentially on the support of nutrients / energy for the microorganisms already present in the site to be decontaminated, capable of carrying out degradation of contaminants. It consists of the administration of adequate times and concentrations of nutrients (nitrogen and phosphorus-containing compounds and oxygen) or chemicals that release oxygen.

1.6.1.4 Permeable Reactive Barrier Design.

The reaction time and the groundwater velocity are used to determine the size of PRB needed to achieve the desired treatment level. Two basic configurations are currently being used for full-scale field application, continuous PRBs or "funnel-and-gate" designs. EPA(1998).

1.   Continuous PRB Trenched System.

In the configuration of continuous permeable wall, the contamination plume is intercepted entirely by the reactant material (Fig. 1.10). In order to prevent the diversion of the flux lines around the barrier the permeability, thereof must be greater than or equal to that of the aquifer. Generally must be guaranteed double permeability at least for the protection from possible problems caused by the precipitation of elements on the surface of the barrier.
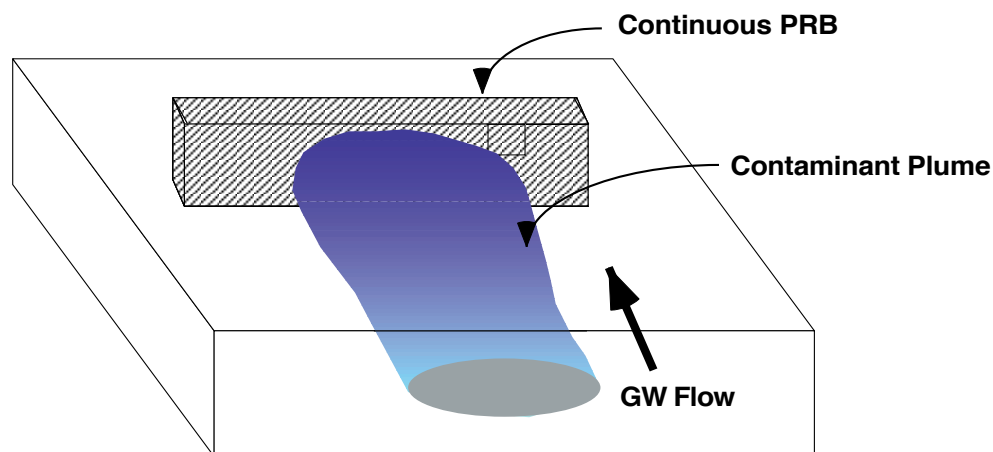
Figure. 1.10 Trenched System continuous Permeable Reactive Barrier. From EPA, 1998.

The continuous trench exploits the natural movement of contaminated water through the reactive medium and, therefore, must be located below the groundwater level. This type of installation can cause problems in the trench stability due to the intrusion of water or the collapse of the trench during the excavation phase. Therefore, it is necessary to carry out accurate geological analysis, hydrogeological and geotechnical, before applying excavation techniques.

2.   Funnels and Gate

In a funnel-and-gate configuration, low permeability funnels direct ground water toward permeable treatment zones or gates. The funnel typically consists of sheet pilings, slurry walls, or some other material and is preferably keyed into an impermeable layer (clay, bedrock) to prevent contaminant underflow. This funnel is emplaced to encompass and direct the flow of contaminated water to a gate or gates containing a permeable zone of granular Fe (0) or other reactive material. (EPA, 1998)
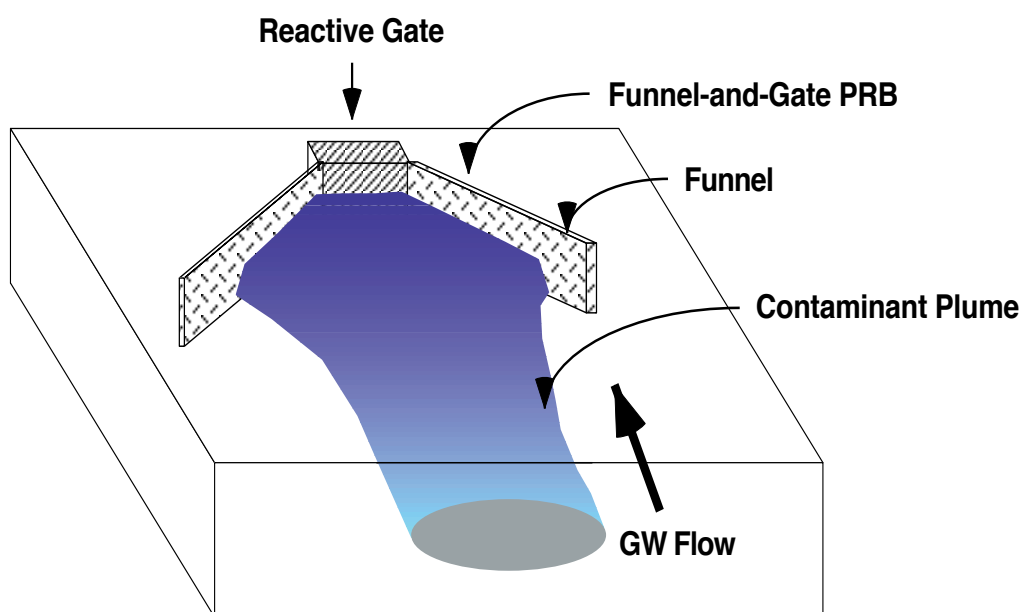
Figure.1.11 Funnels and Gate System Permeable Reactive Barrier. From EPA, 1998.

The funnel and gate system is more economical than the continuous trench system, since it uses a smaller quantity of material and minimize the volume of soil removed for the realization of the trench. In fact the system is more voluminous but requires a minor amount of reactive material. Furthermore, there it is easily maintained since the reactive medium is located in a limited area by the gate and is not distributed as in the case of the continuous trench system.

Usually, the conventional PRB installation techniques require some degree of excavation, which limits the PRB to fairly shallow depths of 20 meters. (R.D. Vidic, 2001.)

3.   GeoSiphon

GeoSiphon is an innovative configuration patented by the Westinghouse Savannah River Company (Fig.1.12) in which the flow of water passes through the reactive material and is induced by a siphon system, which connects the same material with a point in the lower hydraulic load (discharge point). The difference in load is accentuated, making a large diameter well, connected to a siphon (GeoSiphon) or to an open channel (Geoflow).
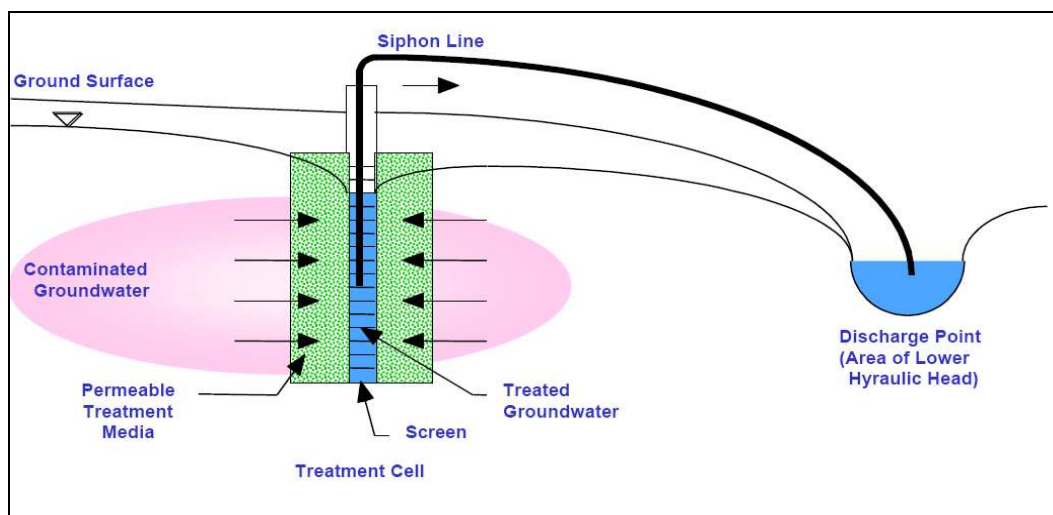
Figure 1.12 Configuration GeoSiphon from (Di Molfetta et al., 2005.)

The first application was in July 1997 at TNX Savannah River Site, for the treatment of an aquifer contaminated with chlorinated solvents.

1.6.2   Specifications of Reagent Materials.

The essential feature for the construction of a permeable reactive barrier is the choice of the most suitable reactive material for the present contaminant. The choice of material must be carried out taking into account the following parameters:

- Reactivity of the material with respect to contaminants: it is preferable to use a reagent medium with high removal rate, which generally increases with the increase of the specific surface area of the material and that allows to minimize the residence time in the treatment zone.

- Stability of the reagent: refers to the timing during which the material maintains the characteristics of reactivity.

- Hydraulic conductivity: the materials must be characterized to obtain a permeability greater than the aquifer, to ensure that the contact time is adequate to react with the contaminants present, moreover permeability must also remain constant over time.

- Environmental compatibility: The material must not give rise to secondary contamination (of side effects) or produce harmful waste. The material, therefore must not contain toxic materials neither generate highly toxic by-products, during the process of degradation of the contaminants.

- Availability and cost effective

There are various types of reactive means, of which some are currently employed and others are still the subject of study in laboratory scale. In fact, since the contaminants present in the aquifers in the world is increasing, researchers conduct constant experiments to find the most effective materials and of low cost. The materials tested to date are:

- Zero Valent iron (ZVI), is the most commonly used reactive barrier material it has a high reactivity with organic and inorganic contaminants, and able to be used in different states: as a pile powder/granular, filing, colloidal, nano sized. It is used for treatment of the organic compounds (Methanes, Ethanes, Ethenes, Propanes, Aromatics), Inorganic compounds (Cr, Ni, Pb, U, Fe, Mn, Se, Cu, Co, Cd, Zn), Anions contaminants (Sulphate Nitrate Phosphate Arsenic) (EPA 1998). Lifetime of the material could be reduced due to the formation of surface coating and due to geological condition of the site. Furthermore, Zero valent iron, is not effective on mercury ions, hence cannot be used for the treatment of contaminated groundwater of mercury.

- Activated carbon. (AC), has vast data on ex situ water and wastewater treatment, however has very limited data on in situ treatment under field conditions. (Thiruvenkatachari et al. 2008)

- Lime (calcium carbonate or hydroxide). Effective in neutralization; reducing the solubility of certain metals or conditioning hydrochemical system to assist with other treatment processes, e.g. bioremediation. Its disadvantages are slow reaction time, loss in efficiency of the system because of coating of the limestone particles with iron precipitates. Limestone treatment is generally not effective for acidities exceeding 50 mg L^{-1}. Voluminous sludge is produced with hydrated lime (calcium hydroxide).

- Zeolites is the second most used material for the design of PRB, due to its high reactivity is used for the removal of heavy metals such as Cu, Co, Zn, Mn, (Erdem et al 2004) As (V), Fe, also for the denitrification of water (Margeta et al, 2013) (Vignola et al 2011), The main disadvantage is that zeolite used in a PRB and has a finite sorption capacity. Regeneration is possible, but would be a complicated process in situ. (Van Nooten et al. 2010).

- Microbial bioremediation. Less expensive and easy to install, natural processes to treat contaminants, capability to degrade organic contaminants into relatively less toxic end products. Reduces risk of human exposure to contaminated media, remediation is not restricted to the treatment zone alone. Works well for dissolved contaminants and contamination adsorbed onto higher permeability sediments (sands and gravels). Disadvantages A perceived lack of knowledge about biodegradation mechanism. (Thiruvenkatachari et al 2008).

In order to be able to offer environmental remediation alternatives to the various ecological problems mentioned above, such as mercury contamination, researchers are making considerable efforts to develop cost-effective adsorbents for Hg removal from groundwater. Murthy et al. 2013, used ß - zeolite, zeolite Y, and mordernite for assesment their adsorption capacity of Hg (II) through batch test. Huttenloch et al, 2003, suggests the used of Copper shavings for removal of Hg(II) from aqueous solutions by amalgamation process, the kinetic sorption experiments showed that 96-98% of Hg (II) was removed within 2 hours.

Nevertheless with the data presented above, we have shown that there are several adsorbents for the removal of Hg in aqueous solutions, that have important values of adsorption capacity, but their application in PRB is complicated, due to the structure and properties of the adsorbent As for example, the AC has a low permeability, which would cause the blocking of the water system flow, or the contact times are very high to reach its maximum adsorption or the pH and temperature conditions of the water changes its performance.   Also its cost of production is high.

Due to the problems mentioned previously, research interest into the production of alternative adsorbents has intensified in recent years. Thus, the most promising path in this race against time seems to be the one using alternative eco-friendly materials, which is able to absorb and separate heavy metals from water. Among these lignocellulosic materials have physical characteristics, such as flexibility, strength,

permeability and are readily available. Spanish broom, a lignocellulosic material with a high diffusion in many areas of the world, is presented in this study as alternative adsorbent. Thanks to functional groups, such as the hydroxyl, aliphatic carboxylic, aromatic carboxylic and phenolic ones that are present in its composition, this material is able to remove Hg from water by absorption (Lv, 2012).

1.7   Spanish broom (*Spartium junceum L.*)

The common broom, also called fragrant broom or Spanish broom (*Spartium junceum*) is a plant that was known even to the ancient Romans. In the past, the Greeks, the Romans and the Carthagians used it as raw material for the manufacture of ropes, nets, bags, and sails. They also used it for covering roofs and even as clothing.

Spanish Broom is a shrub-like plant from the family of legumes (Fig.1.13). It is the only species in the genus Spartium (Table 1.10). It is a native species of the Mediterranean area, which starts from South Europe to North Africa up to the Middle East zones, also reaching some areas of the central and South America. It grows in sunny areas up to an altitude of 1200 m asl,

Figure 1.13 Spanish broom (Spartium junceum L)

characterized by arid and sandy soils. It is a shrubby (from 0.5 to 3.00 m high) and perennial plant with long stems. The stems are green and cylindrically shaped, compressible but tensile resistant, straight and highly branched. The sporadic foliage is almost absent, while the bright yellow flowers are often located in the terminal part of the branches. Historically the Spanish broom was a highly exploited plant and even nowadays it is used for several purposes: traditionally used in the ornamental trade, for yellow dye extraction, cellulose fibers production (Gabriele et al., 2010), reforestation of degraded areas, consolidation of high slope terrains, extraction of essences from flowers for perfumes creation and extraction of fibers for fabrics production or building materials reinforcement. (Chidichimo et al., 2015).

Table. 1.10. Spartium junceum L. Classification

Kingdom	Plantae
Class	Magnoliolipsida
Subclass	Rosidae
Order	Fabales
Family	Fabaceae
Genus	Spartium L
Species	Spartium junceum L.

1.7.1   Distribution of Spanish Broom.

Due to the great migration, this plant managed to expand to other continents such as: Oceania, Asia and even America. In the American continent the Spanish broom is expanded throughout the region due to its physical characteristics and its great power of invasión. This plant managed to adapt in regularly arid areas, changing the natural environment of the site, sometimes displacing native plants of the area. Therefore, some countries such as the United States have considered controlling and even eradicating the growth of this plant to protect the native plants in the area. In figure 1.14 it is possible to observe the distribution of the Spanish broom, worldwide, due to its great presence in the world. This plant is presented as an easily available material.
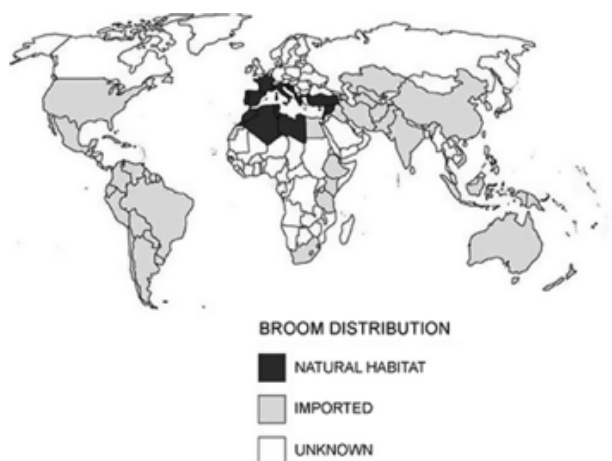
Figure. 1.14 Spanish broom distribution on the earth. From. Lia, 2014

1.7.2   Chemical composition of the Spanish broom.

The elementary fibers in Spanish Broom are bound together by lignin. It shows a thick secondary cell wall indicating high cellulose content. Previous studies have determined the chemical composition of the Spanish broom: (Gabriele, 2010):

Material	Cellulose (%)	Lignin (%)	Pentosans (%)	Pectins (%)	Ash (%)
Spanish broom.	44.5 ±0.2	18.5 ±0.3	16.3 ±0.1	13.3 ±0.1	4.0 ±0.2

Table 1.11. Composition on the Spanish broom (raw material). (Gabriele, 2010)

The composition of the plant is characteristic of materials of lignocellulosic, this composition allows it to have better mechanical properties than flax, and is more elastic and stronger than flax fibers. Moreover, the diameter of the Spanish Broom fiber ultimately ranges from 5 µm to 10 µm, and the diameter of the whole bundle is about 50 µm. (Katović, D., et al 2011.)

As shown in the literature previously regarding the low cost adsorbent materials the process of heavy metals removal from water is directly related whith carboxyl and hydroxyl functional groups, that through chemical and physical adsorption processes, achieved to adsorb the metal ions. Compounds such as lignin, cellulose, hemicellulose have this functional groups on their structure. Considering that Spanish broom is lignocellulosic material may be used as an alternative adsorbent material.

Therefore it is necessary to know more deeply the characteristics of the components present in this material.

1.7.2.1 Lignocellulose

The lignocellulose is an abundant polymer in nature, it covers 50% of the world's biomass.

From a biochemical point of view the lignocellulose is formed by three main components:

• Cellulose (about 40-60% of the dry weight)

• The hemicellulose (about 20-40% of the dry weight)

• The lignin (about 10-25% of the dry weight)
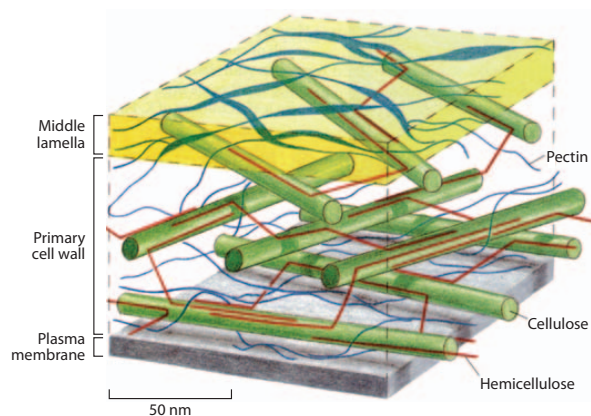
Figure. 1.15 Simplified model of the primary cell wall. From (McCann and Roberts, 1991)

To a lesser extent are present polymers such as starch and pectic substances. The lignocellulose represent 65-70% of the dry weight of the plant. The monomer units of the lignocellulose are represented by simple sugars such as D-glucose, D-mannose, D-galactose, D-xylose, L-arabinose, D-glucuronic acid and to a lesser extent from L-rhamnose and D-fucose. These polymers are rich in hydroxyl groups, which are responsible for moisture absorption in the formation of hydrogen bonds.

1.7.2.2 Cellulose.

It is a linear polymer of high molecular weight. It is found in nature almost exclusively in the membrane (which gives hardness and rigidity to the cell wall) of plant cells, it is also produced by some animals (eg. tunicates) and a few bacteria. Cellulose is a linear homopolymer composed of D-glucopyranose units linked by β-1,4-glycosidic bonds. It mainly contains carbon (44.44 %), hydrogen (6.17 %), and oxygen (49.39 %). The chemical formula of cellulose is $(C_6H_{10}O_5)_n$; n, called the degree of polymerization (DP), represents the number of glucose groups, ranging from hundreds to thousands or even tens of thousands. In the twentieth century, it was proved that cellulose consists of pure dehydrated repeating units of D-glucoses (as shown in Fig. 1.16), and the repeating unit of the cellulose is called cellobiose. (Chen, H., 2014)
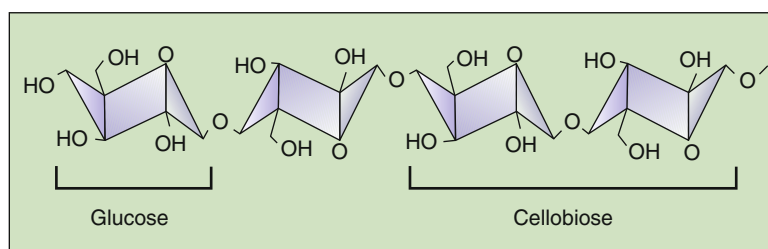
Figure 1.16 Structure of cellulose

1.7.2.2.1 Chemical Properties of Cellulose

Every glucosyl ring of cellulose has three active hydroxyls: one primary hydroxyl group and two secondary hydroxyl groups. Thus, cellulose may have a series of chemical reactions related to hydroxyl. However, these hydroxyl groups also can form hydrogen bonds between molecules, which have a profound influence on the morphology and reactivity of cellulose chains, especially the intermolecular hydrogen bond formed by oxhydryl at C3 and oxygen at an adjacent molecule ring. These hydrogen bonds not only can enforce the linear integrity and rigidity of the cellulose molecule but can also make molecule chains range closely to form a highly ordered crystalline region (Gao J, Tang LG. 1996).

The accessibility of cellulose refers to the difficulty reagents have in arriving at the cellulose hydroxyl. In heterogeneous reactions, the accessibility is mainly affected by the ratio of the cellulose crystalline regions to the amorphous regions. The reactivity of cellulose is the reactive capability of the primary hydroxyl and the secondary hydroxyl at the cellulose ring. Generally, because of the smallest steric hindrance, the reactivity of the primary hydroxyl groups is higher than for the secondary hydroxyl groups, so the reactivity of hydroxyl at C6 with a bulky substituting group is higher. For example, esterification of toluenesulfonyl chloride chiefly occurs in the primary hydroxyl. The reversible reaction occurs mainly in the hydroxyl group at C6, and an irreversible reaction always occurs in the hydroxyl group at C2. Thus, for the esterification of the cellulose, the reactivity of the hydroxyl group at C6 is the highest, but for the etherification, C2 is the highest.

1.7.2.2.2 Physical Properties of Cellulose

Free hydroxyls of cellulose have a strong attraction to many solvents and solutions, but adsorbed water only exists in the amorphous region, not the crystalline region. In the moisture sorption process, the hydrogen bonds of the amorphous region in the dry cellulose constantly could be broken; the hydrogen bonds in the cellulose molecules are replaced by the hydrogen bonds between cellulose molecules and water molecules, even forming new hydrogen bonds, and some hydrogen bonds in cellulose molecules remain. In the desorption process, due to the obstruction from inside, hydrogen bonds between cellulose molecules and water molecules cannot be broken completely and reversibly, resulting in hysteresis. Some water, which is absorbed by cellulose enters into the amorphous region of cellulose and forms the water bound by hydrogen bonds, called bound water. Molecules of bound water attracted by hydroxyl of cellulose are arranged in a certain direction and have a high density, making swelling the cellulose and generating a heat effect. When the celluloses absorb water and reaches the fiber saturation point, water molecules continue to enter into the cell lumina and pores of cellulose to form a main layer adsorbed water or capillary water, which is called free water. No heat effect and swell ability of cellulose exist when absorbing free water (Zhan H.Y. 2005).

1.7.2.3 Lignin

Lignin is one of the most abundant organic polymers in plants, just behind cellulose. It is the exclusive chemical composition of gymnosperm and angiosperm. The content of lignin in wood and Gramineae is 20–40% and 15–20 %, respectively. Lignin is the name of a group of substances; their inhomogeneity is manifested in different species of plants, length of growing season, and different parts of the plants. Even in the different morphologies of cells of the same xylem or different cell wall layers, the structures of lignin are not the same (Jiang TD. Lignin. Beijing: Chemical Industry Press; 2001).
Lignin is composed of complicated phenylpropane units nonlinearly and randomly linked; three main monomers are coumaryl alcohol, coniferyl alcohol, and sinapyl alcohol. Because of the different monomers, lignin can be divided into three types: p-phenyl monomer (H type) derived from coumaryl alcohol, guaiacyl monomer (G type) derived from coniferyl alcohol, and syringyl monomer (S type) derived from sinapyl alcohol (Wei Jh., and Song Yr., 2001)

62

This kind of structural model only describes a hypothetical structure inferred from the average results. Further, different plant sources, or even lignin isolated from the same plant but in different ways, would have different categories of linkages and composition of functional groups, resulting in the complicated lignin structure.

The figure (1.17) follows shows a structural theoretical composition of lignin.
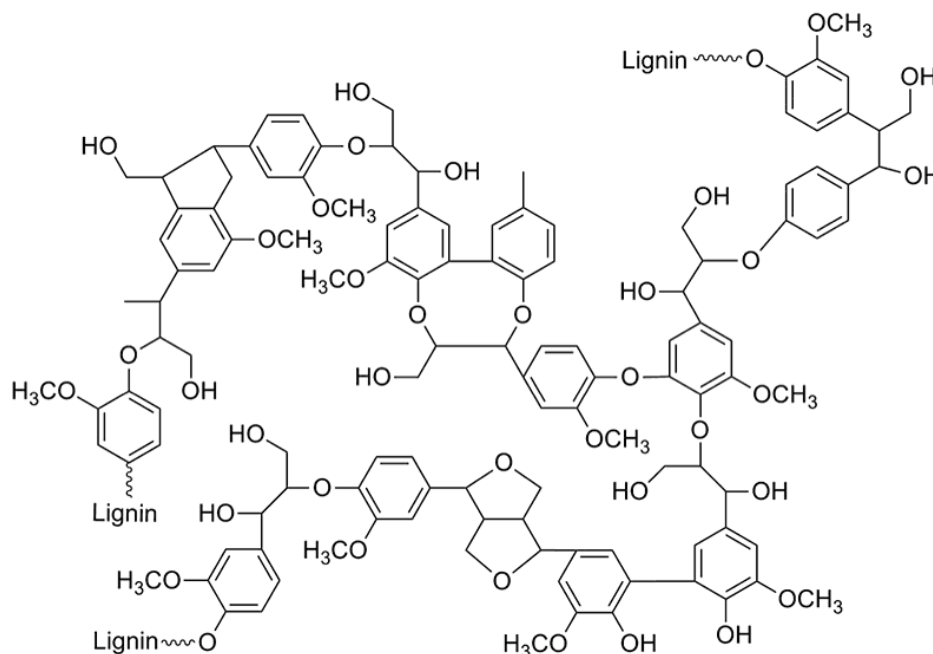
Figure 1.17 Structure Lignin from. (Vanholme et al., 2010)

The distribution of lignin, according to early studies have indicated that the lignin concentration in the complex middle lamella (CML) layer is above 50 % (mass ratio), while it is about 20 % in the second wall (S layer). However, because the volume of the S layer is far greater than the volume of the middle lamella layer, most of lignin still presents in the second wall. The lignin concentration of the cell corner of the middle lamella layer is generally higher than that of the CML layer, even more than 70 % (Lv WJ, et al. 2010.)

1.7.2.3.1 Chemical Properties of Lignin

The chemical properties of lignin include halogenation, nitration and oxidation reactions on the phenyl ring; reactions on the benzyl alcohol, the aryl ether bond, and an alkyl ether bond in the side chain; lignin-modified chromogenic reaction; and so on. The chemical reactions of the lignin structural unit are divided into two major categories: nucleophilic reactions and electrophilic reactions.

1. Chemical reactions of lignin structural unit on the side chain.

Reactions on the lignin side chains are associated with pulping and lignin modification; the reaction is a nucleophilic reaction. The following reagents can conduct nucleophilic reactions with lignin:

a) In alkaline medium, the effect of HO-, HS-, and S2-nucleophilic reagents leads to the cleavage of the main ether bond (e.g., alpha-aryl ether bond, a phenol-type alpha- alkoxy ether bond, and phenol-type alpha-aryl ether bond) and fragmentation and partial dissolution of macromolecule lignin. In alkaline medium, the phenol-type structural unit is separated into phenolate anions, and an oxygen atom that affects the benzene ring by induction and a conjugative effect, which activates their ortho- and para- positions and thereby affects the stability of the CO bond and breaks the alpha-aryl ether bond, then generating a methylene quinone intermediate and resulting in the aromatization of methylene quinone to generate a 1,2-diphenylethene structure.

b) In neutral medium, reaction with nucleophile HSO3 or SO32- leads to the breaking of the ether bond and brings SO32- groups in the degradation of lignin fragments.

c) Acidic media mainly relate to the lignin fragmentation reaction of the acidic sulfite pulping process. SO2 aqueous solution is taken as an affinity reagent, leading to the breakage of phenol-type and nonphenolic-aryl ether bonds, sulfonation of carbon, and increased lignin hydrophilicity. Phenol-type and nonphenolic alpha-alkoxy ether bonds may also have a similar reaction. In addition, C1, C5, and C6 on the high electron density centers of the aromatic ring could also have a condensation reaction with methylene quinone intermediates (Tao Yz, 2003.)

2. Chemical reaction of the aromatic ring in the lignin structure.

Chemical reactions of the aromatic ring in the structural unit of lignin are closely related to the lignin-bleaching process and its modification and have been divided into electrophilic and nucleophilic reactions.

a) Electrophilic substitution reaction: This mainly refers to substitution and oxidation reactions. Electrophilic reagents include chlorine, chlorine dioxide, oxygen molecule, ozone, nitro cation, nitroso cation, and so on. The electrophilic reagent replacement breaks the side chains of lignin and leads to the oxidative cleavage of ß-aryl ether linkages. The aliphatic side chain is oxidized into a carboxylic acid, and the aromatic ring is oxidized into the compound of the o-quinone structure, which will finally be oxidized into dicarboxylic acid derivatives.

b) Nucleophilic reaction: Nucleophilic reagents can react with the aromatic ring of lignin include hydroxide ions, hypochlorite ions and hydrogen peroxide ions. These nucleophilic reagents can react with the chromophoric groups in the degraded lignin fragments, breaking the chromophoric structure to some extent. (Gao J, 1996.)

Chapter 2

2 METHODOLOGIES FOR THE DETERMINATION OF THE PHYSICAL AND CHEMICAL PROPERTIES OF THE ADSORBENT MATERIAL. IN STATIC AND DYNAMIC SYSTEMS.

2.1 Adsorption Experiments.

The adsorption capabilities and chemicals characterization were studied by performing batch tests. The batch method was used for the study of the profiles concentration in a closed reactor and continuous agitation. Generally, these tests are used to test a new material and to determine the kinetics of degradation. The tests in the batch have some advantages such as speed, simplicity and economy of construction. One of the disadvantages is the alteration of the mechanism of transport of the feather pollutant as the reaction takes place in a closed reactor. Also the relationship between material and

reagent solution are generally lower than those achieved with tests in column or in field applications.

The batch tests consist in the interaction of the reactive material (adsorbent) with the contaminant (adsorbate) in an aqueous phase, in constant agitation and with temperature control. To analyze the results, the adsorption capacity, i.e., the amount of adsorbed mercury per unit mass of adsorbent (qt) was determined:

$$q_t = \frac{(C_0 - C_t)V}{W}$$
$$2.1$$

where C_0 and C_t are the initial and mercury ion concentrations (mg L^{-1}) at time t, respectively, V is the volume of the solution (L) and W is the adsorbent mass (g). When the adsorption equilibrium condition holds, $C_t = C_e$ and $q_t = q_e$ where, C_e is the equilibrium concentration and q_e is the equilibrium adsorption capacity.

The Hg(II) removal efficiency (RE%), defined by the equation 2.2, was also used to assess the adsorption performances of the fiber.

$$RE\% = \frac{C_0 - C_e}{C_0} \ x \ 100$$
$$2.2$$

2.2 Adsorptions Kinetics.

Adsorption kinetics depends on the adsorbate-adsorbent interaction and system condition and has been investigated for their suitability for application in water pollution control. Two vital evaluation elements for an adsorption process operation unit are the mechanism and the reaction rate. Predicting the rate at which adsorption takes place for a given system is probably the most important factor in adsorption system design, with adsorbate residence time and the reactor dimensions controlled by the system's kinetics. (Ho, 2006.)

Various adsorption processes for pollutants have been studied in an attempt to find a suitable explanation for the mechanisms and kinetics for sorting out environment solutions. In order to investigate the mechanisms of adsorption, various kinetic models have been suggested.

2.2.1   Pseudo first-order Lagergren model.

Pseudo first-order kinetics equation has been most widely used for the adsorption of an adsorbate from an aqueous solution. Lagergren in 1898 described liquid–solid phase adsorption systems, which consisted of the adsorption of oxalic acid and malonic acid onto charcoal. Lagergren's first-order rate equation is the earliest known one describing the adsorption rate based on the adsorption capacity. (Ho, 2006.)

The pseudo first order kinetics (Lagergren, 1898), assumes that the rate of change of the adsorption capacity is proportional to the concentration of available active sites per unit mass of adsorbent material. This equation can be written as;

$$\frac{d_{qt}}{d_t} = K_1(q_e - q_t) \qquad\qquad 2.3$$

where K_1 (min^{-1}) is the rate constant for pseudo-first-order adsorption, q_e (mg g^{-1}) and q_t (mg g^{-1}) are the uptake amounts of Hg at equilibrium and at time t, respectively.

Eq. (2.3) was integrated with the boundary conditions of $t = 0$ to $t=t$ and $x=0$ to $x=x$ to yield;

$$ln\left(\frac{q_e}{q_e - q_t}\right) = K_1 \qquad\qquad 2.4$$

And

$$q_t = q_e(1 - e^{-K_1 t}) \qquad\qquad 2.5$$

Equation (2.5) may be rearranged to the linear form:

$$log\,(q_e - q_t) = log\,q_e - \frac{K_1}{2.303}\,t \qquad\qquad 2.6$$

The plot of log (q_e - q_t) versus t gives a linear relationship, from which K_1 and q_e can be determined from the slope and intercept of the plot, respectively.

This model has been widely applied by researchers for explaining the liquid–solid adsorption kinetics, (Agrawal et al., 2004, Altundogan, 2005, Vazquez et al., 2007, Wang et al., 2007, Zhang et al., 2003 and Zhang et al., 2005).

2.2.2 Pseudo second order model.

This model assumes that the rate of change of the concentration of occupied active sites per unit mass of the adsorbent material is proportional to the square of the concentration of free active sites per unit mass of sorbent (Ho and McKay, 1999; Kumar, 2006). In terms of adsorption capacity, the pseudo second order rate equation can be written as:

$$\frac{dq_t}{dt} = K_2(q_e - q_t)^2 \qquad 2.7$$

where, K_2 (g mg^{-1} h^{-1}) is the rate constant of the second-order adsorption process.

Separating Eq. (2.7), gives:

$$\frac{dq}{(q_e - q_t)^2} = K_2 dt \qquad 2.8$$

Let the term (q_e - q_t)= X in Eq. (2.8), then

$$q_e - q_t = X \qquad 2.9$$

$$-dq = dX \qquad 2.10$$

Based on Eqs. (2.8) and (2.9), the rate Eq. (10) can be simplified as

$$-\frac{dX}{X^2} = K_2 dt \qquad 2.11$$

Substituting the boundary conditions $q_t = 0$ at $t = 0$ and $q_t = q_t$ at $t = t$, the new boundary conditions for the Eq. (2.10) can be obtained as follows:

$$t = t, \qquad X = q_e \qquad \text{and} \qquad t = 0, \quad X = q_e - q_t$$

Integrating the Eq. (2.9) with respect to the new boundary conditions, Eq. (2.11) becomes

$$\frac{1}{q_e - q_t} = \frac{1}{q_e} + K_2 t \qquad\qquad 2.12$$

Eq. (2.12) can be further linearized to (Ho and Mckay, 1999)

$$\frac{t}{q_t} = \frac{1}{K_2 q_e^2} + \frac{1}{q_e} t \qquad\qquad 2.13$$

The value of q_e and the pseudo second-order rate constant, K_2, can be calculated from the slope and intercept of the straight line obtained from the plot of t/q_t versus t.

The pseudo second order model represents the experimental kinetic data well for the entire adsorption period for most of the systems. The excellent fit of experimental kinetic data for the entire adsorption period makes this model to be widely used by several researchers to represent various sorbate/sorbent systems, e.g. Ho and Mckay 1999, explained the sorption kinetics of divalent metal ions onto peat particles assuming chemisorption. Previously, a similar expression was reported by Blanachard et al. (1984) to explain the kinetics of Exchange reaction of divalent metallic ions onto NH^{4+} ions fixed zeolite particles.

2.2.3 Intraparticle Diffusion Model (IPD)

The intraparticle diffusion model (IPD) proposed by Weber and Morris in 1962 has been widely applied for the analysis of adsorption kinetics, the overall adsorption process may be controlled either by one or more steps, e.g. film or external diffusion, pore diffusion, surface diffusion and adsorption on the pore surface, or a combination of more than one step. One of the first steps is the external surface adsorption or instantaneous adsorption, which is mass transfer across the external boundary layer of liquid surrounding the outside of the particle, then follows of the gradual adsorption step where the adsorption at a site on the surface, (internal or external) and the energy will depend on the binding process (physical or chemical). This step is often assumed to be extremely rapid but depends on the variations of the system including solute concentration, temperature, and adsorbent particle size; and the third step is the final equilibrium step, where the solute moves slowly from larger pores to micropores causing a slow adsorption rate. (Wu et al 2009, Cheung, et al. 2007).

According to Weber and Morris (1963), if the rate-limiting step is intraparticle diffusion, a plot of solute sorbed against the square root of the contact time should yield a straight line passing through the origin (Poots et al., 1976). The initial rate of IPD is obtained by linearization of the curve $qt = \int t^{0.5}$, which is expressed as:

$$qt = K_P t^{0.5} + C \qquad\qquad 2.14$$

where k_p is the IPD rate constant (mg g^{-1} min$^{1/2}$) and C is a constant for any experiment (mg g^{-1}). According McKay et al., C is the interception of the effect of the boundary layer, that means that if the greater the interception, the effect that occurs in the boundary layer increases.

To determine the initial adsorption behavior, the following equations are deduced. First, Eq. (2.14) can be written as:

$$q_{ref} - q_t = k_p\left(t_{ref}^{0.5} - t^{0.5}\right) \qquad 2.15$$

Rearrangement of Eq (2.15) yields

$$\left(\frac{q_t}{q_{ref}}\right) = 1 - R_i \left[1 - \left(\frac{t}{t_{ref}}\right)^{0.5}\right] \qquad 2.16$$

where $R_i = \left(k_p t_{ref}^{0.5}/q_{ref}\right)$, which is defined as the initial adsorption factor of the IPD model

Based the Eqs (2.14) and (2.16), we can obtained R_i

$$R_i = \frac{q_{ref} - C}{q_{ref}} \qquad 2.17$$

where, q_{ref} is the adsorption capacity at the longest time and C can be related to the boundary layer thickness (Wu et al., 2009).

The values of Ri are shown in the table follow.

Table 2.1. Initial adsorption factor (R_i) and kinetic behavior based on IPD model.

R_i	Initial point of kinetic curve (C/q_{ref})	Initial adsorption behavior
$R_i = 1$	$C/q_{ref} = 0$	No initial adsorption
$1 > R_i > 0.9$	$0 < C/q_{ref} < 0.1$	Weakly initial adsorption
$0.9 > R_i > 0.5$	$0.1 < C/q_{ref} < 0.5$	Intermediately initial adsorption
$0.5 > R_i > 0.1$	$0.5 < C/q_{ref} < 0.9$	Strongly initial adsorption
$R_i < 0.1$	$C/q_{ref} > 0.9$	Approaching completely initial adsorption

We can observed that when $R_i=1$ there is no initial adsorption behavior in an adsorption system, however if $R_i = 0$, i.e. $C = q_{ref}$, the adsorption occurs right at the beginning of the process.

The IPD has been used by several researchers for explain the adsorption mechanism on various materials e.g. onto granular ferric hydroxide (GFH) for arsenic removal, (Badruzzaman et al., 2004), Mansonia wood sawdust by lead removal, (Ofamaja, 2010),

acid dye adsorption onto chitosan (Cheung et al., 2007) or on activated carbon (Choy, et al., 2001), etc.

2.3 Adsorption isotherms.

The retention (or release) of a liquid compound on a solid controls the mobility of many substances in the environment and has been quantified in terms of the ''sorption isotherm''. The adsorption isotherms describes the relation of activity or equilibrium, between any solute in solution and the adsorbent (reactive material), at certain physical and chemical conditions (Temperature, pH), which helps to understand the phenomena that govern mobility either in the transfer of substances from a mobile phase (liquid or gaseous) to a solid phase, through a curve describing the retention of a substance in a solid at various concentrations. Equilibrium isotherm equations are used to describe experimental sorption providing fundamental physicochemical data for evaluating the applicability of sorption processes as a unit operation. (Y. S. Ho et al. 2001)

For the different curves that are obtained from the plot q_e vs C_e, Giles et al. (1974) proposed a general modeling of sorption isotherms, in which particular cases are now used as the 4 main forms of isotherm commonly observed. Fig (2.1)
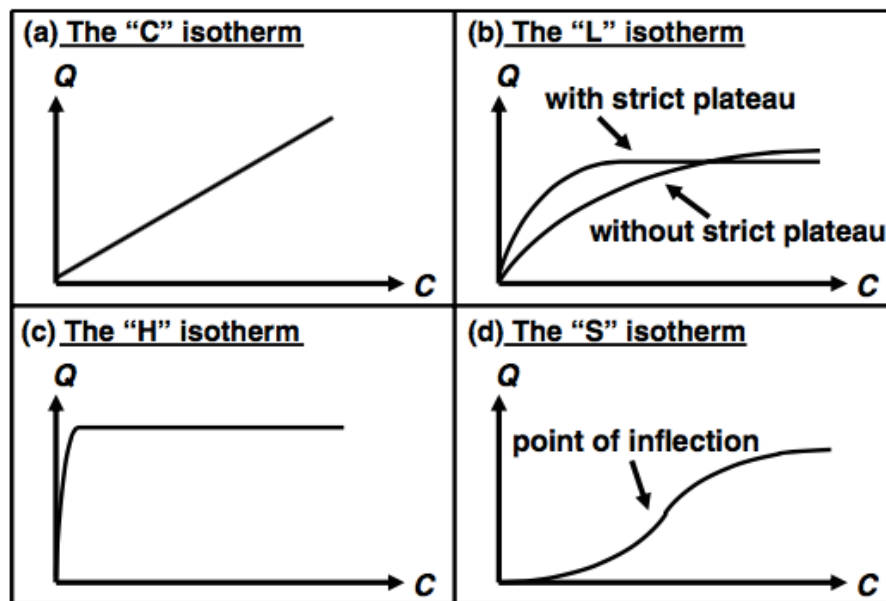
Figure. 2.1. Adsorption isotherms classified by Giles et al. (1960)

(i) The ''C'' isotherm; the curve is a line of zero-origin, It means that the ratio between the concentration of the compound remaining in solution and adsorbed on the solid is the same at any concentration. This ratio is usually named ''distribution coefficient'' or ''partition coefficient'': Kd or Kp (L Kg^{-1}). The ''C'' isotherm is often used as an easy-to-use approximation (for a narrow range of concentration or very low concentrations such as observed for trace pollutants) rather than an accurate description. But the simplicity of this isotherm must not justify its use without verification; otherwise it could lead to erroneous conclusions. For example, if the solid has a limited quantity of adsorption sites, the isotherm could be nonlinear because of a possible saturation plateau. (Limousin et al, 2007)

(ii) Isothermal L; the curve is typically concave with respect to the axis of concentrations (C), and shows a constant initial slope. The strong initial slope is due to the fact that at low concentrations the metal ions have a wide adsorption surface, therefore, it has a high affinity with the metal ions in solution. Nevertheless, as its concentration increases, the adsorption surface area decreases. This results in a decrease in sorption, which is shown by the concave curve section; it suggests a progressive saturation of the solid.

(iii) The ''H'' isotherm; It is a particular case of isothermal type L. This type of isotherm indicates a high affinity between solute and sorbent. The initial part of the curve describing this isotherm is completely vertical, due to that solute in the solution is completely adsorbed (Giles et al., 1960). However according to (Toth, 1995), from point of view thermodynamically this behavior makes no sense.

(iv) The ''S'' isotherm; When the curve has a sigmoid tendency, it indicates that there are at least two mechanisms of adsorption within the system, which is observable in the curve as a point of inflection. This phenomenon was observed in the adsorption of non-polar components (Karimi-Lotfabad et al., 1996), and surfactants (Smith et al., 1990).), and is known as "cooperative adsorption" (Hinz, 2001). In ionic metallic solutions the presence of ligands (ion or molecule "functional group" that binds to a central metal atom to form a coordination complex) within the sorbent-sorbate system form strong complexes with the metal ions that are not adsorbed. At the time when metal ions concentration exceeds the complexion capacity of the ligands, the sorption of the sorbent material increases and the isotherm assumes the characteristic form of S.

2.4   Modeling of the isotherms.

2.4.1   Freundlich isotherms.

In 1909, Freundlich gave an empirical expression representing the isothermal variation of adsorption of a quantity of gas adsorbed by unit mass of solid adsorbent with pressure. This equation is known as Freundlich adsorption isotherm, this model is probably the best known and most widely applied sorption isotherm. The Freundlich equation can be written as:

$$q_e = K_F C_e^{1/n} \qquad 2.18$$

where K_F is a constant indicative of the relative adsorption capacity of the adsorbent $(\text{mg}^{1-(1/n)} \text{ L}^{1/n} \text{ g}^{-1})$ and n is a constant indicative of the intensity of the adsorption, higher the 1/n value, more favorable is the adsorption.

This equation is easily linearizable Eq. (2.19)

$$log q_e = log K_F + \frac{1}{n} log C_e \qquad\qquad 2.19$$

Where the Freundlich constant can be calculated from the slope and intercept of the linear plot *Log q_e vs Log C_e* .

The Freundlich expression is an exponential equation and therefore, assumes that as the adsorbate concentration increases, the concentration of adsorbate on the adsorbent surface also increases. According to the Freundlich equation, the isotherm does not reach a plateau as C increases.

2.4.2   Langmuir isotherms.

The Langmuir isotherm is based on three assumptions:

1. Adsorption cannot proceed beyond monolayer coverage.
2. All sites are equivalent and the surface is uniform (i.e., the surface is perfectly flat on a microscopic scale).
3. The ability of a molecule to adsorbate a given site, independent of the

occupation of neighbouring sites (that is, there are no interactions between adsorbed molecules).

The dynamic equilibrium is:

$$S_v + A \rightleftharpoons SA \qquad (Equilibrium\ 1)$$

where S_v, is the vacant adsorption sites onto adsorbent (mol L^{-1}), A is the adsorbate in solution (mol L^{-1}), and SA is the adsorbate bound to adsorbent site (mol m^{-2}).

At equilibrium;

$$K_{ad} = \frac{[S.A]}{[S_v][A]} \qquad 2.20$$

Consider total number of sites, S_T, (assuming a monolayer coverage) to be fixed:

$$S_T = [S_v] + [S.A] \qquad 2.21$$

Combining the Eqs 2.20 and 2.21 yield:

$$S_T = \frac{[S.A]}{K_{ad}[A]} + [S.A] \qquad 2.22$$

Solving $[S.A]$ and using $C_e = [A]$ gives:

$$[S.A] = \frac{S_T}{1 + \dfrac{1}{K_{ad}.C_e}} = \frac{K_{ad}.C_e.S_T}{1 + K_{ad}.C_e} \qquad 2.23$$

Assuming: $\quad q_e = \dfrac{mg\ adsorbate}{g\ ads\ \square\square\square\square\square\square}$

$$q_e = [S.A].A_{ad}.MW_A \qquad 2.24$$

where A_{ad} = Surface area per g adsorbent (m^2 g^{-1}), and MW_A = Molecular weight of adsorbate (g mol^{-1})

Combining Eqs 2.23 and 2.24:

$$q_A = \frac{K_{ad}.C_e.S_T}{1 + K_{ad}.C_e}.A_{ad}.MW_A \qquad 2.25$$

assuming $q_m = S_T.\ A_{ad}.MW_A$ (mg g^{-1}), gives

$$q_e = \frac{q_m\ K_L\ C_e}{1 +\ K_L\ C_e} \qquad 2.26$$

It can be easily linearized by Eq 2.27;

$$\frac{C_e}{q_e} = \frac{C_e}{q_m} + \frac{1}{q_m b} \qquad 2.27$$

In the model, q_m (mg g-1) is the amount of adsorption corresponding to complete monolayer coverage and b (L mg-1) is the Langmuir constant related to the energy or net enthalpy of adsorption, which can be determined from the slope and intercept of plot of C_e/q_e against C_e. (Langmuir, 1918).

2.4.3   Elovich isotherms.

In multilayer adsorption, it is supposed that molecules are adsorbed in several layers on the adsorption surface. One of the equations that predicted multilayer adsorption with unlimited layers is Elovich equation (Elovich and Larinov, 1962). This model is based on a kinetic principle that the adsorption sites increase exponentially with adsorption, which implies a multilayer adsorption. It is expressed by the relation:

$$\frac{q_e}{q_m} = K_E C_e exp\left(-\frac{q_e}{q_m}\right) \qquad 2.28$$

where K_E is the Elovich equilibrium constant (L mg^{-1}) and q_m is the Elovich maximum adsorption capacity (mg g^{-1}), the constants can be calculated from the slopes and the intercepts of the plot Ln (q_e/C_e) versus q_e . (Hamdaoui and Naffrechoux, 2007)

2.5   Dynamic study in column.

The column test is more effective that batch method, because the column operation creates a continuous concentration gradient and the adsorbent is constantly in contact with spanking new solution (Gupta, 2016. Et al.,) so that the adsorbent material (Spanish broom) is always in contact with a constant concentration of metal ions Hg (II) throughout the duration of the test, unlike to batch where the concentration gradient between adsorbent and adsorbate decreases with time.

For the development of this study, this technique allows us to characterize and determine various properties of the adsorbent material in study, through the breakthrough curves that are plotted. A Breakthrough Curve is a plot of the column effluent concentration as a function of either volume treated or the time of treatment or the number of bed volumes (BV) treated. The important features of a breakthrough curve are breakthrough capacity (BC), exhaustion capacity (EC) and degree of column utilization (DOC) (Snoeyink and Summers 1999), in addition the determination of hydrodispersive properties of the material through a non-reactive chemical tracer (Tracer test).

2.5.1   Thomas model.

For the successful design of a column sorption process, it is important to predict the breakthrough curve for different parameters. Various kinetic models have been developed to predict the dynamic behavior of the column

The Thomas model is another one frequently applied to estimate the adsorptive capacity of adsorbent and predict breakthrough curves, assuming the second-order reversible reaction kinetics and the Langmuir isotherm (Han et al., 2008; Ghasemi et al., 2011). Theoretically, it is suitable to estimate the adsorption process where external and internal diffusion resistances are extremely small (Aksu and Gönen, 2004). The Thomas model is given by;

$$\frac{C_t}{C_0} = \frac{1}{1 + e^{-k_{Th}C_0 t}e^{k_{Th}q_0 m/Q}} \qquad 2.36$$

The linearized form of the Thomas model is as follows:

$$ln\left(\frac{C_0}{C_t} - 1\right) = \frac{k_{Th}q_0 m}{Q} - k_{Th}C_0 t \qquad 2.37$$

where K_{Th} is the Thomas rate constant (L min^{-1} mg^{-1}); q_0 is the maximum solid-phase concentration of solute (mg g^{-1}); m is the amount resin in the column (g); Q is the flow rate (L min^{-1}); C is effluent concentration (mg L^{-1}) and C_0 is influent concentration (mg L^{-1}).

Thomas model is employed by many researchers to predict the breakthrough curves for adsorption and ion exchange (Chu, 2010, Han, et.al. 2009,)

2.5.2   Curve-Fitting procedure and statistical analysis.

The curve-fitting procedures were performed by the Levenberg-Marquardt nonlinear least squares method. It involves an iterative improvement to parameter values in order to reduce the sum of the squares of the errors between the function and the measured data points. At each iteration, the parameters used in the model were varied in order to minimize the chi-square (χ^2):

$$\chi^2 = \frac{1}{n^{eff}-p}\sum_i w_i [y_i - f(x_i; \ p_1, p_2, \dots)]^2 \qquad (2.38)$$

$$\sigma_{i=}\sqrt{C_{ii}\chi_i^2} \qquad (2.39)$$

where, y is the dependent variable, x the independent variables, n^{eff} is the total number of experimental points used in the fitting, p is the total number of adjustable parameters used in the fitting, $p_1, p_2,\dots$ are the model parameters to be varied in order to minimize χ^2.

As a measure to determine the goodness of fit the adjusted r-square (R^2) was used. The closer the fit is to the data points, the closer the adjusted r-square will be to the value of 1.

Standard error on each fitted parameters was calculated in the fitting procedure by equation 39 where, C_{ii} is the diagonal element of the variance-covariance matrix.

Each experiment has been replicated at least three times. The data points on each graph represent the average value calculated over the replicates and the error bars are the corresponding standard deviations.

2.6   Flow model.

Fluid mechanics state that quantities as the density, pressure or velocity at a point in a medium are referred to the so-called fluid particle for fluid mechanics or to the Representative Elemental Volume (REV) for the groundwater flow. In each case, they are referred to a volume of fluid: 1) very large compared to the molecular scale processes and 2) quite small compared to the scale of the flow problems. The introduction of the concept of "fluid particle", then, could see a fluid as a continuous system, whose properties are continuous functions in space and in time taking continuous values throughout the system. Also with reference to the fluid particle, the indefinite equation of motion of a viscous compressible fluid is represented by the Navier-Stokes equation (or Navier-Stokes equations, if written in scalar terms), which translated to a media in the second law of Newtonian dynamics, linking causes and kinematic characters of motion:

$$\rho \left(F - \frac{d\boldsymbol{v}}{dt} \right) = \nabla \rho - \mu \nabla^2 \boldsymbol{v} \qquad (2.40)$$

Where F represents the mass forces remote agents for mass unit (F=g=-g∇z) $[LT^{-2}]$, μ is the dynamic viscosity coefficient $[ML^{-1}T^{-1}]$, v is the velocity $[LT^{-1}]$, ρ is the density $[ML^{-3}]$ and p $[MLT^{-2}]$ is the average pressure. The integration of Navier Stokes equation is impossible for a volume of fluid in a porous medium, because the geometry, at a microscopic scale, is extremely complex and impossible to know and to describe deterministically. These difficulties in the study of the fluid flow in a porous medium are overcoming by the introduction of the concept of REV. Introducing the concept of REV practically means: 1)   averaging physical and hydraulic properties of porous medium on the REV, from microscopic to macroscopic properties, and 2) assuming these macroscopic properties as punctual.

Similar to the role of the fluid particle concept for fluid mechanics, the concept of REV is used to see the porous medium as a continuous system, and own physical and hydraulic properties as continuous functions. In other words, because it is impossible to know the real geometry of a porous medium at a microscopic scale, therefore it is replaced by a continuous mathematical concept, where the physical properties are macroscopic properties (i.e. averaged on REV) described by continuous functions. So, the distribution of pores is described using properties like the porosity, the water content, the degree of saturation and primarily the permeability.

2.6.1 Darcy velocity concept.

Darcy's law expresses the second principle of Dynamic for a fluid within a porous medium. It realizes a relationship between the velocity of a fluid and the causes of its motion.

A general form of the Darcy's law, valid for a variable density fluid, is the following:

$$q = -\frac{k_0}{\mu}(\nabla P - \rho \overline{g}) \qquad (2.41)$$

representing the gravitational acceleration vector [0,0,-g] $[m\ s^{-2}]$, k_0 is the intrinsic permeability $[m^2]$, P is the pressure $[Pa]$ and μ is the dynamic viscosity of fluid $[Pa\ m]$. It was shown that Darcy's law is a solution of the Navier-Stokes equation (2.40) for a very specific configurations (Frega et al., 2004). Moreover, in subsurface hydrology another form of Darcy's law is commonly used, in which the forces that cause the motion are expressed as the gradient of potential function. Explaining the equation in terms of hydraulic head and rewriting it in vectorial terms for a Cartesian system, it's possible to get:

$$q = -\frac{k_0 \rho g}{\mu}\nabla h \qquad (2.42)$$

here, the potential function h(x,y,z) is the hydraulic head associated to the fluid and represents the fluid energy per unit of mass . The best-known form of Darcy's law is obtained using the hydraulic conductivity parameter:

$$K = \frac{k_0 \rho g}{\mu} \qquad (2.43)$$

or, in general terms, the Darcy's law in a tridimensional space becomes:

$$q = -K\nabla h \qquad (2.44)$$

To obtain the governing groundwater flow equation it's necessary to start from continuity equation (conservation mass principle):

$$-\nabla \cdot (\rho q) = \frac{\partial}{\partial t}(\rho n) \qquad (2.45)$$

introducing Darcy's law (2.44) in the balance equation (2.45) of fluid mass, it's possible to get the continuity equation of incompressible fluid in a saturated medium:

$$\nabla \cdot (K\nabla h) = \frac{\partial n}{\partial t} \qquad (2.46)$$

where n is the total porosity of porous medium.

2.7 Model of transport

In this paragraph issues will be discussed relating to transport of a fluid in a porous medium, in which its composition or its properties are variable. This may be the case of two immiscible fluids (e.g. freshwater and saltwater) or a substance dissolved in a fluid with variable concentration (e.g. Mercury in water).

For miscible fluids it will be considered a single flux and it will be defined the concentration of a substance (solute) in a fluid (solvent). There are several ways to define the concentration and here the most common ones will be listed:

1. The volumetric concentration or solute mass per unit volume of solution (kg/m^3 or g/l);

2. The mass concentration intended as mass of solute per unit mass of solution (kg/kg);

3. The molarity standard definition of the concentration in units of the SI, and the number of moles of solute per unit volume of solution (mol/m^3).

In the following it will be used the volumetric concentration C and will be called simply concentration. This concentration varies continuously in the medium; there is no discontinuity between two fluids as occurs between immiscible fluids. When the fluid is moving, the concentration varies in time and space. This type of motion is called mass transport or solute transport in porous medium. In order to clearly differentiate between laws of the transport and the laws of interaction among the substances transported and the medium, it will initially be treated as transport of substances, which are not subject to variations, exchanges or reactions while crossing the porous medium. These are non-reactive substances or conservative, for example, it is excluded radioactive decay as well as adsorption (S. Straface, 2015).

Afterwards, it will treat the issue of reactive substances and it will be possible to see how special laws governing their behavior must be added to the transport equations. It is important to establish, from the outset, what is the mean of transport of a solute. First of all, it is necessary to identify the constituents of elements, which are soluble in water. These items can themselves be ionized more or less according to their Ionic charge. However, these dissolved substances may also be present as electrically neutral chemical elements or complex created by aggregates of molecules or ions versions. In addition, intractable salts can be carried as trace concentrations because this insolubility is not total.

Since certain radionuclides, for example, are toxic even in low concentrations, these tracks can be important in calculations for the radiological security. Finally, must also consider the constituents delivered in the form of larger molecular aggregates, such as colloids, which may eventually be subject to mechanical filtration through the network of the porous medium. All these substances are known as solutes transported until, they do not constitute a mobile phase distinct from carrier fluid but integrated themselves into the single phase fluid (natural water), possibly changing physical and chemical properties (e.g. mass per unit volume, viscosity).

The solute transport is therefore different from immiscible fluids like oil and water, which obey to laws completely different (S. Straface, 2015).

2.7.1 Non-reactive transport.

The mass dissolved in solution in a particular volume of solid matrix can vary over time due to several factors: a different concentration of moving water or water injected through wells, for phenomena of diffusion or dispersion of solute, adsorption, production or decay caused by chemical or biological reactions.
The transport of a solute is studied through the mass amount of single species dissolved in solution (solute) and bulk quantities of the species deposited (adsorbed).

The concentration of solute, C, and that of adsorbed Cs, is linked through the adsorption isotherms in equilibrium. Ignoring the phenomenon of adsorption and decay the dispersive phenomenon can be divided (artificially) into three separate mechanisms: 1) advection, 2) molecular diffusion and 3) kinematic dispersion (S. Straface, 2015).

2.7.1.1 Advection.
This phenomenon occurs when the dissolved substances are carried by the medium through its displacement. If it is assumed that the transport is governed only by the phenomenon of advection, the resulting transport equation is obtained from a simple mass balance applied to macroscopic scale, the REV.
Due to the advection, if it is injected at the moment t_0 a tracer concentration C_0 in section x_0 in a flow column with an average velocity u, the same concentration C_0 will be found in section $x_1 = x_0 + u \Delta t$.
The mass balance of the solute requires that the mass flux of transported substance in the volume D is equal to the change of mass of the substance in the volume D per unit time. The mass balance crossing the boundary of the volume D returns the following equation:

$$\int_{\Sigma} Cq \, \vec{n} \, d\sigma \qquad\qquad (2.47)$$

where C (volumetric) is the concentration of the solute, q is the (average) velocity of Darcy and $\vec{n}$ is the normal to the boundary surface. The mass of solute contained in the elementary volume V is:

$$\int_V nC \, dv \qquad\qquad (2.48)$$

where n is the total porosity. The mass variation in the time unit can be written as:

$$\frac{\partial}{\partial t}\int_V nC \, dv = \int_V n\frac{\partial C}{\partial t} \, dv \qquad (2.49)$$

The passage from the first to the second form is allowed by the Leibnitz law as V is fixed and n is constant. The mass balance equation becomes:

$$\int_\Sigma (Cq)\,\vec{n}d\sigma = \int_V n\frac{\partial C}{\partial t} \, dv \qquad (2.50)$$

using the Ostrogradsky rule it is possible to turn the surface integral into a volume integral:

$$-\int_V \nabla(Cq) \, dv = \int_V n\frac{\partial C}{\partial t} \, dv \qquad (2.61)$$

This is the balance equation for advection.

$$-\nabla(Cq) = n\frac{\partial C}{\partial t} \qquad\qquad (2.62)$$

2.7.1.2 Molecular diffusion.

This physical phenomenon is related to the molecular agitation. In an immobile fluid, Brownian motion throws the particles in all directions of space. If the concentration of fluid is uniform in space, each one of two neighboring points sends on average the same

number of solute particles towards the other, and molecular agitation does not change the concentration of the solution. However, if the concentration of the solution is not uniform, points with higher concentration sends on average a greater number of particles in space compared to points with less concentration.

The result of this molecular agitation is that some particles have transferred from areas of higher concentration toward points with lower concentration. Fick has found that the flow of particles of solute in an immobile fluid is proportional to the gradient of concentrations, through the note report:

$$\phi^{diff} = -d_0 \nabla(C) \qquad (2.63)$$

where d_0 is called molecular diffusion coefficient and is:

$$d_0 = \frac{RT}{N} \frac{1}{6\Pi\mu r} \qquad (2.64)$$

indicating with R the ideal gas constant, dynamic viscosity μ of fluid, T the temperature in kelvins, N the number of Avogadro and average radius of molecular aggregates of fluid.

In order to take account of the tortuosity of porous medium and the obstacle of grains, it is possible to use a smaller coefficient of molecular diffusion, as defined d = d0/(Fn), indicating with F the ratio between the electrical resistivity of the soil and the electrical resistivity of the water contained in it and with n total porosity. Considering both the convective phenomenon that diffusive, the equation becomes:

$$\int_\Sigma (Cq)n \, d\sigma + \int_\Sigma n\phi^{diff} \, nd\sigma = -\int_V \nabla(Cq)dv - \int_V \nabla(n\phi^{diff})dv \qquad (2.65)$$

total porosity comes into play here because the integral of diffusive flow on Σ is zero on the solid part [(1 − n) Σ] and nonzero on pores, while [nΣ] the velocity of Darcy is defined as if the whole area were open. Substituting:

$$\nabla \cdot (nd\nabla C - Cq) = n \frac{\partial C}{\partial t} \qquad (2.66)$$

Due to the presence of blind pores and more or less irregular shape of grains there is a part of fluid that does not participate at the motion. There is also the part of fluid that remains attached on surfaces because of forces between molecules and interactions of physical and chemical phenomena on electrical sheets around the grains.

Thanks to molecular diffusion, immobile fraction contains the part of the dissolved substance and it is therefore necessary to insert it into the balance.

The mass continuity equation of solute becomes:

$$\nabla \cdot (nd\nabla C - Cq) = n\frac{\partial C}{\partial t} + (n - n_c)\frac{\partial C'}{\partial t} \qquad (2.67)$$

where C' is the concentration of immobile flow and n_c is the kinematic porosity (S. Straface, 2015).

2.7.1.3 Kinematic Dispersion.

This phenomenon of mixing is mainly due to microscopic velocity heterogeneity within the porous medium on any scale of observation:

1) Inside the pores, the velocity distribution is not uniform but parabolic with highest velocity at the centerline of the pores. This causes faster propagation along the axis of the pores and progressive spreading of the transported substances compared to the mean movement of advection;

2) The different sizes of pores throws velocity gradients that give rise to greater dilution and a transverse propagation of the solute.

3) Tortuosity of paths yields in dispersion of fluids due to the pore geometry. The division of transport in an adjective term, related to speed of Darcy, and a dispersive term, that integrates the effects of heterogeneity, is somewhat arbitrary. The mathematical formulation adopts a transport law for dispersion of Fick that takes into account the phenomenon of mixing:

$$\phi^{diff} = -D'\nabla C \qquad (2.68)$$

that is applied to the entire section of medium, as well as the Darcy velocity, but with a dispersion coefficient D' that has these characteristics:

It is a symmetric tensor of the second order:

$$D' = \begin{bmatrix} D'_{xx} & D'_{xy} & D'_{xz} \\ D'_{yx} & D'_{yy} & D'_{yz} \\ D'_{zx} & D'_{zy} & D'_{zz} \end{bmatrix}$$

the main directions are formed by the direction of the velocity vector (longitudinal direction) and the other two orthogonal directions;

the values of diagonal coefficients are variable and they depend from velocity.

The mixed terms of tensor matrix are zero and for isotropic and homogenous medium, it is possible to write:

$$D' = \begin{bmatrix} \alpha_L IqI & 0 & 0 \\ 0 & \alpha_T IqI & 0 \\ 0 & 0 & \alpha_T IqI \end{bmatrix}$$

where α_L is the longitudinal dispersion and α_T is the transverse dispersion. Anisotropic condition is due at the velocity of dispersion, which is major along the motion direction. To take in account the advection, molecular diffusion and kinematic dispersion the balance equation of solute mass becomes:

$$\nabla(D'\nabla C + nd\nabla C - Cq) = n_c \frac{\partial C}{\partial t} + (n - n_c)\frac{\partial C'}{\partial t} \tag{2.69}$$

It is possible to define a new dispersion tensor of second order, which takes in account molecular diffusion and kinematic dispersion, and to write a new equation:

$$\nabla \cdot (D\nabla C - Cq) = n_c \frac{\partial C}{\partial t} + (n - n_c)\frac{\partial C'}{\partial t} \tag{2.70}$$

If the concentration of mobile fluid reaches the immobile fluid instantaneously, the equation is the following:

$$\nabla \cdot (D\nabla C - Cq) = n \frac{\partial C}{\partial t} \tag{2.71}$$

On the other hand, if concentration C' is zero, there is no transfer of solute in the immobile part of fluid, the equation becomes

$$\nabla \cdot (D\nabla C - Cq) = n_c \frac{\partial C}{\partial t} \qquad (2.72)$$

If the both considerations are not true, it is possible to insert a new variable and define a new equation:

$$(n - n_c)\frac{\partial c'}{\partial t} = \tau(\text{C-C'}) \qquad (2.73)$$

where τ is the coefficient of transfer between immobile and mobile phase.

2.7.2   Reactive transport.

The immobile phase mainly includes the solid phase, but also the fluid related to the solid part by molecular forces of attraction. During the transport, it can happen to establish mechanisms that tend to change the mass balance. Such mechanisms, due to the interaction between the immobile phase and the transported substances, can make the transport non-conservative (Jackson, 1980). The main reactive mechanisms are:

Physical mechanisms. Transported substances can be stopped by filtration physics through the pores. This can happen even if the transported substances are smaller than the pore size.

Geochemical mechanisms are mainly due to:

- Combinations of ions inside the electrically neutral molecules.
- Acid/base reaction as a function of pH of the solute and rocks that it crosses.
- Oxide-reductions, which affects the State of valence of ions transported.
- Dissolution/precipitation, which can immobilize or dissolving substances.
- Adsorption/desorption limited definition, strictly speaking, usually to trade of ions (primarily cations), that attach to the surface of colloidal or clay minerals.

Radiological mechanisms. These are radioactive decay (disappearance of substances) and creation of by-products of decay (appearance of new substances).

Biological mechanisms. Biological activity in porous media that can decompose or transform certain elements.

Assuming equilibrium between immobile and mobile phase, taking into account the mechanisms in the transport equation, which introduces a generic source term Q:

$$\nabla \cdot (D\nabla C - Cq) = n_c \frac{\partial C}{\partial t} + Q \qquad (2.74)$$

where the source term Q represents the mass of solute, added (or subtracted) per unit of time. This source term represents a sink or a source of solute mass or an amount of solute that is stored or disappeared in the volume.

In case of adsorption, degradation or decay, the solute removed from the solution and stored in the volume represents a source term, so it is positive. Below is a summary of the laws that allow estimation of the source term.

2.7.2.1 Filtration

In this case the transported items are filtered by medium; this happens when the pore size is smaller of particles in solution. Greenberg gives the following estimates for the size of the pores in the clays:

Clay particle diameter ~ 20,000 Å and sometimes much smaller.

The spacing between layers of clay minerals. 9 – 15 Å.

In the sands, the order of magnitude of pore diameter, is usually in the range of 10^{-2} and 10^{-1} mm (100.000 to 1.000.000 Å).

Soluble ion diameter smaller, such as Na^+ or Cl^-: 1 – 10 Å.

Diameter of the larger organic molecules with a higher molecular weight.

Diameter of bacteria: 5.000–30.000 Å.

Diameter of Colloids: highly variable, usually in the range 1000-50000 Å.

Therefore, it is necessary to admit that the direct filtration can be only for much larger molecules, bacteria or colloids, silt or clay soils.

2.7.2.2 Ion Exchange

The adsorption capacity of certain minerals or colloids is due to the existence of electrical unbalanced charges on the surface or inside of these minerals. Ions with an opposite charge will stick to it, creating a double layer that can belong to one of the following two types:

Imperfections or replacement of ions in the crystal lattice of the mineral cause positive or negative electrical imbalance. The mineral surface has called stable layer and ions with an opposite charge attracted by stable layer are called moving electrical layer. Specific adsorption of certain ions by the mineral surface creates a stable layer to which other ions of opposite charge stick by creating a mobile layer.

2.7.2.3 Adsorption.

As solutes stick to mineral particles there are a number of substances that bind to the solid phase. The mass concentration F, dimensionless, has typically used in representing substances adsorbed mass per unit mass of the solid.

In a unit volume of the porous medium, solid mass is $(1 - n)\rho_s$, where n is the total porosity and ρ_s mass per unit of volume of solid particles. The mass of adsorbed solute in unit volume is then $(1 - n)\rho_s F$. The source term must be added into the equation of continuity, it is the variation of the mass of adsorbed solute per unit volume in the time (De Marsily, 1986):

$$Q = (1 - n)\rho_s \frac{\partial F}{\partial t} \qquad (2.75)$$

The problem of adsorption is to define the relation between the concentration F and C. This relationship can be defined through different isotherms such as those mentioned above in section 2.3 Adsorption isotherms.

Chapter 3.

3 CHARACTERIZATION OF THE ADSORBENT MATERIAL AND BATCH TESTS.

3.1 Spanish broom characterization.

To have a good knowledge of the solid materials used as adsorbents it is necessary to make a correct characterization of their properties, from the point of view: chemical, physical, mechanical, morphological, textural, etc. In addition is also important to know the reactivity of the material against different adsorbate contact conditions, evaluating the adsorption capacity, the equilibrium relationship between the phases, the bonding mechanisms, the kinetics between the material surface and the metal ions, the determination of the physical properties and size of the particles, its mechanical resistance to guarantee the ease of handling, and to avoid the least possible loss of load in fixed and mobile beds, and a low cost of both the raw material and the manufacturing process.

The chemical composition of the broom used in the present study has been previous determined (Gabriele et al., 2010): 44.5 (0.2)% of Cellulose; 18.5 (0.3)% of Lignin; 16.3 (0.1)% of Pentosans; 13.3 (0.1)% of Pectins and 4.0 (0.2)% of Ash.

3.1.1 Fourier Transform Infrared Spectroscopy (FTIR) analysis

Fourier Transform Infrared Spectroscopy (FTIR) is the most frequently used technique in the analytic laboratories for identification of organic (carbon-based) materials. The technique involves the interaction of infrared radiation (IR) with a sample by either transmission of an IR beam through the sample or by reflection of an IR beam off of the sample. Absorbance of certain wavelengths of the IR beam by the sample can be related to the presence of specific functional groups present in the sample. Thus, we can determine chemical information based on the wavelengths and intensities of IR bands absorbed by the sample.

Image. 3.4 Bruker ALPHA FT-IR. Analysis of Spanish broom.

To characterize the SB fibers FTIR spectra between 375 and 4000 cm^{-1} were directly collected on dry samples by a Bruker ALPHA FT-IR spectrometer equipped with a A241/D reflection module.

 Only 1 gram of sample is needed for FTIR analysis, it must be finely ground. The material (SB) powder is placed on the ATR diamond crystal stage and clamped in place. Each sample measurement takes less than a minute to run. The sample is then removed, and the ATR stage cleaned, before the next sample is placed on the stage for measurement.
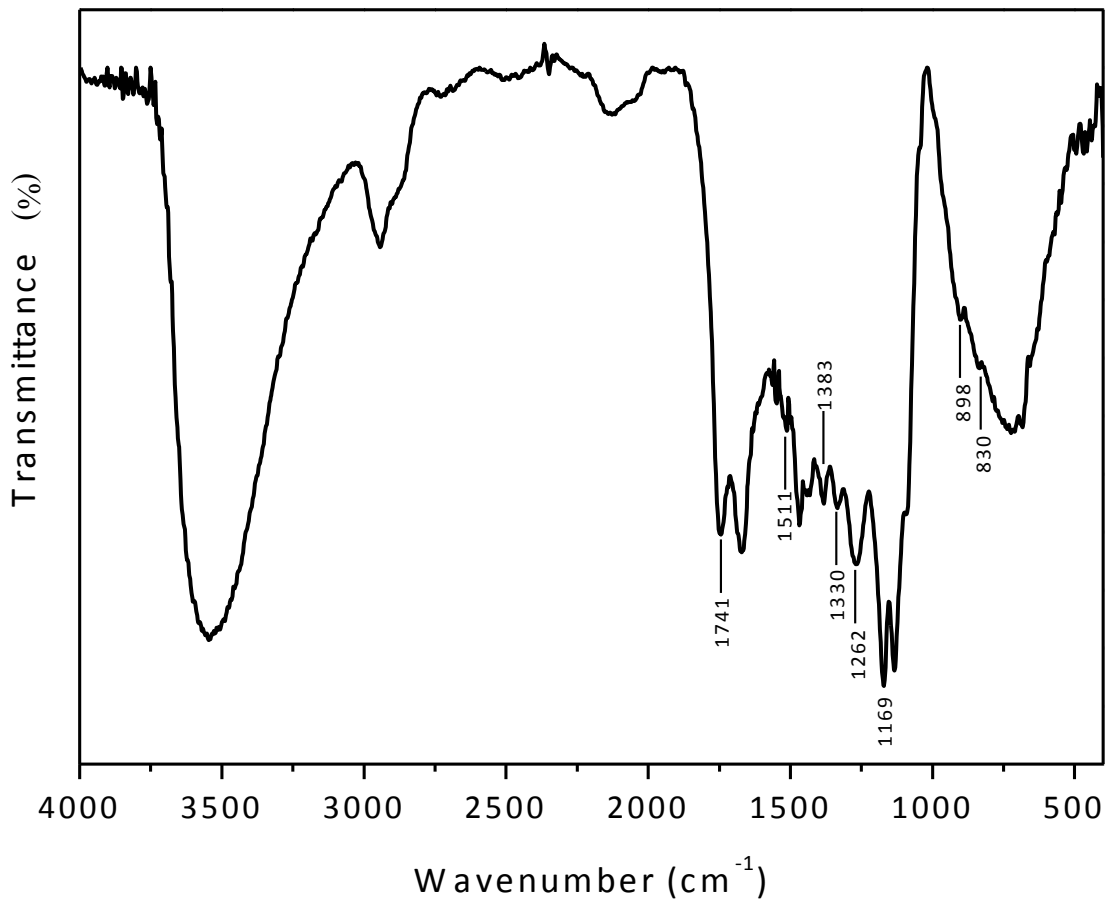
Figure. 3.1 FTIR spectrum of Spanish broom

Figure 3.1 shows the typical FTIR spectrum of Spanish broom (SB). The peaks picked are characteristic of lignocellulosic materials (Casas et al., 2012). Clearly distinguishable are the peaks related to the cellulose fraction and those of the lignin one. Firstly it's shown a strong broad O-H stretching at 3300–4000 cm^{-1}, C–H stretching in methyl and methylene groups at 2800–3000 cm^{-1} are typical base structure of the all cellulose (wood) samples.

Thus, the peaks at 1169 cm^{-1} and at 898 cm^{-1} are attributed to the C – O – C asymmetric stretching vibration and C_1– H deformation in cellulose. On the other hand, the intense peak at 1741 cm^{-1} is related to the C = O stretching vibrations of the carboxyl groups of lignin. Moreover, vibrations at 1330 cm^{-1} and 830 cm^{-1} are typical of the syringyl unit, while the guaiacyl ring vibration occurs at 1511 cm^{-1}. Other characteristic peaks of lignin are that at 1383 cm^{-1} attributed to the phenolic hydroxyls and the small peak at 1511 cm^{-1} related to the aromatic skeletal vibration.

The presence of these functional groups within the structure of the material increases the possibility of reaction of the mercury species in solution with the adsorbent's surface, decreasing the concentration of Hg in contaminated water sources.

3.1.2   Scanning Electron Microscopy (SEM) analysis.

The scanning electron microscope (SEM) uses a focused beam of high-energy electrons to generate a variety of signals at the surface of solid specimens. The signals that derive from electron-sample interactions reveal information about the sample including external morphology (texture), chemical composition, and crystalline structure and orientation of materials making up the sample.

The structure of the Spanish broom fibers was analyzed by a SEM LEO 420 (LEO Electron Microscopy Ltd., Cambridge, England). Fiber samples were gold sputter-coated with an Auto Sputter Coater, AGAR. Images were acquired under an accelerating voltage of 15.00 kV.
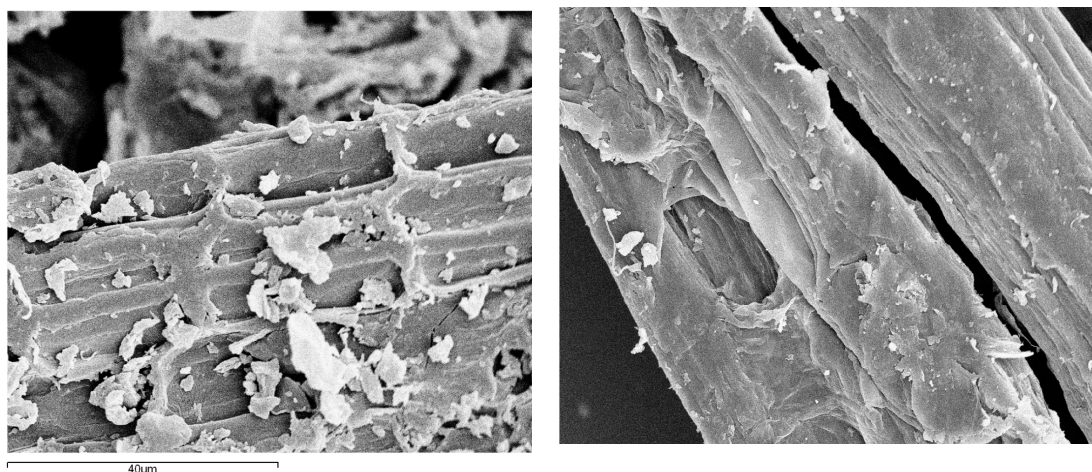
Figure 3.2 SEM images of the Spanish broom a) 200x; b) 1000x

The characterization results demonstrated a representative image of the structure of the lignocellulosic fiber that is reported in Figure 3.2. It shows that the Spanish Broom fibers are organized in parallel bundles of cylindrical microfibers glued together by lignin. Each microfibers has a diameter of about 40 μm, and thanks to its microfibers arrangement and the presence of lignin linked to other cellular components such as

cellulose and hemicellulose, provides to the structure of the SB an ideal mechanical strength for to be use as a filter within a continuous flow system.

3.2 Spanish broom pretreatment and solutions preparation.

Cost is an important parameter for comparing the sorbent materials. However, cost information is seldom reported. In general, a sorbent can be assumed as ``low cost'' if it requires little processing, is abundant in nature, or is a by-product or waste material from another industry.

As noted previously in Chapter 1, various by-products from industry have been used as low-cost raw material to produce adsorbents, but the various treatments they need have raised their cost, reducing them to use exclusive for water treatments to small and laboratory scale. Therefore the production of alternative adsorbents to replace the costly activated carbon is one of the objectives of this research.

The pretreatment of the material under study is a simple process, which does not require high production costs. The Spanish broom was collected from the area of Arcavacata of Rende - Italy, pruning the extreme branches of the tree, eliminating theirs flowers and seeds. The branches were chosen that presented a thick and firm structure, later a manual cleaning was carried out for the elimination of insects, contaminated branches by pests that could be present in the plant.

Subsequently a continuous washing with distilled water was performed until a clear wash water was obtained, and then placed in a Binder model E028-230V-T Hot Air Oven, with temperature control, it is was set at 105 ° C to dried it and remove all water from the material, then it was grinded by an industrial mill and sieved the material through an industrial sieve with a 5 mm opening.

Image. 3.5 Process of treatment and obtaining of the adsorbent material (Spanish broom), by all laboratory test.

All chemicals and reagents used for the experiments had an analytical grade of purity. Ultrapure water (18.3 MΩ cm, Arioso-Human Corporation) was used for all the

solutions. A stock solution of Hg(II) with a concentration of 1000 mg L^{-1} was prepared starting from Hg(NO$_3$)$_2$ •H$_2$O (Sigma-Aldrich, 99.99 % purity) in agreement the Guidelines EPA, Inductively Coupled Plasma-Atomic Emission Spectrometry (Method 6010C). Chloride ions at a concentration of 150 mg L^{-1} were also added to the stock solution through the addition of concentrated HCl. This was done in order to have Cl$^-$ ions concentration in the range of the groundwater samples collected in important aquifers involved by Hg pollution (INIGEMM, 2013). The working standard solutions, adopted in the tests were prepared by means of serial dilutions of the Hg stock solution using the equation:

$$C_1 * V_1 = C_2 * V_2 \qquad\qquad 3.1$$

where: C$_1$= Initial concentration (element stock dissolution); V$_1$= Initial volume (element stock solution); C$_2$ = Final concentration; V$_2$= Final volume.

HNO$_3$ and NaOH solutions were used to adjust the pH of these solutions. Mercury concentration in the samples collected during the experimental activities was measured by an Inductively Coupled Plasma Mass Spectrometer (ICP/MS, iCapQ Thermofischer). ICP/MS technique consists of the separation and subsequent determination of the ions present in a sample as a function of their atomic mass. The sample, in a first stage, is subjected to high temperature by means of a plasma (8000°K). This plasma achieves breaking the chemical bonds of the atoms present in the sample and ionizing them. Then these ions are subjected to electromagnetic fields, causing their separation, according to the mass/charge ratio. Thus, the different ions arrive at the detector separated and ready to be quantified.

The instrument was calibrated using different analytical standards concentrations (TraceCERT® certified reference materials (CRM)): 1, 5, 10 and 20 ppb, obtaining linear regressions greater (R^2) > 0,995. All samples were purified with a 0.45μm filter and then acidified with HNO$_3$ (pH = 2). The instrument was operated in Collision Mode; that uses a non-reactive gas and a process called kinetic energy discrimination (KED) to selectively attenuate all polyatomic interferences based on their size. The sample introduction system used consisted of a Peltier cooled (3 °C), baffled quartz cyclonic spray chamber, PFA-ST nebulizer and quartz torch with a 2.5 mm i.d. removable quartz injector. All samples were presented for analysis using a SC-4DX

autosampler with integrated 7-port FAST valve from Elemental Scientific before ICP/MS analysis. All analysis operations were in agreement with Guidelines iCAP Q Operating Manual Thermo Fisher Scientific.

All results were analyzed through **Origin 8.0** that is a proprietary computer program for interactive scientific graphing and data analysis interactive scientific graphing and data analysis.

Image. 3.6 Inductively Coupled Plasma Mass Spectrometer (ICP/MS, iCap Q Thermofischer).

3.2.1 Potentiometric titrations

Potentiometry is an electrochemical analytical method based on the measurement of the potential difference between electrodes immersed in a solution, where the potential of one of the electrodes is a function of the concentration of certain ions present in the solution. The measure of the electrode potentials allows to obtain of direct form the concentration of a substance or to follow its evolution along a chemical reaction (titration reaction).

The use of this technique allows us to determine different characteristics of the material in studio (SB), for this research have been used the technique of Gran, 1952, which is detailed below.

3.2.1.1 Gran's method.

The potentiometric titration experiments were carried out through a Hanna HI 221 potentiometer calibrated with different buffer solutions (pH = 4.01; 7.00 and 10.00) following Hanna Instruments HI 221 Instruction Manual, employing at constant

temperature (25 ± 1°C). Titrations were performed on suspensions of the absorbent material (2 g L^{-1}) or on blank control samples not containing the absorbent. The suspensions were acidified using HNO_3 0,01N (Sigma-Aldrich Cod. 13-1760 SAJ) at pH 3 and then the suspensions were slowly back-titrated in 0,1mL increments of standard NaOH 0.01 N (Sigma-Aldrich Cod. 1.60309) up to about pH 10.

The Gran's graphical method was used to determine the equivalent points in the acid titration of Spanish broom. It is applied when working with very diluted solutions of weak electrolytes, where the slope of the curve around the point of inflexion varies slowly and it is difficult to determine exactly the point of equivalence. Therefore Gran through Nernst's law derives a function in which the potential oscillate in a linear way with the addition of the titration reagent. (Gran, 1952; Rossotti and Rossotti, 1965).

The linearizing functions of the Nernst equation is:

$$E = E_1 + S \log \{H^+\} \qquad 3.2$$

where {H+} is the activity of the hydrogen ion measured. S is the slope of the electrode used, typically +or- 59.2 mV for a univalent ion at 25° C. Solving for C and multiplying by the volume to get millimoles the function yield: $(V_0 + V_a + V_b) * 10^{\frac{E-E_1}{S}}$ where $H^+ = 10^{\frac{E-E_1}{S}}$ or $H^+ = 10^{-pH}$ become:

$$Acid\ side. = (V_0 + V_{at} + V_b) * 10^{pH-7} \qquad 3.3$$

$$Alkaline\ side. = SF * (V_0 + V_{at} + V_b) * 10^{4-pH} \qquad 3.4$$

where V_0, V_{at}, and V_b are, respectively, the initial volume of the suspension, the total volume of acid solution and the total volume of OH– added at the titration points.

The specific volume of titrant added at the equivalent point (V_e) was determined by plotting the function Eq. 3.3 on the acidic side and the function Eq. 3.4 on the alkaline side, as a function of the volume of NaOH added.
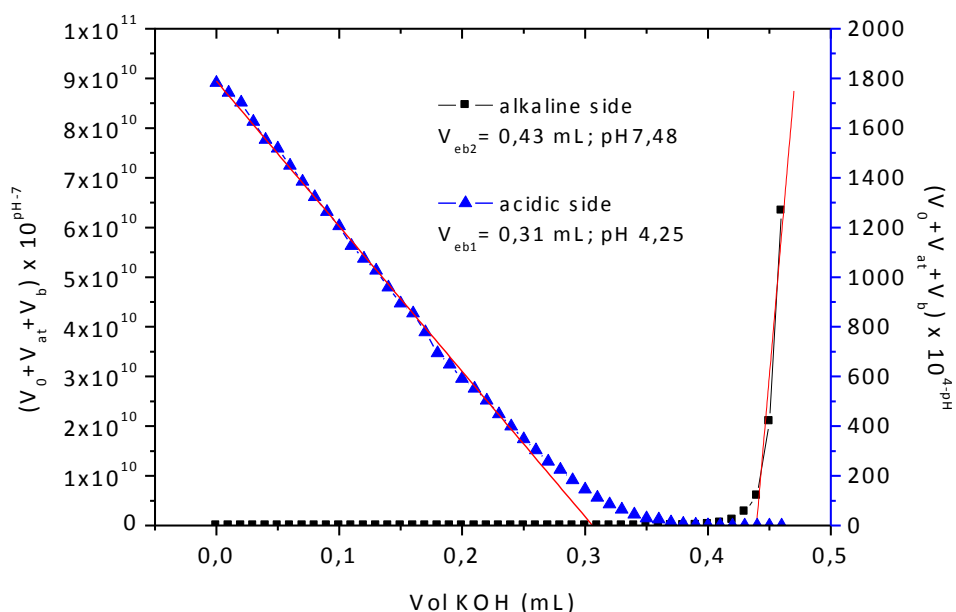
Figure 3.3 Gran's plot relative to the Spanish broom titration

The ionic strength was maintained constant throughout the titration experiments by the addition of $NaNO_3$ (0.1 M), with constant agitation using a magnetic stirrer and purged with pure N_2. Nitrogen gas was prepurified by passing through wash bottles containing NaOH (0.1 M) and HCl (0.1 M), and then saturated with distilled water.

The data analysis and graphics software Origin 8.0, was used to construct the Gran plot, using the data obtained from the titration, once the data was plotted, we have fitted a line to only the linear part of the Gran plot of Acid side and Alkaline side curves and extrapolate it to the abscissa (x) to find the equivalent points Veb_1 and Veb_2 respectively as shown in **Figure 3.3.** Through these values, it was possible to determine the pH value where the equivalence points of the material are presented at **4.25** and **7.48**, due to the origin of the adsorbent material. These points can be attributed to the ionization of the carboxyl and phenolic hydroxyl groups of the lignin, respectively (Lv et al., 2012; Guo et al 2008).

3.2.2 Speciation study of Mercury (II) in the presence of chloride.

The study of the adsorption of heavy metals on an adsorbent material is linked on the complexation that the metal forms with the different ionic or cationic species within the solution. Distribution of mercury compounds depends to a significant degree on reduction-oxidation conditions. Another important aspect to be considered in the Hg(II) speciation within the solution is the influence of the pH.

Previous studies (Zhang et al., 2005) have shown that, in the absence of chelating agents, Hg^{+2} is the dominant species in solution at pH < 3, Hg (OH)$_2$ is the dominant one at pH > 5, while for pH values between 3 and 5, both species coexist Moreover, small traces of $HgOH^+$ ranging from 1% to 13% of the total mercury Hg(II), were also detected for pH values between 2 and 6. When agents able to complex the Hg(II) ions are present in solution, the speciation of Hg(II) significantly changes. In order to explain the pH-dependent adsorption of Hg (II) on SB, speciation study of Mercury (II) in the presence of chloride was investigated.

The hydrogen ion concentration in the metal cation stock solution was determined potentiometrically with a glass electrode using Gran's method (see. Section 3.2.1.1).

The complexation equilibria were studied in 0.1 M NaNO$_3$ and at 25°C by measuring with a glass electrode the competition of chloride for H^+ and the metal cation. The cell arrangement and the electrodes employed was Ag/AgCl reference electrode manufactured by Metrohm, it acquired a constant potential within 10 min after the addition of the reagents and remained unchanged to within ± 0.1 mV for several hours. The titrations were carried out with a programmable computer controlled data acquisition switch unit 34970 A supplied by Hewlett-Packard. The EMF (the potential difference between the anode and cathode) values were measured with a precision of +10-5 V using an OPA 111 low-noise precision DIFET operational amplifier. (Furia et al. 2009).

The metal (C_M) and ligand (C_L) concentrations were ranged from 0.5 to 5 mM, the ligand–to–metal ratio was varied between 1 and 10 and pH was ranged from 2 to 9. The test solution's acidity was varied stepwise by adding C_B M NaOH stock solution.

Under the conditions of work of our research, detailed above, by analysis complexes of chloride with Hg^{2+}, the general equilibrium can be written, schematically, as: eq. (3.5)

$$p\ Hg^{2+} + r\ HCl \rightleftarrows Hg_pH_{-q}(HCl)_r^{(2p-q)} + q\ H^+ \qquad\qquad \beta_{pqr} \qquad\qquad (3.5)$$
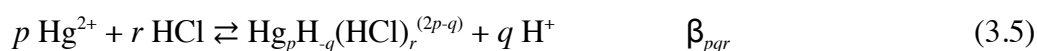
which takes into account the possible formation of simple ($q=r$), mixed ($q \neq r$), mononuclear ($p=1$) and polynuclear ($p>1$) species. The interpretation of the potentiometric data in terms of complexes and equilibrium constants was carried out with computer program Superquad in which formation constants are determined by minimisation of an error-square sum based on measured electrode potentials. The program also permits refinement of any reactant concentration or standard electrode potential. (Gans et al., 1985). During the numerical treatment the equilibrium constants for the hydrolytical species (eqs. 3.6-3.8) of the metal ion, which were took from literature (Baes and Mesmer, 1976), were kept fixed.

$$Hg^{2+} + H_2O \rightleftarrows Hg(OH)^+ + H^+ \qquad \log K_{11} = -3.40 \qquad (3.6)$$

$$Hg^{2+} + 2\,H_2O \rightleftarrows Hg(OH)_2 + 2\,H^+ \qquad \log K_{12} = -6.17 \qquad (3.7)$$

$$Hg^{2+} + 3\,H_2O \rightleftarrows Hg(OH)_3^- + 3\,H^+ \qquad \log K_{13} = -21.1 \qquad (3.8)$$
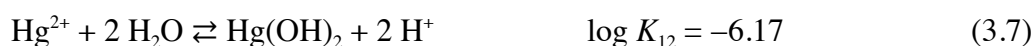
The results obtained were reported in Table 3.1 with the relative standard deviations, which represent 3 σ

(p,q,r)	Species	$\log \beta_{pqr} \pm 3\sigma$
(1,1,1)	$HgCl^+$	7.2±0.2
(1,2,2)	$HgCl_2$	14.0±0.1
(1,3,3)	$HgCl_3^-$	15.1±0.3
(1,4,4)	$HgCl_4^{2-}$	15.4±0.2
(1,2,1)	$Hg(OH)Cl$	4.1±0.3

Table 3.1. Survey of the $\log \beta_{pqr} \pm 3\sigma$, eq. (3.5), for Hg-Cl complexes obtained by numerical procedure

103
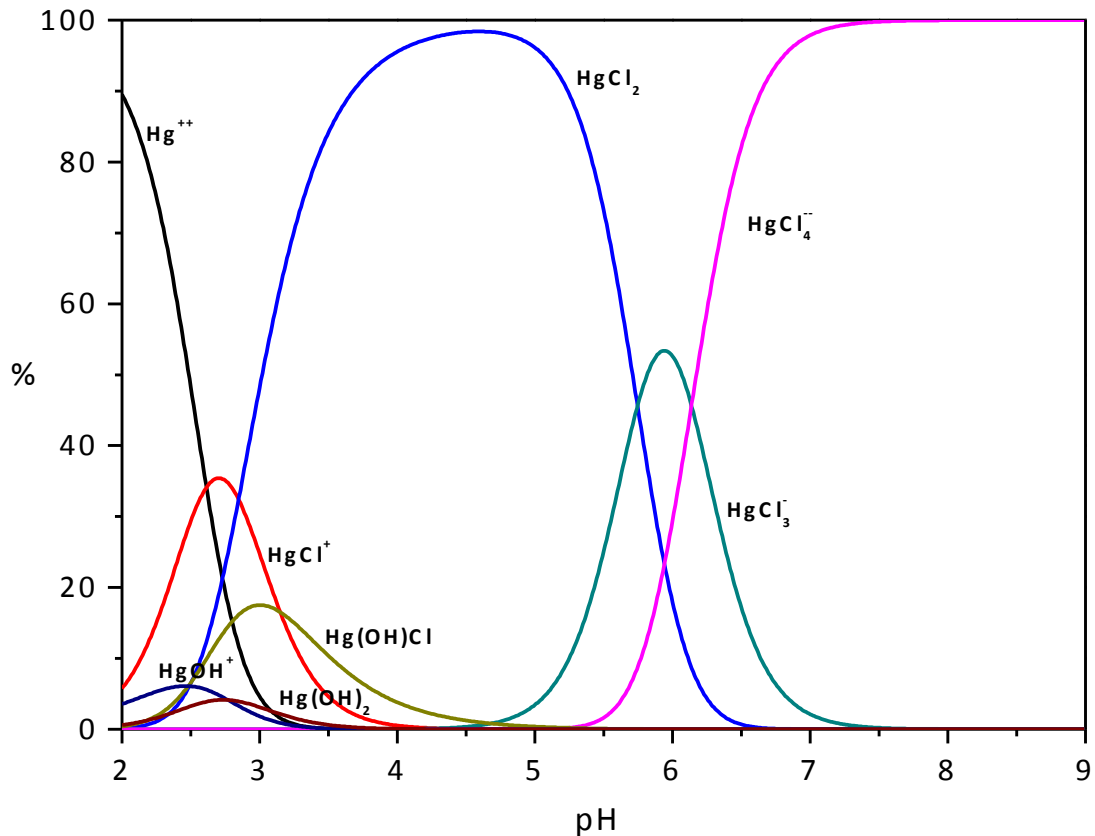
Figure 3.4. Distribution diagram of Hg^{2+} in the presence of chloride ($C_M = 5 \cdot 10^{-4}$ M and $C_L = 4 \cdot 10^{-3}$ M)

The results obtanied by computer program Superquad about equilibrium of hydrolysis of Hg^{+2}, as shown in **Figure 3.4**, Hg(II) forms several stable products related either to the equilibrium of hydrolysis of Hg^{2+} ($Hg(OH)^+$, $Hg(OH)_2$, $Hg(OH)3^-$) or to the complexation equilibrium with the chloride ($HgCl^+$, $HgCl_2$, $HgCl_3^-$ and $HgCl_4^{2-}$), together with the mixed species Hg(OH)Cl. It can be seen that, for pH values between 3.5 up to 5.5, the predominant species is the $HgCl_2$ complex.

3.3   Adsorption Experiments Test Batch.

The effect of pH on Hg adsorption, was studied by performing batch tests in which 0.5 g of Spanish broom were suspended in 50 mL of 80 mg L^{-1} Hg(II) solution at room temperature. The pH was varied in the range 2-9 by adding HNO_3 or NaOH solution. Adsorption kinetics and the influence of the contact time were evaluated in similar batch tests using the following conditions:

1) Initial Hg(II) concentration = 100 mg L^{-1}, solution volume = 0.400 L, mass of sorbent = 40.00 g;

2) Initial Hg(II) concentration = 200 mg L^{-1}, solution volume = 0.400 L, mass of sorbent = 20.00 g;

3) Initial Hg(II) concentration = 100 mg L^{-1}, solution volume = 0.400 L, mass of sorbent = 2.00 g, at pH 5.02 ± 0.3.
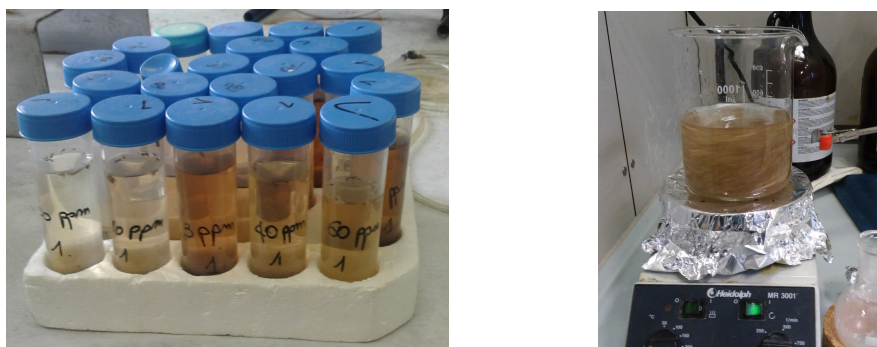
Image. 3.4 Batch Method Samples

Adsorption isotherms at different temperatures were obtained from similar batch experiments in which 0.5 g of Spanish broom were suspended in 50 mL of Hg(II) solutions with different concentrations in the range 1-180 mg L^{-1}. The suspensions, contained in 50 mL Falcons, were immersed in a water bath and incubated in an oven at the set temperature for eight hours. During the incubation time, each suspension was subjected to vigorous agitations by inversion for 30 s every hour.

These experiments were also useful to assess the influence of the Hg(II) initial concentration on the Spanish broom adsorption capacity and removal efficiency.

Another set of batch experiments were also carried out in order to test the effect of the increasing adsorbent dosage (mass of Spanish broom) on the adsorption capacity and mercury removal efficiency. In each experiment, the Hg(II) solution concentration was fixed at 80 mg L^{-1} and gradually increasing the amounts of Spanish broom, in step of 0.5 g, from 0.5 g to 7.0 g. Each amount was suspended in 50 mL of the above Hg(II) solution.

To analyze the results, the adsorption capacity, i.e., the amount of adsorbed mercury per unit mass of adsorbent (q_t) was determined for equation (2.1). And the Hg(II) removal efficiency (RE%), defined by the equation (2.2).

3.3.1   X-ray Fluorescent Spectroscopy (XRF) analysis.

The analysis in XRF is well established among the qualitative analysis techniques, with a broad field of practical applications, especially when require non-invasive analytical methods, thereby the XRF is constitute one of the most used and profitable methodologies.

Image. 3.5 Bruker Tracer III. XRF analysis of Spanish broom.

In order to show the presence of mercury on the lignocellulosic fibers, XRF analysis was performed with a Bruker Tracer III, equipped with a Rh/Pd source, at a voltage of 40kV, a current of 11f and an acquisition time of 15sec. Spanish broom samples, before and after suspension in Hg(II) solution, were dried in a desiccator, and pelleted to form disks that were subsequently placed directly onto the probe of the instrument for the measurement.
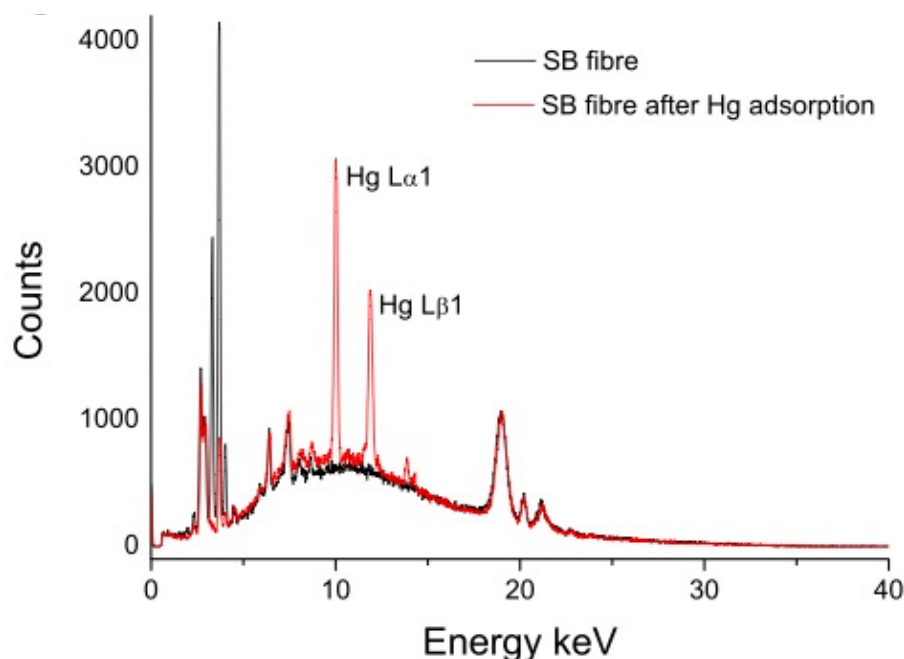

Figure 3.5 XRF Spectra of the Spanish broom before (black line) and after adsorption (red line)

.

As shown in Figure 3.5. The spectrum of the adsorbent material (black line) before contact with the Hg solution, the presence of the Hg metal in its structure is not observed. Nevertheless after the exposure of the adsorbent with the mercury solution, the presence of the mercury Hg αL and Hg βL was observed in the adsorption experiment (red line), thus confirming the adsorption of mercury by the lignocellulosic material.

3.4 Effects of various parameters on Mercury (II) removal

The adsorption of heavy metals within a reactive material varies according to the chemical conditions and the medium in which it reacts, these conditions may be favorable for the adsorption obtaining large yields or may decrease its reactive power. The effect of these parameters on the adsorption are evaluated in this section to obtain a better evaluation of the adsorption capacity of the material to different conditions, in order to determine which are the most appropriate conditions in which the adsorbent material obtains a better performance.

3.4.1 pH Influence

Figure 3.6. shows the influence of initial pH on the adsorption capacity of the Spanish broom. As can be seen, adsorption increases with pH starting from removal percentages of about 67 % at pH 2 up to about 85% for pH $\geq$ 6. There is a step-wise increase of the removal efficiency % above pH 4 and another stepwise increase above pH 7 that can be only seen at its initial stage in Figure 3.6. This is in agreement with the titration curve of the Spanish broom, which shows two equivalent points at pH 4.25 and 7.48, as determined by the Gran plot's method (section 3.2.1.1) (Figure 3.3). It is clear that, as the acidic functional groups present on the broom are ionized due to the increase of the pH, the adsorption efficiency increases.

This effect can be partly explained by the increase of the negative charge on the surface of the material that is therefore able to more efficiently attract positive ions and partly by the ability of the oxygen atoms to make stable complexes with the mercury (II)

species present in solution. The adsorption properties of the broom are due to its composite material nature, where cellulose and lignin play the major role. Indeed, metal cations can interact with the hydroxyl groups of cellulose and lignin as well as with the carboxyl functional groups of lignin. The chelating action of hydroxyl and carboxyl groups toward several metals, is known (Porwal et al., 2015; Beneduci, 2011; Furia and Sindona, 2012; Adamo, et al. 2009; Furia et al., 2013). Specifically, the monomers constituting the lignin polymer, p-Coumaryl alchol, Conferyl alcohol, and their derivatives (Henriksonn, 2009), provide exceptional moieties for heavy metal binding under different pH and other solution conditions (Furia and Sindona, 2012; Furia et al., 2013; Porwal et al., 2015).
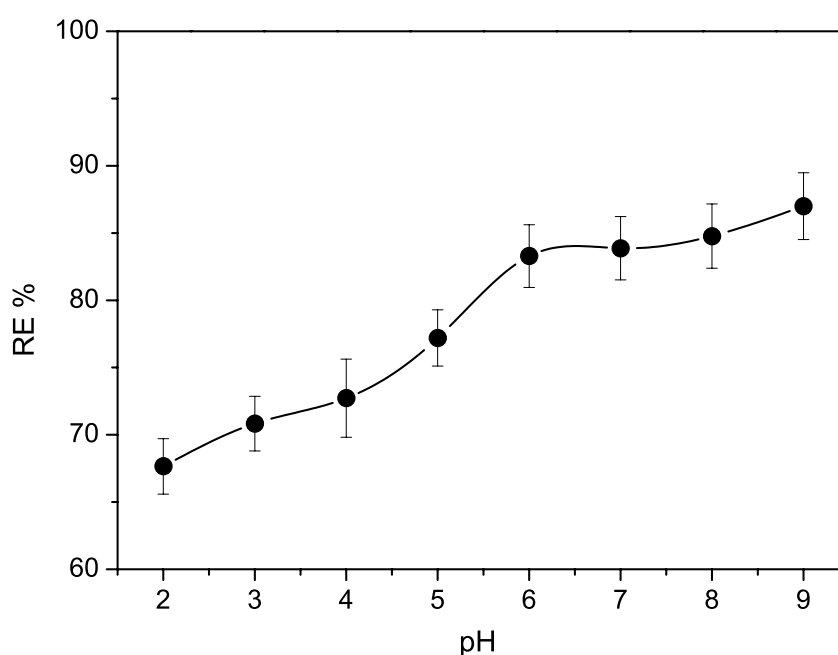
Figure 3.6 Hg(II) adsorption as a function of the initial pH ($C_0 = 80$ mg L^{-1}; W = 0.5 g, T = 298 K)

It is worth noting that all the adsorption experiments were carried out at pH = 5 and in the presence of chloride. These conditions served to approximate those of typical groundwater (INIGEMM, 2013), where the predominant species is $HgCl_2$ (Figure 3.4). Therefore, all the results reported in this work mainly reflect the adsorption of $HgCl_2$ and represent a lower limit of adsorption performances for SB. At increasing pH, the RE% increases (Figure 3.6), but other species come into play in the adsorption mechanism.

3.4.2 Effect of the contact time.

The experiment was featured varying mass of adsorbent (20 and 40 g) and the initial concentrations of Hg (II) (100 and 200 mg L-1), in agreement with exposed in the section 3.3. for evaluating the effect on the adsorption Hg. These parameters are very important for the subsequent analyzes, since it allows to determine the necessary time of contact of the adsorbate with the adsorbent, in order to reach its maximum adsorption performance under different conditions.

Figure 3.7 shows the trend of the Hg(II) concentration as a function of the contact time between the solution and the broom. There is a fast Hg concentration reduction during the first 60 minutes (Figure 3.7a), which leads to a removal percentage of over 70% in both tests (Figure 3.7b). The rate of mercury removal becomes subsequently much slower, until it reaches a plateau value, corresponding to the equilibrium condition. As can be seen from **Figure 3.7**, the equilibrium time, i.e. the time required to reach the maximum Hg(II) adsorption, it is not influenced by the Hg(II) concentration or by the amount of adsorbent material. Indeed, in both cases the equilibrium was reached after about 480 min (8 hours), resulting in an adsorption of more than 86%.
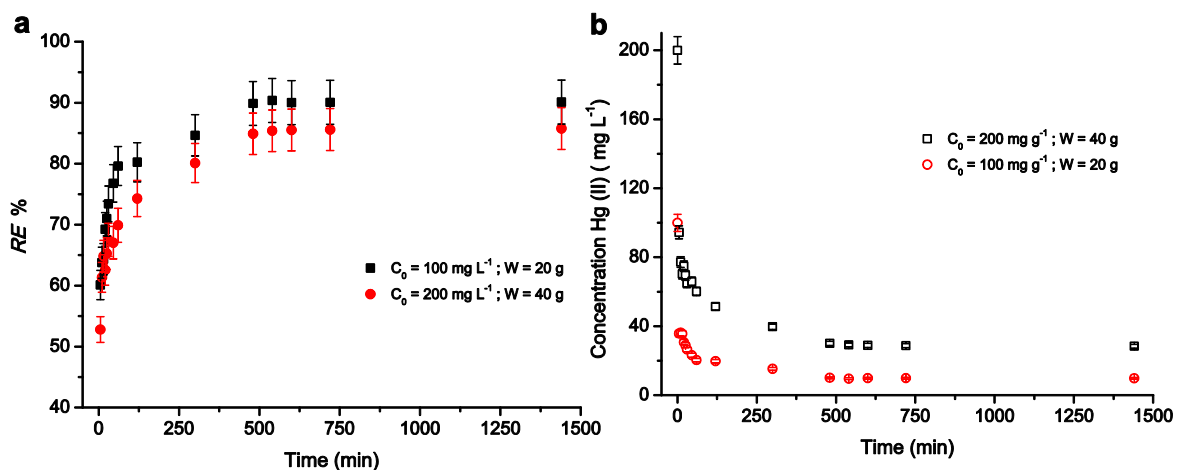
Figure 3.7 Removal efficiency (RE%) (a) and Hg(II) concentration (C_t) as a function of the contact time (b), at two different Hg(II) initial concentration (Hg 100 and 200 mg L^{-1}).

3.4.3 Effect of the initial concentration and of the adsorbent dosage.

The adsorption capacity (q_e) of the Spanish broom increases quite linearly with the initial concentration of Hg(II) in solution (C_0) almost in the whole range of initial concentrations considered, though at high concentrations a deviation from linearity does

occur (**Figure 3.8c**). This suggests that the Spanish broom has a limited number of adsorbent sites, which is fixed by its amount and by the experimental conditions adopted (mainly pH, temperature, solution volume/adsorbent mass ratio, etc.). Thus, q_e increases as long as free active sites are available on the broom. When all the active sites are involved by the adsorption process, the saturation and therefore the maximum adsorbent capacity per unit mass of adsorbent material (q_m), is achieved.

Due to the above trend, the adsorption efficiency of the broom, defined as the percentage of mercury removal from the solution, is almost independent of C_0, assuming an average value of (67 ± 5) %, (**Figure 3.8a**). In contrast, the equilibrium concentration of Hg(II) in solution monotonically increases with C_0 (**Figure 3.8a**). However, it is worth noting that at low initial concentrations (< 10 mg L^{-1}), the equilibrium concentration falls in the ppb range (**Figure 3.8a**).

Figure 3.8. (a) Effect of the initial concentration on the adsorption process (W = 0.5 g, V= 50 mL); (b) effect of the adsorbent dosage on the efficiency of the adsorption process (C_0 = 80 mg L^{-1}, V= 50 mL); (c) Adsorption capacity of the Spanish broom as a function of the initial Hg(II) concentration. Experimental conditions: 1.0 g of Spanish broom, 100 mL of Hg(II) solution, pH = 5, T = 294 K.
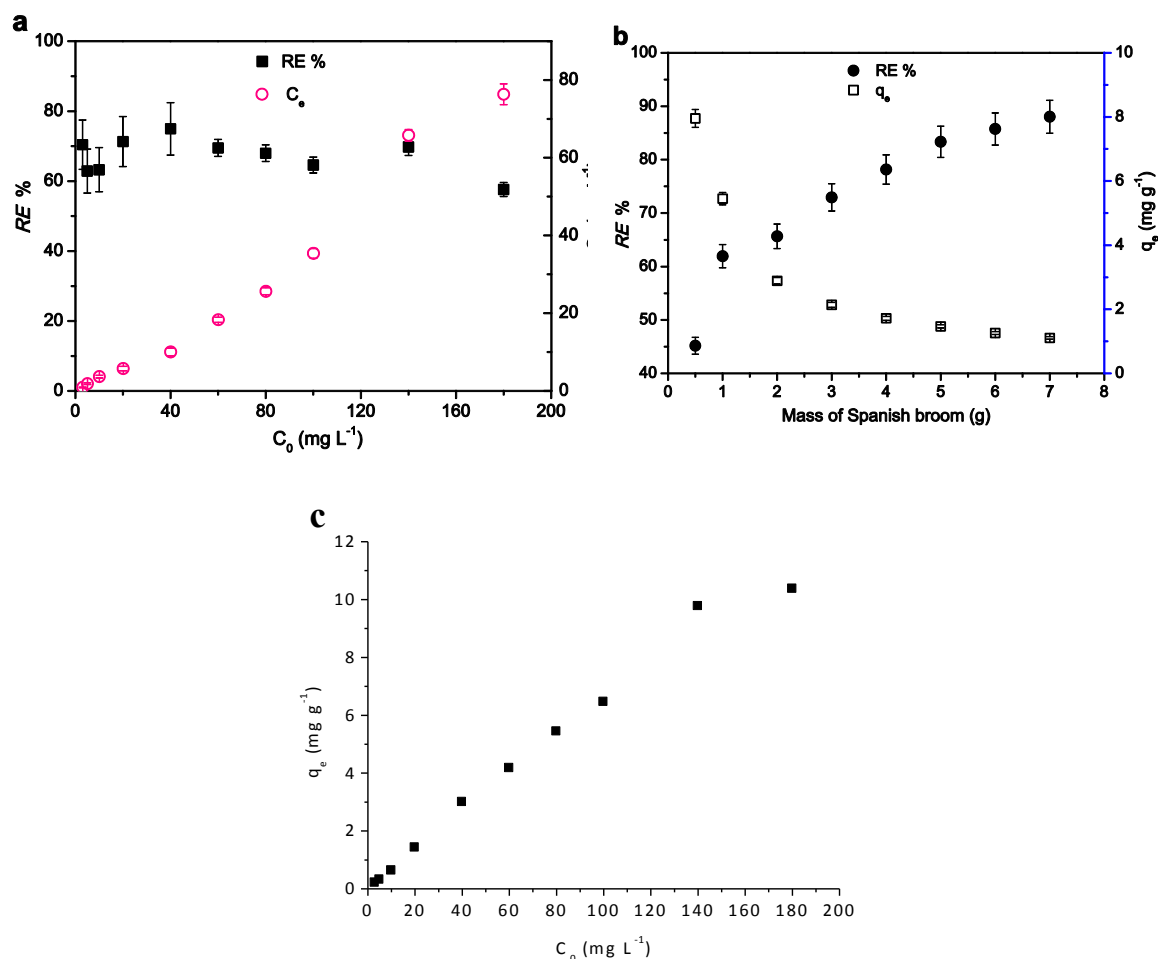
It is expected that the percentage of mercury removal depends on the adsorbent dosage, being the other conditions the same (Rao et al., 2009). This is actually the case, as illustrated in **Figure 3.8b**. Adsorption efficiencies as high as 87 % were found at 7 g of Spanish broom suspended in 50 mL of a 80 mg L^{-1} solution of Hg(II).

It is also evident from the plot in **Figure 3.8b** that the efficiency increases with the increase of the mass of Spanish broom. On the other hand, the adsorption capacity has an opposite trend and decreases with the adsorbent mass. Both these trends strongly indicate a situation far from the saturation, due to the large excess of available active sites. Moreover, it is interesting to note that the above trends are nonlinear and both the observables seem to tend to a plateau value that is determined by the thermodynamic of the adsorption processes.

3.5   Adsorption kinetics of the adsorbent.

The mechanism of adsorption of ions and other substances such as dyes on solid porous surfaces (particle), generally involves several steps characterized by different rates, in which the solute diffuses into the adsorbent material.

In the Chapter 2 section 2.2 were described the models used for adsorption kinetics study and the section 3.3 was detailed the conditions for all batch experiments, the results obtained was evaluated and plotting, by Origin 8.0. The graphs show the standard deviations of the data and the captions describe the conditions of the experiment.

The complexity of the adsorption process can be fully displayed in a q_t *vs.* t$^{1/2}$ plot, according to equation (2.14) (Weber and Morris, 1962), generally showing a multilinearity in the set of kinetic data in any adsorption experiment where intraparticle diffusion (IPD) occurs (Wu et al., 2009). **Figure 3.9a** shows the IPD plot for the Hg(II) on the Spanish broom fiber. As can be observed, three linear regions were identified corresponding to different diffusion steps.

The initial, most rapid one, is related to the external surface adsorption during which the Hg(II) species moves from the bulk of the solution to the fiber surface. The second linear region may be related to the gradual diffusion of the solute into the pores of the lignocellulosic matrix. The final equilibrium process may involve a very slow diffusion

of the Hg(II) species from larger pores to smaller ones or from lignin rich to cellulose rich regions, being the adsorbent material a lignocellulosic composite.
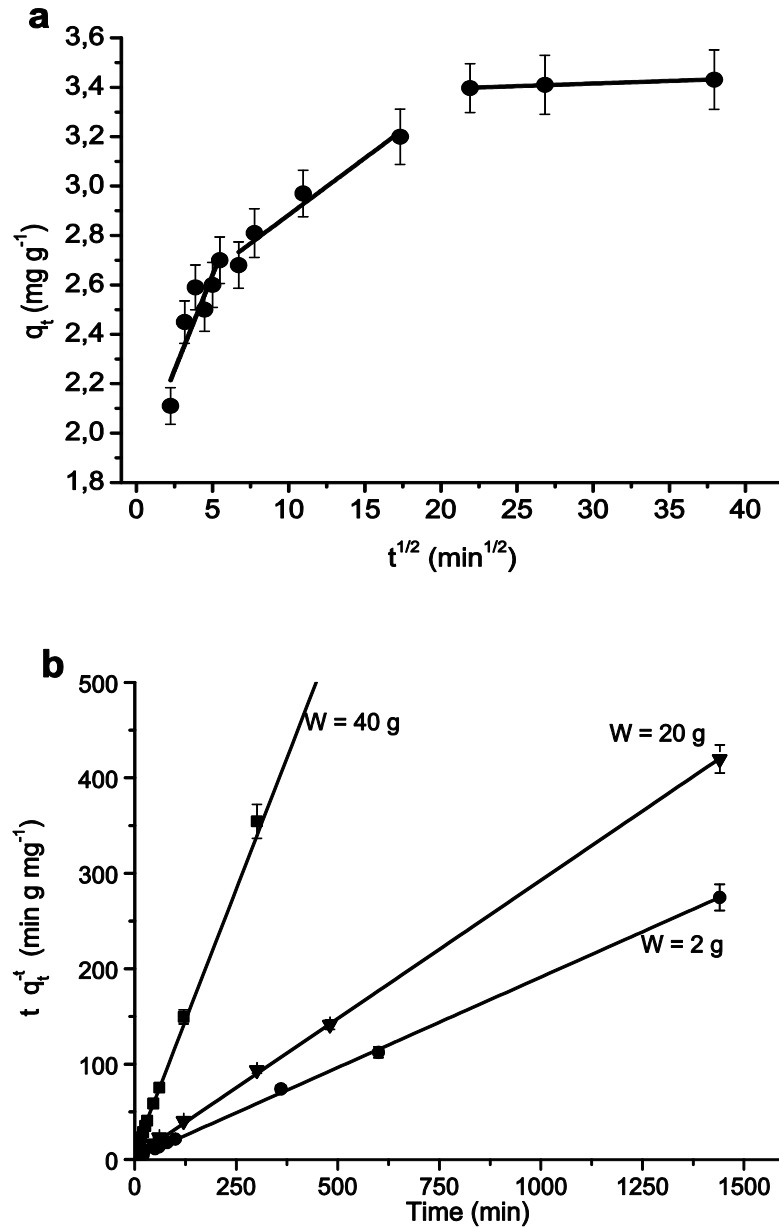
Figure 3.9. Adsorption kinetics. (a) Intraparticle diffusion plot showing three regions of linearity (C_0 = 200 mg/L, V = 0.100 L, W = 5 g, T = 298 K). (b) Pseudo second order plots showing the fitting between the experimental data points, obtained for three different adsorbent material masses, and the linear function described by eq. (2.13)

The values of k_p and R_i are reported in **Table 3.2** for three batch experiments which only differ for the employed mass of fiber. The calculated R_i ratio is less than 0.5 (**Table 3.2**) indicating that the adsorption kinetics has a strong extent of surface adsorption that accounts for more than 80% increase of q_t (Juang et al., 2002; Tunali et al., 2006), that

is to say that most of the adsorption of Hg(II) occurs on the surface of the Spanish broom fiber.

The IPD model provides a fractional description of the adsorption kinetics of Hg(II) species on the fiber, highlighting that a variety of processes takes place according to the existence of active binding sites either on the surface of the fiber or at its interior. However, it does not provide a whole description of the entire set of kinetic data. A complementary approach is to calculate the number of free active sites per unit mass of fiber at time t (S_f) by assuming a pseudo first order or a pseudo second order kinetics (Ho, 2006). These models rely on the assumption that the following adsorption equilibrium holds:

$$S_f + Hg(II) = S\text{-}Hg(II) \qquad\qquad \text{(equilibrium 2)}$$

where, S-Hg(II) is the mercury-fiber complex formed upon adsorption, corresponding to the number of occupied active sites per unit mass of fiber (S_o).

The pseudo first order kinetics was fitting through the plot of log (q_e - q_t) versus t (eq. 2.6), its plot failed to reproduce the entire set of data (Figure 3.10), in agreement with similar observation on different adsorbent materials (Zabihi et al., 2010).
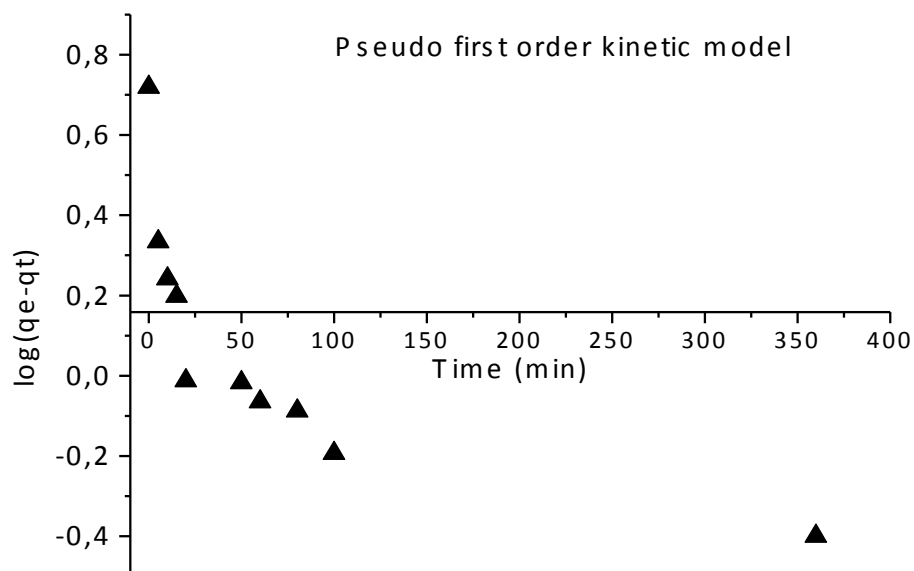

Figure 3.10. Pseudo first order kinetic plot

In contrast, very good fitting results were obtained with the pseudo second order model (Figure 3.9b and Table 3.2). It assumes that the rate of change of the concentration of occupied active sites per unit mass of the adsorbent material, is proportional to the

square of the concentration of free active sites per unit mass of sorbent (Ho and McKay, 1999; Kumar, 2006). Where the values of R^2 obtained from the fit the data plotting, of the ratio t/q_t as a function of t (eq. 2.13), are higher of 0.999.

The key parameters k_2 and q_e can then be directly extracted from the linear fitting (Figure 3.8b), whose results are reported in **Table 3.2**.

In agreement with the results discussed before in **Figure 3.7b**, the equilibrium adsorption capacity decreases with the increase of the adsorbent mass. In contrast, the pseudo second order rate constant decreases with the reduction of the mass of fibers due to the decrease of the total number of active sites.

Table. 3.2. Fitting results of the pseudo second order kinetic model.

| W (g) | IPD model | | | Pseudo second order model | | |
	K_p (mg g^{-1} min-$^{1/2}$)	R_i	R^2	k_2 g mg^{-1} min^{-1}	q_e (mg g^{-1})	R^2
40.00[b]	0.040 (0.004)	0.36	0.9493	0.137 (0.031)	0.908 (0.003)	0.9998
20.00[c]	0.15 (0.04)	0.31	0.7643	0.0280 (0.007)	3.45 (0.02)	0.9995
2.00[d]	0.10 (0.02)	0.22	0.9025	0.0193 (0.006)	5.29 (0.04)	0.9997

[a]Values in parentheses are the standard deviation of the data. [b]C_0 = 100 mg/L, V= 0.400 L, W = 40.00 g; [c]C_0 = 200 mg/L, V= 0.400 L, W = 20.00 g; [d]C_0 = 100 mg/L, V= 0.400 L, W = 2.00 g;

The above results support a chemisorption mechanism in which the interaction between the functional groups of the sorbent and $HgCl_2$, leads to the formation of mercury-lignocellulosic complexes (S_f-Hg(II)), as supposed with the equilibrium (1). This interaction may involve either the hydroxyl groups of cellulose and lignin or the carboxyl groups of lignin. However, it is known that cellulose is a poor sorbent of heavy metal cations and that it should be activated by chemical modification in order to improve its adsorption capacity (Demirbas, 2008). This is due to the unfavorable interaction between the soft Hg(II) metal (Pearson, 1963) and the hard hydroxyl groups of cellulose. On the other hand, Hg(II) may better interact with the more acidic carboxyl groups of lignin. This hypothesis is in agreement with the fact that lignin can form both monodentate and bidentate complexes with $HgCl_2$ through the involvement of both carboxyl and phenol binding sites (Lv et al., 2012).

This mechanism should lead to a pH decrease following adsorption due to the concomitant release of chloride acid into the aqueous medium. We verified this mechanism by observing that the final pH of the solution after adsorption is lower than

the initial one (pH = 5), ranging from 4.3 to 4.8 and systematically decreases with the increase of the initial Hg(II) concentration (Table 3.3). This indicates that the above reaction do effectively occurs with the release of hydrochloric acid in solution. Thus, the complexation of HgCl$_2$ by the lignocellulosic fibers, evidently involves the acidic functional groups of the fibers, mainly located on lignin.

Hg(II) Concentration (mg L^{-1})	pH
10ppm	4.80
20 ppm	4.73
40 ppm	4.72
60 ppm	4.65
80 ppm	4.64
100 ppm	4.29
180 ppm	4.28

Table. 3.3. Final pH values as a function of the initial Hg(II) concentration

3.6 Adsorption isotherm of adsorbent.

The plot of the adsorption capacity (q_e) versus the equilibrium concentration of a solution (C_e) at constant temperature is called adsorption isotherm. The mercury adsorption isotherms at several temperatures are reported in **Figure 3.11**. They show a rather rapid increase of the adsorption capacity for low C_e values and a decrease of the slope at higher equilibrium concentrations, suggesting the existence of plateau values for the adsorption capacity.
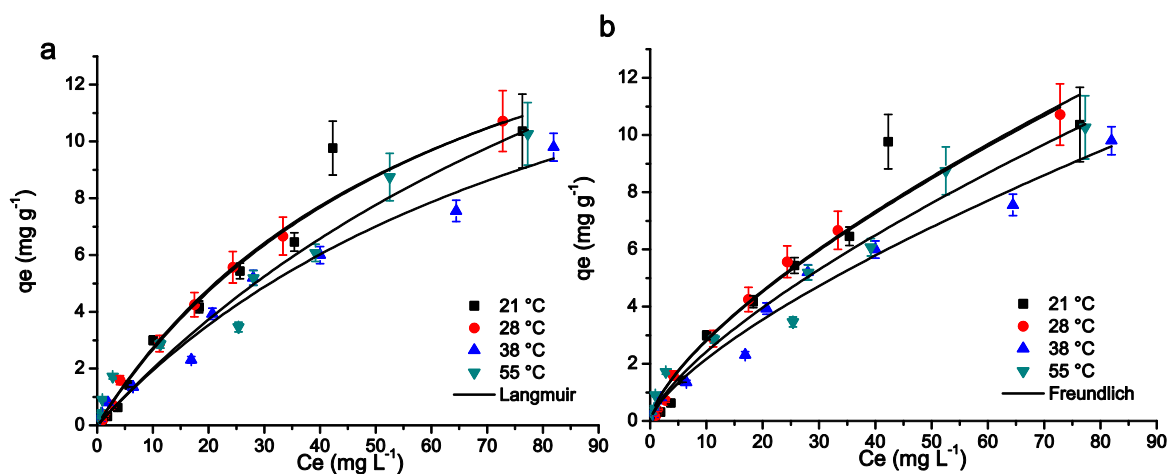

Figure 3.11 Experimental adsorption isotherms for mercury at different temperatures and nonlinear curve fitting with the Langmuir (a) and Freundlich model (b)

This trend should correspond to an L-type isotherm according to Giles et al. (1974), which can be suitably described by the Langmuir model (eq. 26) (Limousin et al., 2007; Atkins et al., 2006). This model assumes that the adsorption process is restricted to a monolayer surface coverage on a uniform surface exhibiting equivalent binding sites and that there are not interactions among the adsorbed solute species that may affect the adsorption mechanism (Atkins et al., 2006). Due to the limited number of active sites on the surface of the adsorbent material, the maximum adsorption capacity, q_m, and K_L can be determined from the slope and intercept of plot of C_e/q_e against C_e. Where, K_L is the Langmuir adsorption constant related to the equilibrium distribution constant K_d at very low q_e far from the saturation (eq. 3.9):

$$K_L = \frac{q_e}{C_e(q_m - q_e)} \cong \frac{q_e}{C_e q_m} = \frac{K_d}{q_m} \text{ , in the limit } q_e \ll q_m; \text{ with } K_d = \frac{q_e}{C_e} \tag{3.9}$$

The results of the nonlinear curve fitting with the Langmuir model are summarized in **Table 3.4**

Good results were obtained also with the Freundlich model (Table 3.4 and Figure 3.11b), which does not introduce any limitation on the mechanism of surface coverage (eq. 2.18) (Limousin et al., 2007; Haghsererth and Lu, 1998).

The mechanism of monolayer adsorption is further supported by the fact that a multilayers model, such as that of Elovich (Hamdaoui and Naffrechoux, 2007), is not able to reproduce the experimental set of data (Figure 3.12), with R^2 values lower than 0.7 in all test.
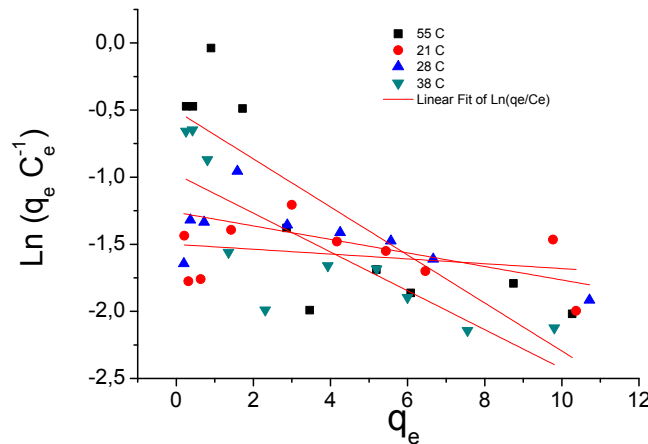

Figure 3.12. Linear fitting with the Elovich model of the adsorption isotherm data

Table. 3.4 Langmuir and Freundlich adsorption isotherms parameters

T (K)	Langmuir model			Freundlich model		
	K_d [a] $(cm^3 g^{-1})$	q_m $(mg\ g^{-1})$	R^2	K_F $(mg^{(1-n)}\ g^{-1}\ L^{1/n})$	n	R^2
294	315 (6)	20 (4)	0.96038	0.6 (0.2)	1.5 (0.2)	0.93719
301	307 (5)	20 (1)	0.99752	0.58 (0.07)	1.46 (0.07)	0.99090
311	223 (3)	20 (4)	0.97901	0.43 (0.09)	1.4 (0.1)	0.97997
328	213 (4)	28 (11)	0.95729	0.5 (0.1)	1.4 (0.1)	0.96730

[a] Calculated with eq. (10); K_d becomes dimensionless if the density of the solution is assumed equal to that of water. Values in parentheses are the standard deviation of the data.

3.7 Thermodynamic of the adsorption.

The Langmuir model has been used to extract the thermodynamic quantities related to the adsorption isotherms. The distribution constant K_d has been used to calculate the Gibbs free energy ΔG^0_{ads} using equation 3.9. The value of ΔG^0_{ads} = -14.2 (0.3) kJ mol^{-1}, averaged over the temperature range considered, clearly indicates that the adsorption process is spontaneous (Mondal et al., 2013; Gupta and Nayak, 2012). By applying the van't Hoff equation (3.6), the adsorption enthalpy was also derived from the slope of the plot of lnK_d versus T^{-1} (**Figure 3.12**), with the assumption that ΔH^0_{ads} is independent on T in the restricted temperature range considered.

$$\frac{d}{d(T^{-1})} lnK_d = -\frac{\Delta H^0_{ads}}{R} \qquad\qquad (3.10)$$

The negative enthalpy value ΔH^0_{ads} = -10 (3) kJ mol^{-1}, indicates that the adsorption of mercury on Spanish broom fiber is exothermic, in agreement with the decreases of the equilibrium distribution constant with T (**Table 3.4** and **Fig. 3.13**).
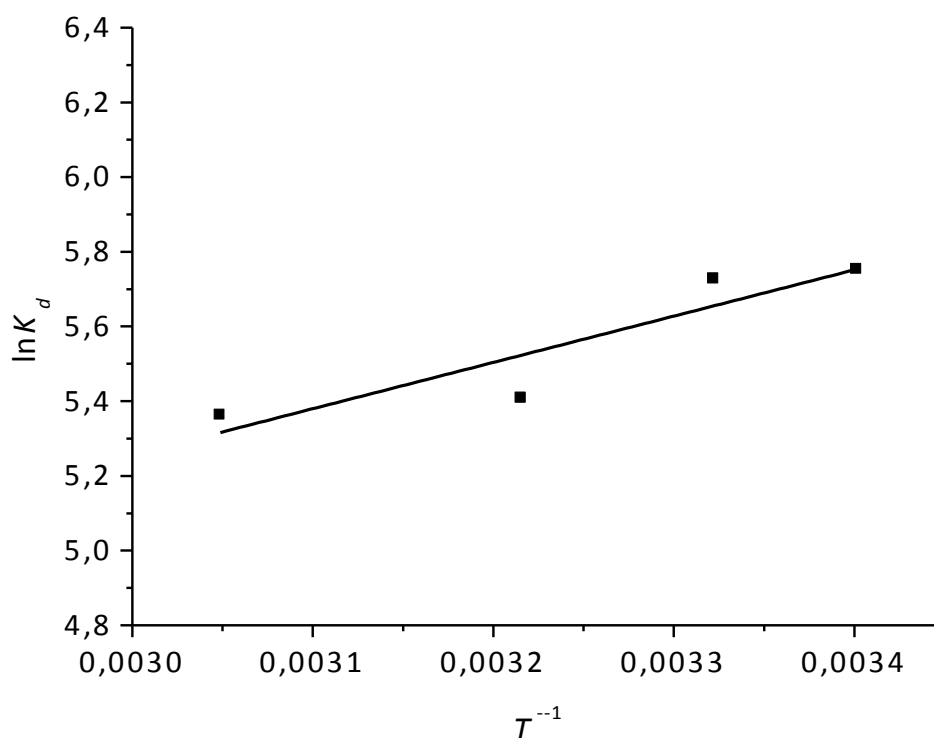
Figure. 3.13. Dependence of the distribution constant on T and extraction of the adsorption enthalpy from the slope of the line fitting the data.

Finally, the maximum adsorption capacity does not change significantly with T, indicating that the adsorption efficiency of the Spanish broom is quite independent of the temperature. The Spanish broom shows a good adsorption capacity compared to other materials (Zabihi et al., 2009; Gupta et al., 2015; Lv et. al, 2012; Yee et al., 2013; Bag et al., 2007; Shin et al., 2007; Feng et al., 1997; Liu et al., 1998; MacKay et al., 1989; Li et al., 2014) which, however, must be activated with chemical or physical pretreatments or even prepared by chemical synthesis (**Table 3.5**).

Table. 3.5 Adsorption capacity of mercury(II) by various materials

Adsorbent material	q_m (mg g^{-1})	Reference
Thiol functionalized porous organic polymer-based nanotrap (PAF-1-SH)	1,014	Li et al., 2014
Chitosan	815	MacKay et al., 1989
Thiol-monolayer-functionalized mesoporous silica	505-600	Feng et al., 1997 Liu et al., 1998
Thiopyrene-featured porous carbon	518	Shin et al., 2007
Chalcogel-1	645	Bag et al., 2007
Rice husk (sulphuric acid treatment)	384.62	Gupta et al., 2015
Cystoseira baccata	329	Gupta et al., 2015
Electrospun sulfur copolymer. Poly(sulfur-statistical-diisopropenylbenzene)	19.7-327.7	Thielke et al., 2016
MOF Zr-DMBD	197	Yee et al., 2013
Tolypocladium sp. (residue from fermentation industry)	161.1	Gupta et al., 2015
Walnut shell (ZnCl$_2$ chemical activation)	151.50	M. Zabihi et al., 2009
Furfural	174	M. Zabihi et al., 2009
Lignin	77.7	Lv et. al, 2012
Wheat bran (chemical modification)	70.00	Gupta et al., 2015
Coal adsorbents (Seyitorner)	56	M. Zabihi et al., 2009
Carbon Aerogel	34.96	M. Zabihi et al., 2009
***Spanish broom* (bulk)**	**20**	**This study**
Commercial activated carbon	12,38	M. Zabihi et al., 2009
Coconut (chemical modification coir pith PGCP-COOH)	13.73	Gupta et al., 2015
Sulfo-calcic ashes	4.9	M. Zabihi et al., 2009
Waste Rubber	4	M. Zabihi et al., 2009
Silico-aluminous ashes	3.2	M. Zabihi et al., 2009
Fuller's earth	1.145	M. Zabihi et al., 2009
Granular activated carbon	0.8	M. Zabihi et al., 2009
Activated carbon (fertilizer waste)	3.62×10^{-3}	M. Zabihi et al., 2009

Chapter 4.

4 DYNAMIC STUDY IN COLUMN

4.1   Flow cell experiments

Adsorption experiments were also carried out by pumping the Hg(II) solution within a Spanish broom filter. The grinded plant was packed into a clear acrylic column (flow cell) of 15 cm length and an inner diameter of 56 mm. Packing was conducted taking care to create an homogeneous porous medium. At both ends of the column, the broom was retained by a non-woven membrane, a metal plate 2-mm thick with 2.5-mm wide openings and a closing flange. The aforementioned configuration ensures that the entire cross section of the filtering material is affected by the flow of the solution. The inlet flow rate (at the bottom of the column) was fixed by a peristaltic pump (model PD 5101, Heidolf). The outlet flow rate (at the top) was sampled in time to trace the breakthrough curves describing the adsorption performances of the broom in the different conditions adopted for each experiment (Figure 4.1). For this purpose different amounts of adsorbent material were used (80 g and 115 g) and subjected to different flow rates (19, 15, and 10 mL min^{-1}) having the same mercury concentration of 100 mg L^{-1}.
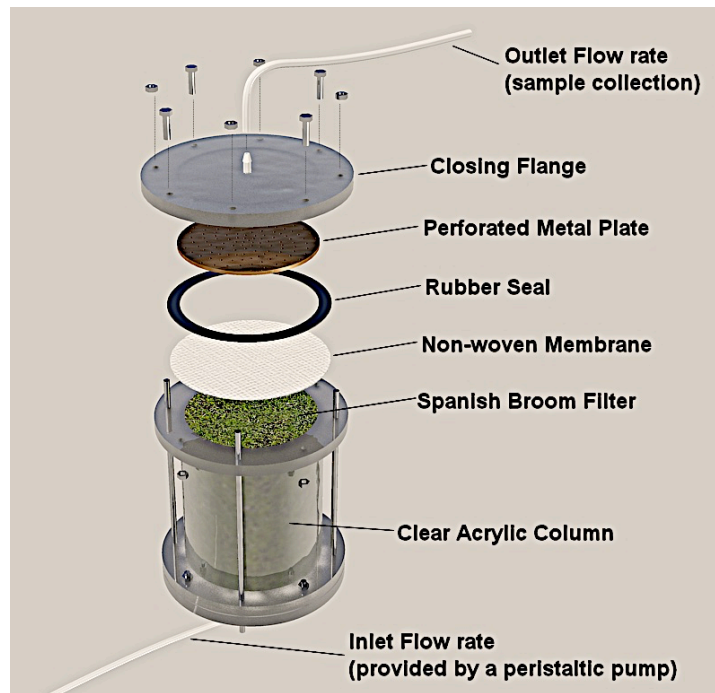
Figure 4.1 Sketch of the experimental apparatus

The following tests were designed and performed (mass of adsorbent material – flow rate): a) 80 g – 19 mL min^{-1}; b) 115 g - 19 mL min^{-1}; c) 115 g - 15 mL min^{-1} and d) 115 g – 10 mL min^{-1}. Sampling was realized every 30 minutes.

121

4.2   Hydrodynamic characterization of Spanish broom.

The material adopted for the production of filters and barriers for water remediation from heavy metals, need to be investigated, its physical properties. The knowledge on how the material allows the water to flow through it, depending on its packing and compaction status, plays a fundamental role in the design of the filtering system. Several laboratory tests were performed to obtain the hydrodynamic properties of the woody fibres. A constant head permeameter was used in order to find the variation law of the hydraulic conductivity with respect to the density of the Spanish broom. The permeameter (Fig. 4.1) above mentioned has been used for the test. The cell was packed with the Spanish broom and eight samples with different density, were analyzed.

A Mariotte bottle was used to maintain a constant hydraulic head condition at the inflow section of the cell. The same hydraulic head of 15 cm was imposed for all the analyzed samples. The Mariotte bottle was completely filled with tap water for all the performed measurements, ensuring an entering volume to the cell of 76 mL. Once a sample was arranged in the flow cell, the time necessary to a given water volume to pass through the material was recorded. The aforementioned water volume was monitored by reading the variation of the water level in the Mariotte bottle. Five identical water volume were observed for the same investigated sample, and five flow rate values were evaluated as well. The hydraulic conductivity value, corresponding to each flow rate, was estimated by using Darcy's Law.

The average value of hydraulic conductivity, calculated from the five determined for each sample, was finally adopted. The sample weight, employed between the different test series, was increased, each time, of 10 g: starting from 70 g (sample 1) to 140 g (sample 8).

The obtained variation law is shown in the following graph:
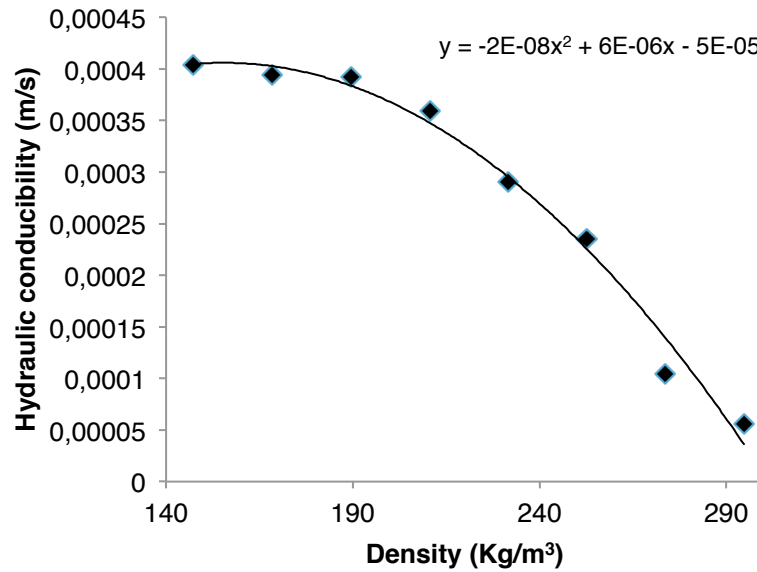
Figure 4.2 Density vs. Hydraulic conductivity

A parabolic law was found. The curve is a branch of a parabola showing that an increase of the sample density results in a hydraulic conductivity decrease.

Moreover, the relation between the density with the porosity was established too. Several samples, with different density, were analyzed by means of the double-weight method in order to measure the total porosity. In this case a linear law was found between the porosity and the density (Fig. 4.3)
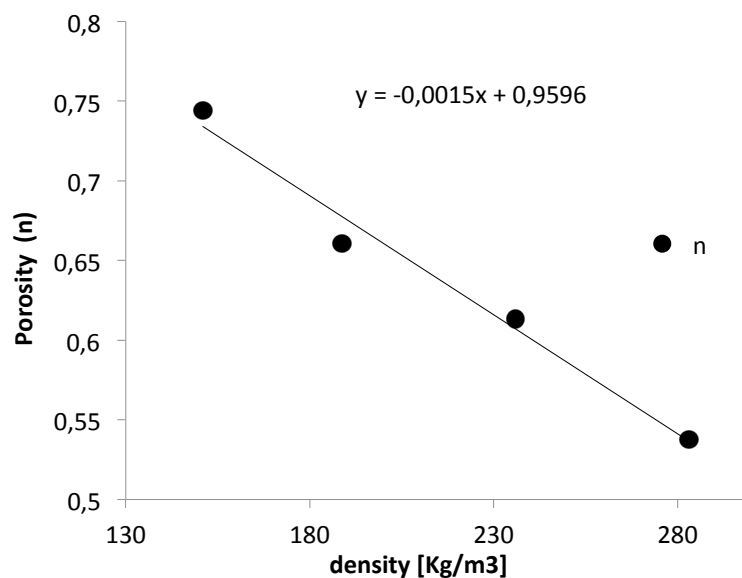
Figure 4.3 Density vs. Porosity

123

Thanks to this characterization we can predict how much material should be used in a PRB to reach a hydraulic conductivity value higher than the one of the soil in which the barrier must be inserted.

4.3 Application Thomas model.

Figure 4.4 shows the breakthrough curves obtained by plotting the ratio between the outlet (C_t) and inlet (C_0) concentration of Hg(II) as a function of time, under different sorbent mass (*m*) and different flow rates (Q). It can be seen that, for a given mass, as the flow rate decreases the exhaustion point, i.e., the point at which the adsorbent bed is fully saturated, shifts forward in time.

According to the literature (Bear, 1972; Dagan, 1989; Neuman, 1990), this is a typical behavior and is due to the fact that at decreasing flow rates the concentration of mercury per unit time flowing through the column is lower, being the other conditions the same. Therefore, the exhaustion point occurs later.

On the other hand, at the same flow rate, as the adsorbent mass increases the exhaustion point occurs later. This can be explained by taking into account the increase of the overall number of active sites as the m/C_0 ratio increases.
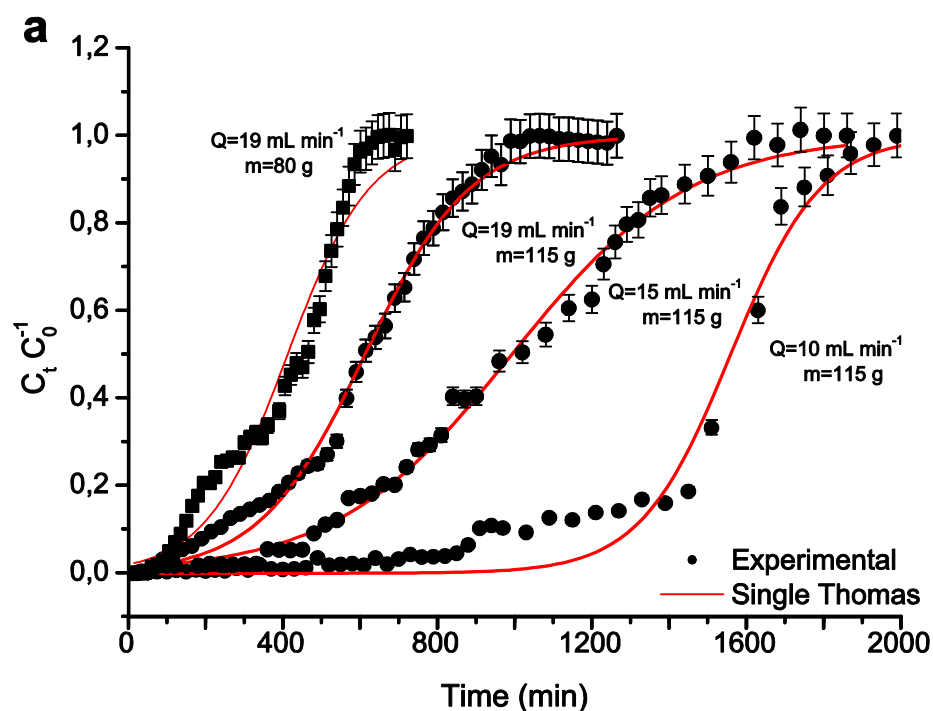
Figure 4.4 Breakthrough plots showing the C_t/C_0 ratio as a function of time with an inlet Hg(II) concentration $C_0 = 100$ mg L^{-1}. Solid lines are the fitting curves modeled by a Single Thomas (a) and a Double Thomas model (b). The two breakpoints, common to all the S-shape curves, are indicated by arrows.

However, in contrast to a typical S-shape trend generally observed for a breakthrough curve collected during constant injection tracer tests (De Marsily, 1986; P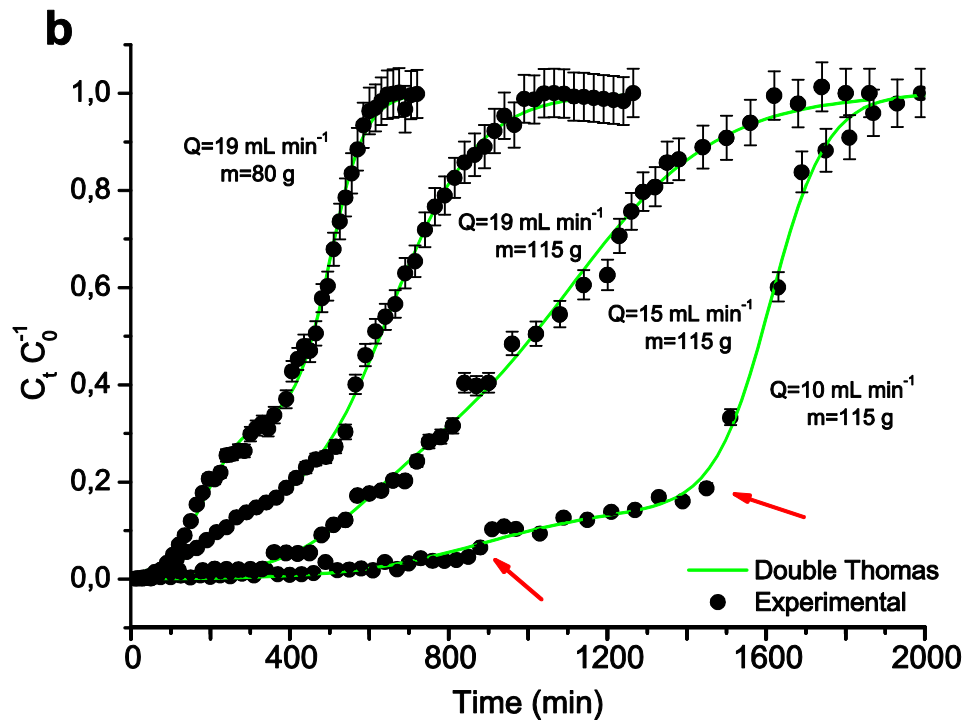ugliese, 2013), here we observed a systematic double S shape behavior. Indeed, we can clearly identify two breakpoints, one intermediate and a final pseudo-exhaustion point on each curve reported in **Figure 4.4**. This suggests that mercury adsorption occurs in at least two processes with different timescales. According to the batch results regarding the adsorption kinetics (**Figure 3.8**), it can be advanced the hypothesis that, during column operation, the adsorption mechanism involves the surface active sites in the first events until they become totally occupied, and then the inner ones which, however, contribute to a lesser extent to the overall adsorption. As highlighted in section 3.4, in which the adsorption kinetics of the batch tests have been discussed, Spanish broom fibers are responsible of a diffusion process involving different solute transport steps (IPD). This process is probably the same observed during column dynamic tests and causing the occurrence of the double S shape curves. The hypothesis is that the adsorption mechanism should first involve all the external superficial active sites of the fibers, and then the ones settled within the fibers which, however, give a minor contribute to the overall adsorption process. When a solution flows within a porous medium, the solute is

125

transported according to three main processes: advection which is originated from the fluid's flow which in turn is determined by the fluid's physical properties and by the geometry and physicochemical properties of the bounding solid, kinematic dispersion causing macroscopic mixing because of local velocity variations, and diffusion resulting from the molecules thermal motion (De Marsily, 1986).

The flow rates adopted for the column tests were calibrated to reproduce a velocity field typical of groundwater systems. In such systems, the relative importance of the three aforementioned solute transport phenomena is indicated by a dimensionless parameter known as the Peclet Number (Pe). It is defined as:

$$Pe = \frac{q\sqrt{k_0}}{nD_0} \qquad (4.1)$$

where q (m s^{-1}) is Darcy's velocity, k_0 (m^2) is the intrinsic permeability of the porous medium, n is the porosity, an D_0 (m^2 s^{-1}) is the diffusion coefficient. When $Pe \gg 1$ transport by advection is faster than transport by diffusion, and the system is advection dominated. As the Peclet Number decreases the three processes become comparable. For small values ($Pe < 1$), diffusion dominates (De Marsily, 1986). **Table 4.1** shows the Peclet Numbers calculated for all the column tests performed in this study.

The results demonstrate that the transport process occurred in the experiments is mainly driven by diffusion, confirming the theory on how the double S curves have been generated.

In the hypothesis of Langmuir adsorption isotherm and a second order adsorption kinetics, the breakthrough curves can be modeled by the Thomas model (Mustafa and Ebrahim, 2010), given by equation 4.2:

$$C_t / C_0 = \frac{1}{1 + e^{-k_{Th}C_0 t} e^{k_{Th}q_0 m/Q}} \qquad (4.2)$$

where, k_{Th} (mL min^{-1} mg^{-1}) and q_0 (mg g^{-1}) are the Thomas constant and the maximum adsorption capacity, respectively.

4.4   Double-Thomas Model

However, the fitted curves reported in **Figure 4.4b**, clearly evidence that the Thomas model is not able to reproduce the experimental trend. Actually, strong deviations from the Thomas model occur in the intermediate portion of the breakthrough curves. This is due to the fact that this model does not take into account the two processes mentioned above, both contributing to the adsorption. Since the experimental points describe a double S-shape curve, we tried to fit them with a double Thomas model given by equation 48:

$$C_t / C_0 = \frac{f}{1 + e^{-k_{Th\_1}C_0 t} e^{k_{Th\_1}q_{0\_1}m/Q}} + \frac{1-f}{1 + e^{-k_{Th\_2}C_0 t} e^{k_{Th\_2}q_{0\_2}m/Q}} \qquad (4.3)$$

where, the new parameter f, was named Active Surface Sites Fraction (ASSF). Obviously, if f assumes a value equal to 1 the equation 4.3 (Double-Thomas Model) becomes identical to equation 4.2 (Single-Thomas Model). This parameter can be mathematically described as the difference between the C_t/C_0 ratio at the beginning and at the end of the first breakthrough curve while 1-f is the analogous difference for the second breakthrough curve; k_{Th_1}; k_{Th_2} and q_{0_1}; q_{0_2} are the Thomas constants and the maximum adsorption capacities for the first and second process, respectively. The parameter f also takes a clear physical meaning from which its name derives. Being a number in the 0-1 range, it discriminates the fraction of Hg(II) species adsorbed by the superficial active sites from that adsorbed by the inner ones (1-f). For a given adsorbent mass, f is a function of the contact time between the aforementioned mass and the solution flowing through it. As can be seen in **Table 4.1**, the ASSF decreases with decreasing injected flow rates (row 2-4). A lower flow rate results in a higher contact time which allows the ions to reach and involve, in the adsorption process, more inner active sites. Considering hence the experiments performed with the same flow rate and different adsorbent mass, f decreases with the increase of the latter (row 1 and 2). The increase in mass, for a given volume, of the adsorbent material causes a density variation of the filter which in turn results in a porosity decrease. The lower porosity reduces the effective transversal area available for the solution flux, resulting in a reduced involvement of the superficial active sites. The Double-Thomas Model fitting

127

lines are displayed in **Figure 4.4b** and the related fitting parameters are collected in **Table 4.1**.

This model better fits the experimental data with respect to the Single-Thomas Model, with R^2 values always larger than 0.996. Interestingly, the Thomas constants associated to the two processes have quite similar values, suggesting that the kinetic mechanism undergoing the two processes is the same.

Notably, the breakthrough step of the S-shape curve (*f*) related to the first process has a tendency to decrease with decreasing flow rate, and tends to be vanishingly small for very low flow rates. It can be argued that, in such a case, the second process is quite indistinguishable from the first (the two are quite overlapped) because the system has enough time to equilibrate under low flux conditions.

As **Table 4.1** shows, the maximum adsorption capacities increases as the flow rate decreases, being the other conditions the same. As a matter of fact, the overall adsorption capacity, q_{0_2}, assumes values close to the batch ones (**Table 3.4**).

Table 4.1 Double-Thomas model fitting parameters

m (g)	Q (mL min^{-1})	$k_{Th\_1} \times 10^{-4}$ (mL min^{-1} mg^{-1})	$k_{Th\_2} \times 10^{-4}$ (mL min^{-1} mg^{-1})	q_{0_1} (mg g^{-1})	q_{0_2} (mg g^{-1})	f	Pe 1.	EC1/EC2	R^2 Double-Thomas	R^2 Single-Thomas
80	19	2.0 (0.2)	2.3 (0.1)	4.4 (0.2)	11.95 (0.07)	0.33 (0.01)	0.637	2.	0.9971	0.9652
115	19	0.98 (0.01)	0.99 (0.03)	4.5 (0.2)	11.22 (0.06)	0.23 (0.01)	0.577	5.1	0.9980	0.9953
115	15	1.0 (0.2)	0.54 (0.02)	4.9 (0.3)	9.6 (0.1)	0.20 (0.01)	0.455	3.4	0.9961	0.9964
115	10	0.6 (0.1)	1.41 (0.08)	7.7 (0.5)	14.02 (0.04)	0.15 (0.02)	0.303	1.4	0.9975	0.9764

Values in parentheses are the standard deviation of the data

The contribution of the two processes to the overall adsorption can be estimated by the ratio of the exhaustion capacities between the first (EC1) and the second process (EC2). The exhaustion capacity is defined as the mass of the adsorbate removed per unit mass of adsorbent at the saturation point (Gupta et al., 2016). It can be estimated by calculating the area overlaying the breakthrough curve up to the exhaustion point (Gupta et al., 2000; Gupta et al., 1997; Medvidovic´et al., 2008)

4.4.1   Exhaustion capacity calculation

The total mass (m) of mercury (II) retained in the column is given by the following integral:

$$m = Q \int_0^{t_e} (C_0 - C_t)dt \qquad (4.4)$$

where, t_e is the time at the exhaustion point.

Equation 4.4 can be re-written as the mass of solute retained in the column normalized with respect to the initial mercury concentration (C_0) at the volume of exhaustion (V_{ec}):

$$\frac{m}{C_0} = \int_0^{V_{ec}} (1 - \frac{C_t}{C_0})dV \qquad (4.5)$$

In order to estimate the contribution of the first and second adsorption process to the overall Hg(II) adsorption in the column, the following ratio was calculated, that is the ratio between the exhaustion capacity relative to the first adsorption process (EC1) and to the second one (EC2):

$$\frac{\frac{m_1}{C_0}}{\frac{m_2}{C_0}} = \frac{m_1}{m_2} = \frac{EC1}{EC2} = \frac{\int_0^{V_{ec1}}(1-\frac{C_t}{C_0})dV}{\int_{V_{ec1}}^{V_{ec2}}(1-\frac{C_t}{C_0})dV} \qquad (4.6)$$

where, m_1 and m_2 are the mass of Hg(II) retained in the column due to the first and the second process respectively; V_{ec1} and V_{ec2} are the volume at the intermediate and final exhaustion points, respectively.

As shown in **Table 4.1**, this ratio is larger than one, in agreement with the condition $m_1 > m_2$, i.e., the mass adsorbed in the first adsorption process is larger than that adsorbed in the second one.
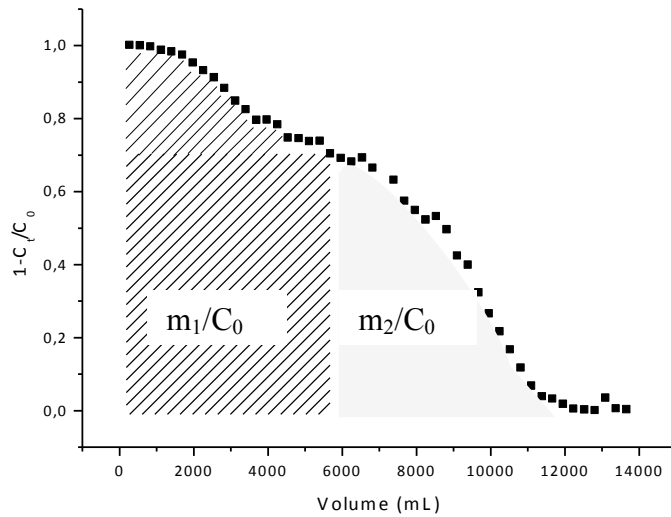
Figure 4.5 Illustration of the graphical integration of the breakthrough curve for the exhaustion capacities calculation.

If we compare the experiments performed under identical conditions (**Table 4.1 row 2-4**), we find that this ratio is always higher than 1 indicating that the first adsorption process contributes mainly to the overall adsorption. However, the EC1/EC2 ratio decreases in time with the flow rate (**Table 4.1**), indicating that, if the adsorbent bed is allowed to stay in longer contact with the solution, the second process becomes more important.

Chapter 5

5 DESIGN OF A REACTIVE PERMEABLE BARRIER (PRB), CASE STUDY.

Introduction.

The South American continent is rich in reserves of precious minerals exploited for centuries, and even today they represent a significant wealth source in many countries. However, the extraction methods of these metals have a high environmental impact, mainly caused by illegal mining and inadequate "handmade" mining practices which lead to the contamination of different water sources such as groundwater that is the most valuable stock of drinkable water.

Ecuador is a country that has a potential estimated (according to the National Development Plan of the Mining Sector 2011-2015) of 36.9 million ounces of gold, 72.4 million ounces of silver, 8.1 million tons of metallic copper, 28 471 tons of lead and 209 649 tons of zinc. Today the mining activities are an important economic resource contributing with the 1.30% of the Gross National Product (GNP).

Since the pre-Columbian era, Ecuador mined deposits of precious metals, concentrated mostly in the southern part of the country and primarily located in four regions: Ponce Enriquez, Santa Rosa, Zaruma and Portovelo Nambija. Among these stands, the Ponce Enriquez region which central town has the same name have the most significant

mineral deposits of Ecuador. The borders of Camilo Ponce Enriquez region are the province of Azuay on the West, Cuenca, and Naranjal at South. Guabo and Pucara on East by Santa Isabel and Cuenca, and to the West with the region of Guayaquil and Balao.

Figure 5.1 Localization of region of "Camilo Ponce Enriquez".

5.1   The importance of gold to the region of Ponce Enriquez.

The first economic activity in Ponce Enriquez region is the gold mining. According to Census carried out in 2010 (INEC, 2010), the majority of the population (42,6%) is dedicated to the extraction of metal ores, followed by 30,2% agriculture and animal farming. In the region, there is one of the most valuable and productive gold deposits in all the country; despite some technological improvements in recent years, the traditional mining continues.

According to the Ecuador Mining Regulatory Agency (ARCOM), in 2015, Province of Azuay secured 3.236.002,26 grams of gold, which 2.138.170,83 came from the Bella Rica mining settlement (Canton Ponce Enriquez) obtaining an economic income of 74.856.247,84   USD.   (http://www.controlminero.gob.ec/biblioteca/)Descargas   / Estadisticas Mineras 2015). In this Canton, there are close to 71 mining concessions, of which 51 are in force, and the others continue the process of conceding. Near to 70% of

the Canton area is in concession with permits of 15 to 20 years to small miners, national companies and some foreign.

Small-scale mining (including clandestine mining), as mentioned before, still using artisanal extraction processes. Foremost utilized technique for gold extraction uses metallic mercury (Hg) in a process called amalgamation. This procedure consists of the mixture of mercury in liquid form with the extracted mine material. When gold particles come into contact with mercury, the two substances mix to form a compound called amalgam. At the end of the process, the separation of gold from the collected amalgam mainly by heating. Roughly, two grams of mercury extract an ounce of gold.

5.2   Problems due to gold amalgam.

The gold mining that uses amalgamation process is a very polluting practice because only around 10% of added mercury reacts with the gold particles in the ground material that came from the mining.The remaining mercury (90%) is removed and recycled or discharged through the nearest receptor or directly dispersed into the environment which is the most dangerous practice. But even when the mercury is recycled results in a high polluting practice. Because it is common to place the solution in open tubs carved crudely into the soil that leads mercury infiltration to deep layers and become a broad focus of mercury contamination due it spread into the local environment becoming a threat to the ecosystem and surrounding people.

According to study by Carling et al. 2013, in the River Siete area of Canton Ponce Enriquez, we determined high levels of Methyl mercury in this water stream, compared with other rivers that are in other areas with mining activity, such as the river Calera (Portovelo) and the river Calixto (Nambija). Another investigation by Diaz X, 2015. Reports the presence of Mercury in hair samples of the inhabitants that drink water from wells (groundwater) in Tenguel and in the lower area of Ponce Enríquez, these values vary 500 ng/g in the Conchero well up to 2000 ng/g in the San Rafael Well. These studies reveal that the population is continually in contact with a source of mercury contamination that can lead to serious consequences on the health of the population.
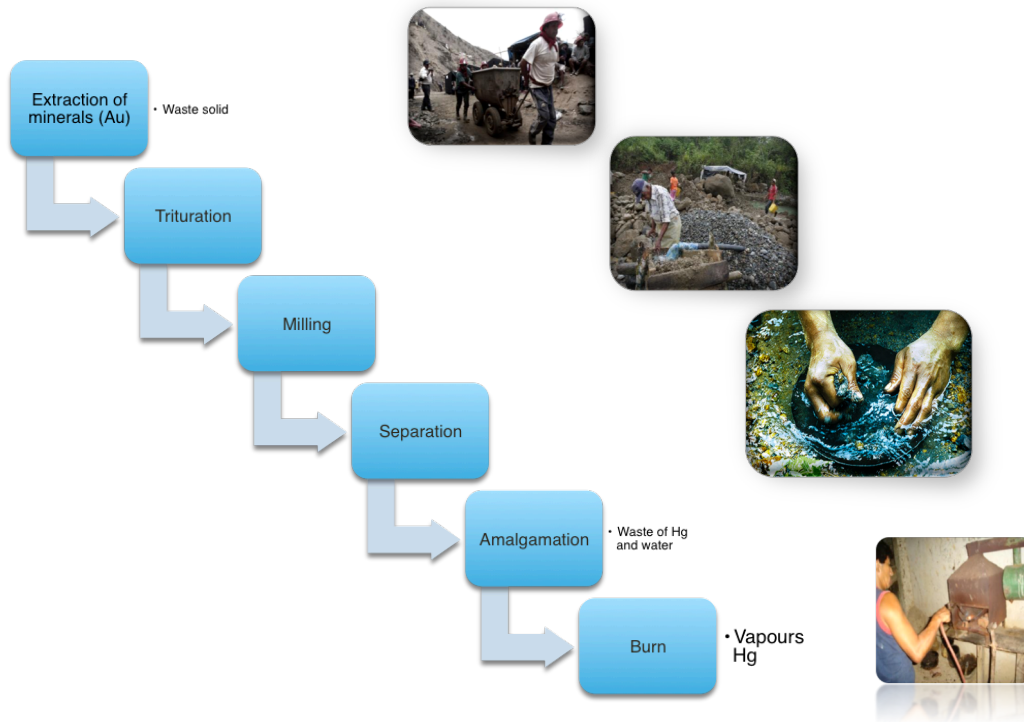
Figure 5.2 Gold extraction process.

5.3 Analysis of the area.

The canton Camilo Ponce Enríquez is constituted by the locality of the same name and they conform rural communities like: La Rica, Bella Rica, Nueva Esperanza, Hermano Miguel, Shumiral, Union of San Pedro, Liberty and White River. It is located in the extreme west of the Cordillera de Mollepongo (Door of the tree), in the province of the Azuay approximately to 200 km to the southwest of the city of Cuenca. (GAD Municipal Camilo Ponce Enriquez. (2012). Plan de Desarrollo y Ordenamiento Territorial Camilo Ponce Enriquez 2012-2026. Camilo Ponce Enriquez.)
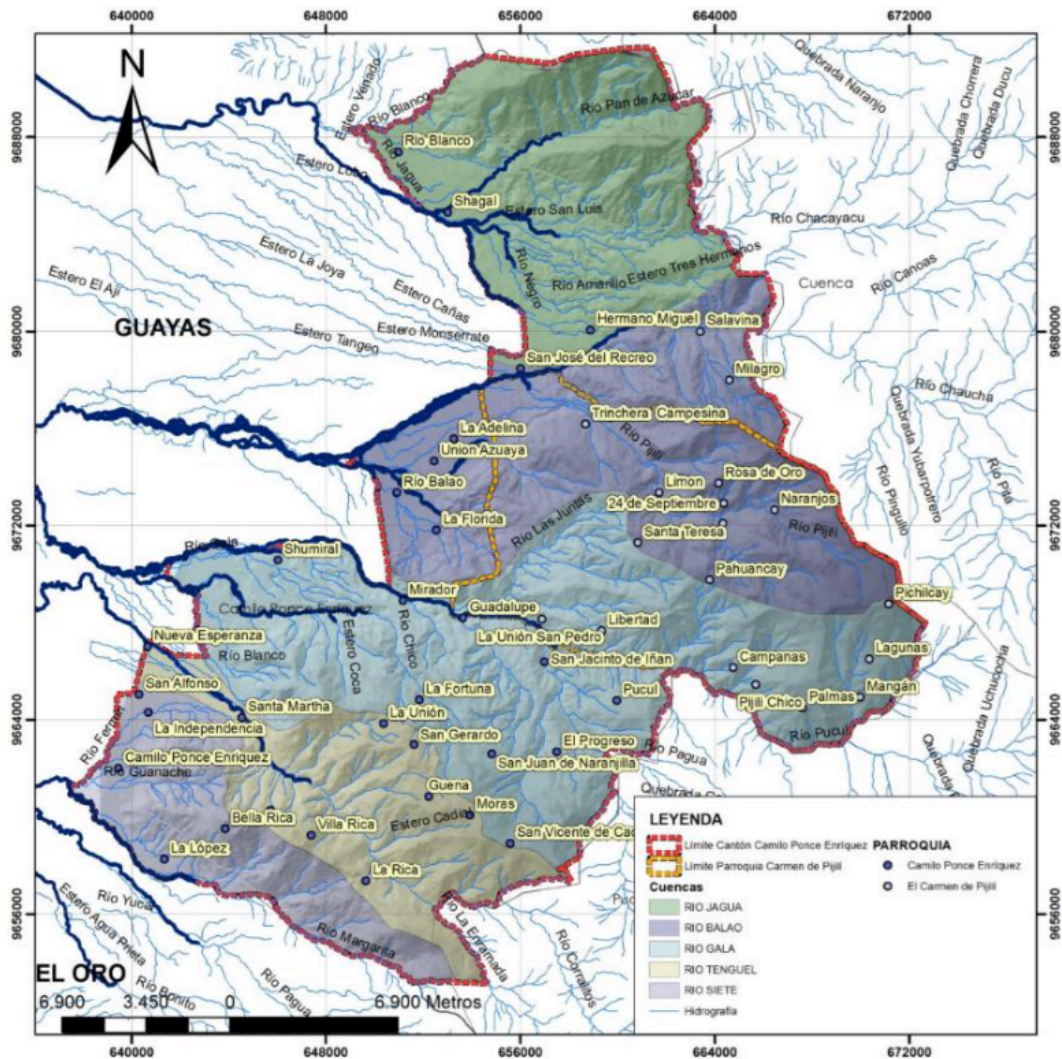
Figure 5.3. Map Basin Rivers of the canton Camilo Ponce Enríquez. (from GAD Municipal de C.P.E., 2014).

The canton and its parishes are crossed by five important rivers basin (rivers Jagua, Balao, Gala, Tenguel and Siete), which run in parallel form from the western cordillera to the Pacific Ocean. A majority of the processing plants of gold in the Ponce Enriquez area are located along River Siete.

The study area corresponds to recent unconsolidated deposits of alluvial origin that correspond to the Holocene of the Quaternary. Superficially there is a cover of gray or brown clay, whose thickness varies from about 5 to 10 meters. The sediments found in the area come from the western cordillera, which the rivers of the area, have transported, these sediments are mostly made up of silt and sand. This area has a cumulative average precipitation of 1102.6 mm of rainfall and an average annual temperature of 21.5 ºC, typical values of a humid tropical climate, which results in a

general net recharge of 305.2 mm for the Camilo Ponce Enríquez zone. (INIGEMM 2012).

In the study of the hydrogeological units of the zone realized by the Inigemm 2012, we can see in **Figure 5.4**, a set of geological formations where the different types of aquifers of the zone are identified, observing that there is an extensive and productive aquifer of high permeability (blue zone), that covers the western zone of the canton and the rivers Tenguel, Siete and Gala. While in the Eastern zone of the canton (green zone) the aquifers of low permeability and the aquitard are predominating.
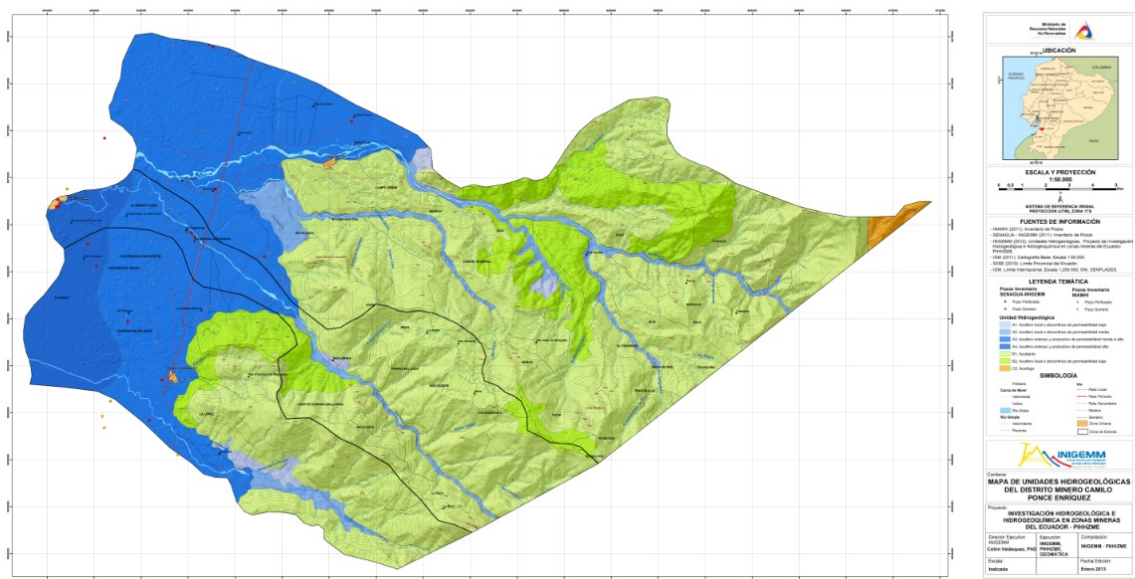
Figure 5.4 Hydrogeological study Canton Ponce Enriquez. (from Inigemm, 2013).

The susceptibility to contamination of the groundwater resource in the Ponce Enriquez canton is represented in **Figure 5.5**, where the zones with very low susceptibility are located in the extreme East on the slope of the Tengel river, where there are sectors without contamination due to mining activity or with very low levels of affectation. The zones corresponding to the low susceptibility levels are located in sectors partially contaminated by the mining activity. These zones are located in the extreme east of the study area as well as in the sector of Shumiral and in the average slopes of the Chico river and the river Tenguel. (yellow zone). Sectors with moderate levels of susceptibility are located in the upper and middle slopes of the Cachi, Tenguelillo, San Miguel rivers, on the lower slopes of the Chico river and in the Bella Rica sector.

Areas of high susceptibility (red zone) are located in areas affected by pollution from mining activity on the lower slope of the Fermin and Siete rivers. Finally, zones of very high susceptibility are located in the alluvial colluvial valleys and alluvial terraces of the Chico, Iñán, Gala, Tenguel and Siete rivers, forming local aquifers of medium permeability, which are found in areas directly affected by the mining activity (Inigemm 2012)
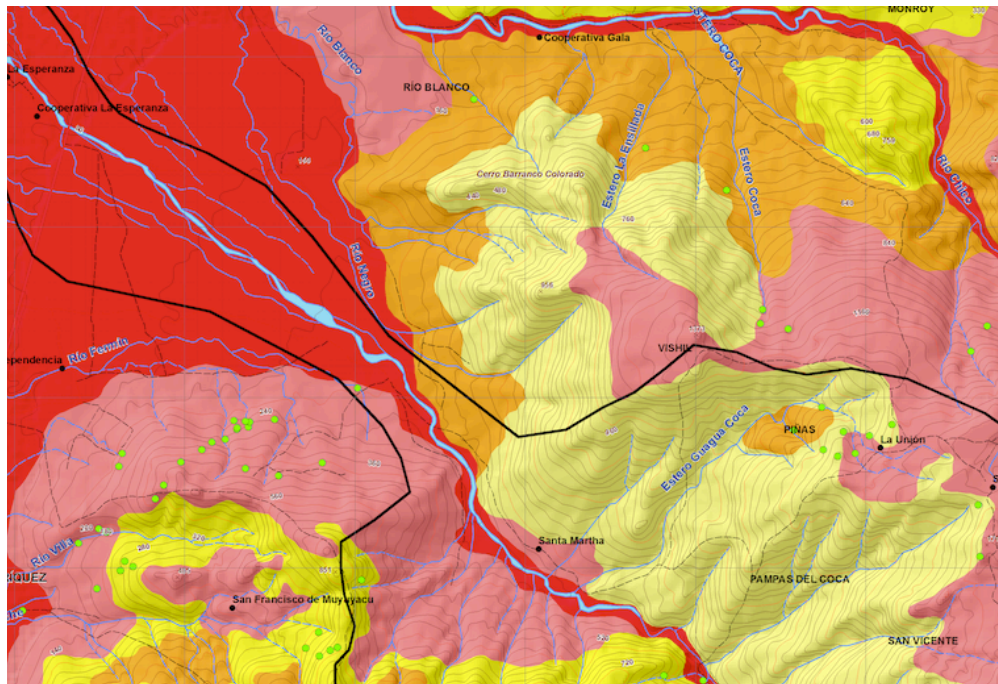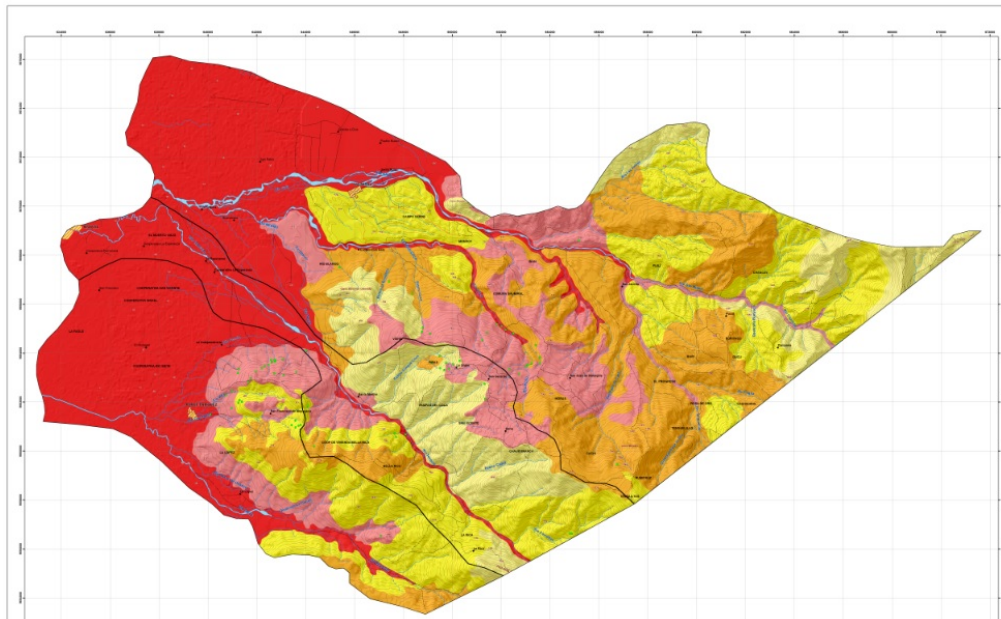

Figure 5.5. Map of the susceptibility to contamination of the groundwater resource. From Inigemm, 2012.

The green points indicate the zones of mining activity observing a great concentration in the zone of Bella Rica, a mountain very rich in gold, copper, bronze; but in this place not only shines the gold, but also a beautiful nature that between excavators, tubes and mills resists to disappear.

5.4   Study of the water quality of the canton Ponce Enriquez.

The Ministry of Environment through the law TULSMA, 2012, provides the protocols and laws for the protection of the environment within the Ecuadorian territory. In which, in Book VI, Annex I, referred to the Environmental Quality Standard and discharge of effluents, in Section 3.1 literal 3. Groundwater Quality Standard; Table 5. Reference quality criteria for groundwater, considering soil with clay content between (0-25.0)% and organic matter between (0 - 10.0)%. As far as Mercury is concerned, it sets the maximum permissible limits. Table 5.1, for the conservation and protection of water sources.

Parameter	Unit	Maximum Permissible limit
Total Mercury (Hg)	ug/L	0.18

Table 5.1 Maximun permissible limit of Hg for Groundwater. TULSMA, 2012.

A previous study carried out in Canton Ponce Enriquez by National Institute of Mining and Metallurgical Research of Ecuador (Inegemm), Evaluation of Susceptibility to Contamination of Underground Water Resources in the Camilo Ponce Enríquez, Mining District investigated the impact of the gold extraction mining activity, in the sources of waters that are within the mining zone. This study shows the presence of heavy metals, mainly of Mercury in surface water and groundwater.

The study area was previously described in section 5.3, the results obtained from this investigation (Fig. 5.6), it can be observed that in the hydrographic basins of Tenguel and Siete of the Ponce Enriquez canton, the underground waters of San Gerardo and Muyuyacu have values of mercury greater than limit of law 0.18 ug / L, mainly in the San Gerardo area mercury concentration is located at 7 ug / L and 5 ug / L, downstream in the Muyuyacu zone the mercury level is at 5 ug / L, the high level of Hg concentration in these areas is consistent with the contamination susceptibility assessment. The pH values reported for groundwater in this study ranged from 3.4 to 7.94.
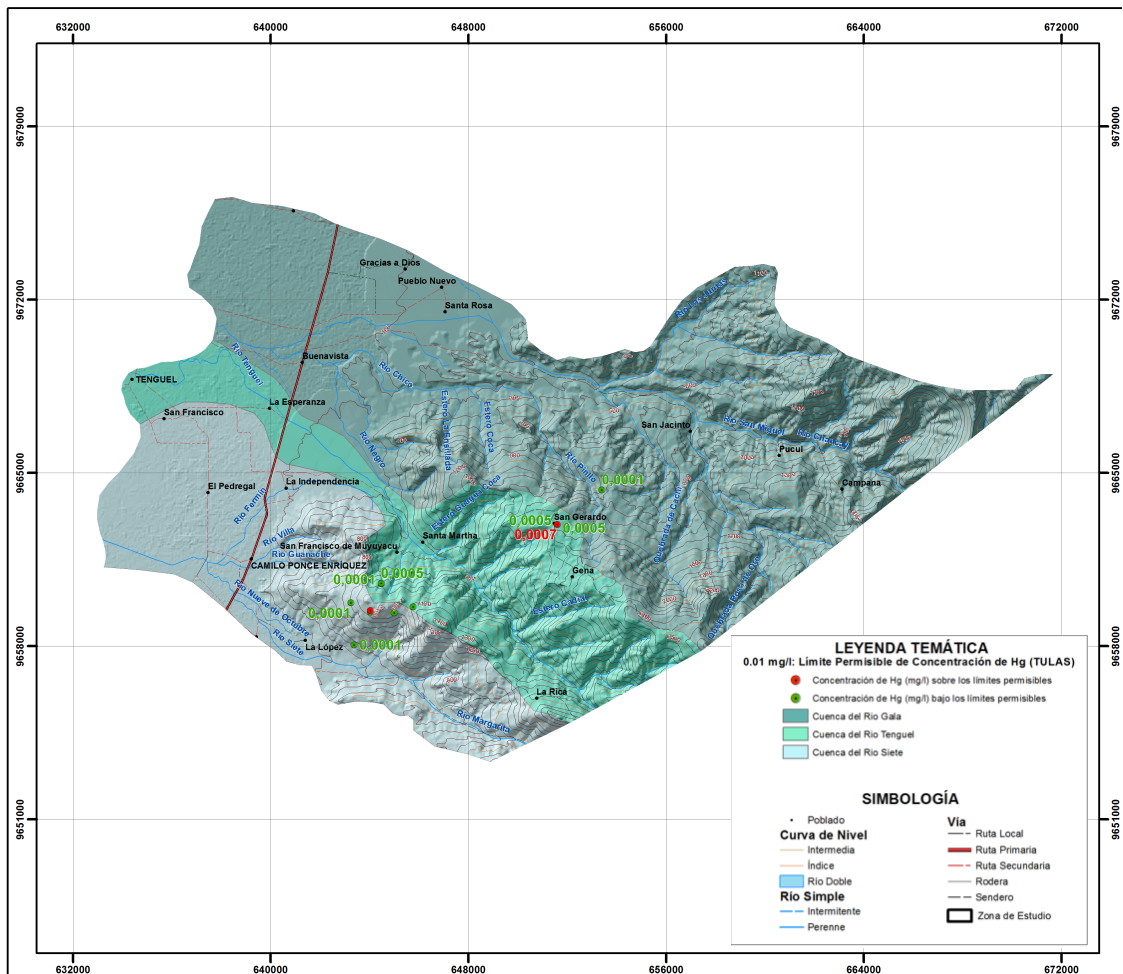
Figure 5.6 Map District Camilo Ponce Enriquez. Concentration of Hg in groundwater. Inegemm 2012.

These research data carried out on the mining sector in the region "Ponce Enriquez," demonstrate that gold mining activity through mercury amalgam has produced a strong impact on the environment, particularly in the surrounding areas, causing a severe anthropogenic disturbance. This results in a danger to the health of workers, of the settled population in those areas, as well as the flora and wildlife.

5.5 Study of the potential solution for groundwater remediation.

Given the hydrogeological nature of the contaminated areas and the shallow depth of the underground strata, the most suitable technique for the treatment of the underground aquifer may be the design of a permeable reactive barrier (PRB) containing a specific reactive material for the reduction of mercury. This technique is particularly effective when the contaminant infiltration into the areas susceptible to contamination are not too

large, so it can be intervened using a PRB type (Funnel and Gate) that allows the centralization of the flow in favor of a volume of reactive material necessary.

The projection of a PRB for the case study presented in canton Ponce Enriquez is one of the objectives of this research, providing a valid option for the conservation and remediation of the aquifer source, using a material of low cost with an important capacity of adsorption of Hg.

According to the data presented in section 5.4 the concentration of Hg in groundwater will be established with a safety factor of 3 times higher than the highest value determined in the study. The output concentration of the PRB is given by the current Ecuadorian law TULSMA (2012), which sets as maximum limit value of Hg concentration for groundwater 0.18 ug/L.

As regards the minimum lateral extension of the reactive barrier, it depends on the extent of the polluting plume within the aquifer, and the configuration of PRB that we will choose (Funnel and Gate or Continuous). The transportation of the contaminant plume within the aquifer will be determined with the GMS modeling software and through the equation Thomas Double model developed for dynamic study of adsorption in column for SB, there will calculate the quantity of necessary reactive material for PRB.

5.6   Permeable Reactive Barrier Design.

Groundwater flow and transport modeling has become an important tool for research. Flow modeling deals with the movement of water, while transport modeling is focused on the distribution and migration of solutes or heat in the subsurface. Flow modeling is relevant for the management of water supply systems and supervision of hydraulic works. Transport modeling is mainly applied to problems in which groundwater quality is involved (Holzbecher and Kohfahl, 2009). Reactive transport modeling is the one that best fits our case study, its results will give us the necessary information to design the PRB. GMS (Groundwater Modeling System), will be used to reach the aforementioned goal, as it is one of the most used tool for engineering applications.

5.6.1   Groundwater flow and transport numerical models.

Groundwater models require a tremendous amount of information and understanding of the aquifer in order to be accurate, reliable, and robust. The first step in developing a

groundwater model, and perhaps the most important, involves the design of a conceptual model. Conceptual modeling can lead to more efficient model development, and opportunity for multiple interpretations. A conceptual model is a simplified, high-level graphical representation of the site to be modeled, that represents the simplest scheme on how the aquifer works and can be easily adjusted to better describe the real situation of the investigated system, before the implementation of the final numerical model.

This approach simplifies the field problems, such as data organization and system analysis. The closer the conceptual model approximates the field situation, the more accurate is the numerical model. The failure of numerical models to make accurate predictions can often be attributed to errors in the conceptual model. (Schlumberger, 2009).

Developing a good conceptual model requires the knowledge of detailed information on geologic formations, groundwater flow directions, hydrologic boundaries (recharge, rivers, lakes, wetlands, etc), hydrogeologic parameters (conductivity, storage, porosity, etc), the presence of extraction or injection operations from wells (location, depth, screens, rates), and observations of groundwater hydraulic heads and water quality. All this amount of information, generated from different sources, is used to process the model, which varies according to the complexity of the study. A general outline for the development of groundwater modeling process is presented below.
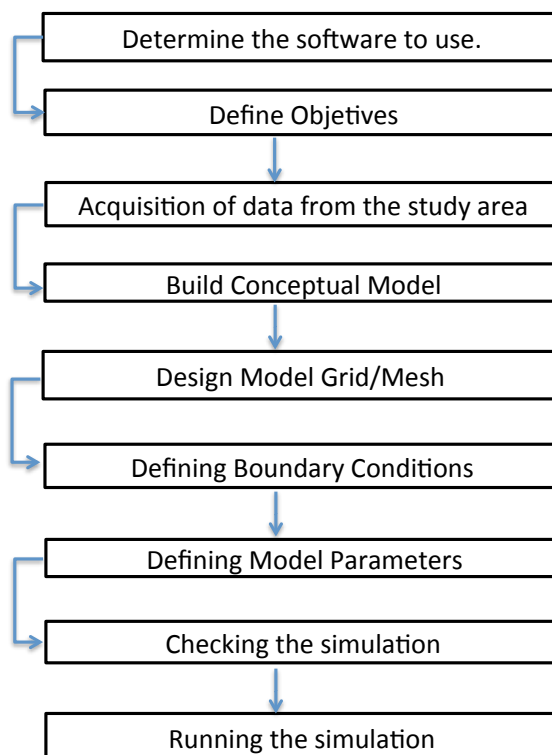
Figure 5.7 Groundwater modeling Process.

GMS 7.1 has been used, in this research, to perform groundwater flow and transport modeling within the area of high contamination susceptibility in the Ponce Enriquez District.

The Groundwater Modeling System (GMS) is a comprehensive graphical user environment for performing groundwater simulations. The entire GMS system consists of a graphical user interface and a number of analysis codes (Modflow, MT3D, MODPATH, SEEP2D, FEMWATER). The GMS interface, was developed by the Engineering Computer Graphics Laboratory of Brigham Young University in partnership with the U.S. Army Engineer Waterways Experiment Station in the late 1980s currently the developer of this program is Aquaveo company. (Ewell, Christopher, 2015).

GMS is a comprehensive modeling environment. Several types of models are supported and facilities are provided to share information between different models and data types. In order to continue the process of build conceptual models the analysis codes Modflow will be used for the simulation of the groundwater flow and MT3D analysis code for transport modeling.

5.6.2 Modflow.

Modflow numerical code solves the three-dimensional problem of flow in porous media, using the groundwater flow equation using the finite differences method. The resolution of the flow problem leads to the estimation, for each cell of the grid, of the hydraulic head and hence the water velocity. The partial derivative equation of the flow implemented by Modflow is: (McDonald and Harbaugh, 1988)

$$\frac{\partial}{\partial x}\left(K_x \frac{\partial h}{\partial x}\right) + \frac{\partial}{\partial y}\left(K_y \frac{\partial h}{\partial y}\right) + \frac{\partial}{\partial z}\left(K_z \frac{\partial h}{\partial z}\right) + W = S_s \frac{\partial h}{\partial t} \qquad 5.1$$

where K_x, K_y and K_z are the values of hydraulic conductivity along the x, y, and z coordinate axes (L/T), h is the potentiometric head (L), W is a volumetric flux per unit volume representing sources and/or sinks of water present within the system (T^{-1}), S_s is the specific storage of the porous material (L^{-1}) and t is the time (T).

Two approaches can be used to construct a Modflow simulation in GMS: the grid approach or the conceptual model approach.

1. The grid approach involves working directly with the 3D grid and applying sources/sinks and other model parameters on a cell-by-cell basis.
2. The conceptual model approach involves using the GIS tools in the Map module to develop a conceptual model of the site being modeled.

The location of sources/sinks, layer parameters such as hydraulic conductivity, model boundaries, and all other data necessary for the simulation can be defined at the conceptual model level. Once this model is complete, the grid is generated and the conceptual model is converted to the grid model and all of the cell-by-cell assignments are performed automatically. The steps involved in performing Modflow simulation for Ponce Enriquez district using the conceptual model approach are described below. Firstly we have to describe the problem to solving which is to determine course of groundwater flow within the study area with respect to possible contamination of Hg in this source water. The results of this simulation will be used as the flow field for a transport simulation using the MT3DMS code.

5.6.3 Discretization and boundary conditions.

The flow problem was implemented on a large-scale three-dimensional model working in stationary conditions. In order to define the domain of the modeling, a format map (.shp) geo-referenced with coordinate WGS 84 UTM - 17 S domains was imported from the QGIS software. The area was identified to the north by the Negro River and to the south by Tenguel River. West and East limits are determined by two closing sections between the above-mentioned rivers, and were set to be constant hydraulic head boundaries. The whole domain has an area of about 73.74 km^2. The geological composition of the study area is primarily made of clay and loam sediments where was localized two different areas. The first (Area 1) extended zone predominantly consisting of alluvial deposits and other Area 2 consisting of franco-clay-lays deposits. Therefore two different horizontal hydraulic values in the flow model were used. The aquifer will be modeled as an unconfined one.

Recharge packet which simulates a distributed recharge, was used to assign a recharge rate value to each model cell. The east and west contours conditions are Specified Head type, piezometric load values assigned for each nodes were 105 m and 8 m respectively. (INIGEMM, 2012). As for the north and south contours were be used a River type contour condition for the Negro and Tenguel rivers. River pack function is to simulate the interaction between a surface water body and a groundwater. Therefore, the two rivers have been divided into several segments, each of them were assigned a conductivity value, equal to the value of hydraulic conductivity and each node of the segments, a value of the free quota "head stage" and the bottom "bottom elevation" of the river was distributed, according to the values of the topography surface "Top Elevation" (Appendix 1).

All data used to perform the conceptual model approach were obtained from the study "Assessment of the susceptibility to contamination of underground water resources, mining district of Camilo Ponce Enriquez – Ecuador", carried out by Inegemm (2012).
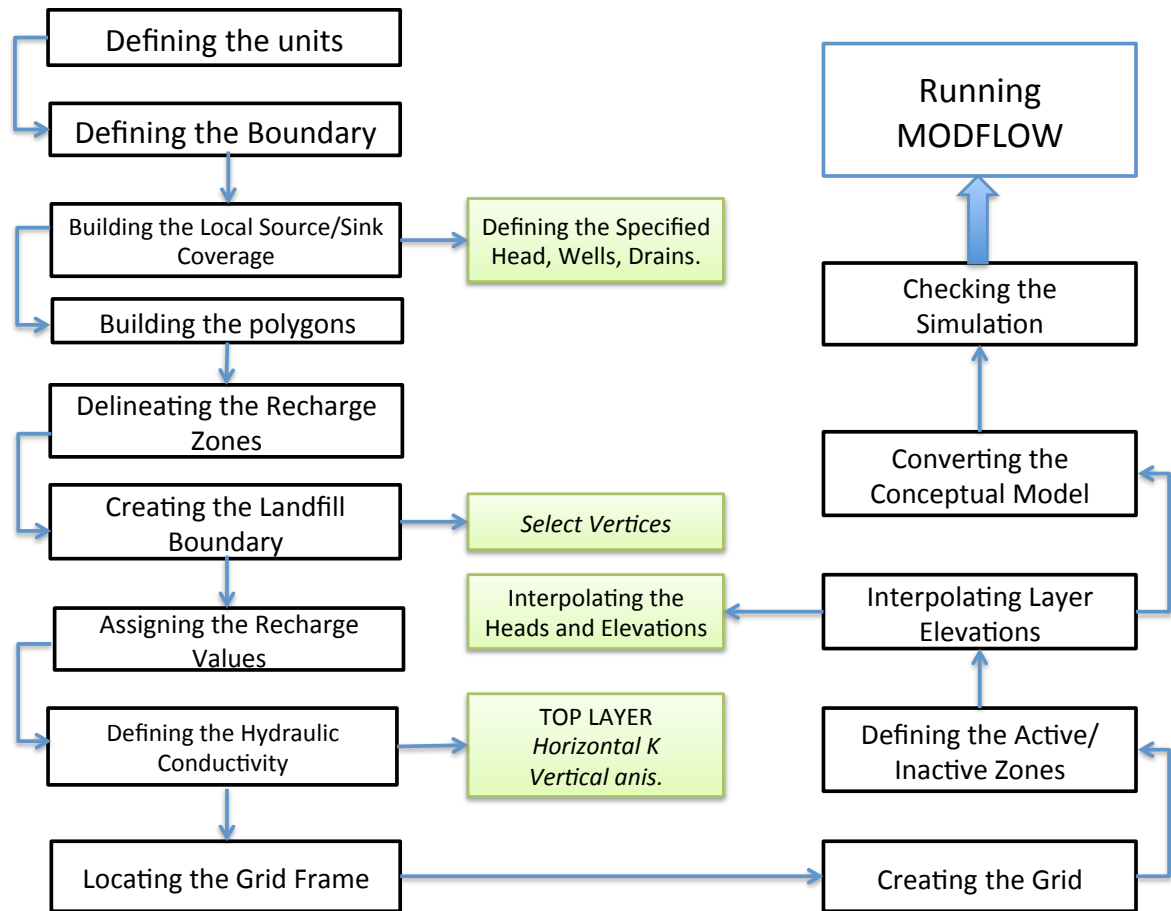
Figure 5.8 MODFLOW - Conceptual Model Approach Process.

In agreement with Figure 5.8 that explains the methodology to follow for Modflow modeling, you need to first launch GMS and import the background image of the site to be modeled (.shp), once the image is imported to GMS, it can be displayed in the background as a guide for on screen digitizing and placement of model features.

Model boundaries are created with the arc tool, which forms a closed loop around the site and constitutes the local Source/Sink coverage. This coverage defines the boundary of the region being modeled and it defines local sources/sinks including wells, rivers, drains, and general head boundaries. The next step is the definition of the specified head boundary along the south and north sides of the model, afterwards we defined the active region of the grid building the polygons. Subsequently the recharge zones are created, assigning the Recharge Values and defining the Hydraulic Conductivity (K) for the layer. The values used in this model are presented in the following table:

Parameters	Value
Recharge rate	9.6e-09 (m/s)
Horizontal K(Area 1)	4.2e-05 (m/s)
Horizontal K(Area 2)	1.6e-6 (m/s)
Vertical anisotropy	1
Starting Head	8 (m)
Bottom Layer	-10 (m)
Average elevation	130 msnl
Porosity	0.3
Longitudinal dispersivity	20
Ratio of horizontal transverse dispersivity to longitudinal dispersivity (TRPT)	1.0
Ratio of vertical transverse dispersivity to longitudinal dispersivity (TRPT)	1.0
Length Period	3.0 e+09 (s)
Maximum transport steps	10 e+04 (s)
Starting concentration (Hg)	0.01 (mg/L)

Table 5.2 Descriptive parameters of the District Ponce Enriquez used for the code MODFLOW y MT3D. GMS 7.1

The ground surface morphology of the study area is generated by importing punctual altitude data from a text file UTM coordinates, and by interpolating them using a Geostatistical approach. The Inverse Distance weighted (IDW) interpolation with Sheppard's method has been chosen between the several ones supported by GMS. The active zones of the model have been defined and all the input data have been checked to avoid possible errors, which can affect the simulation results.
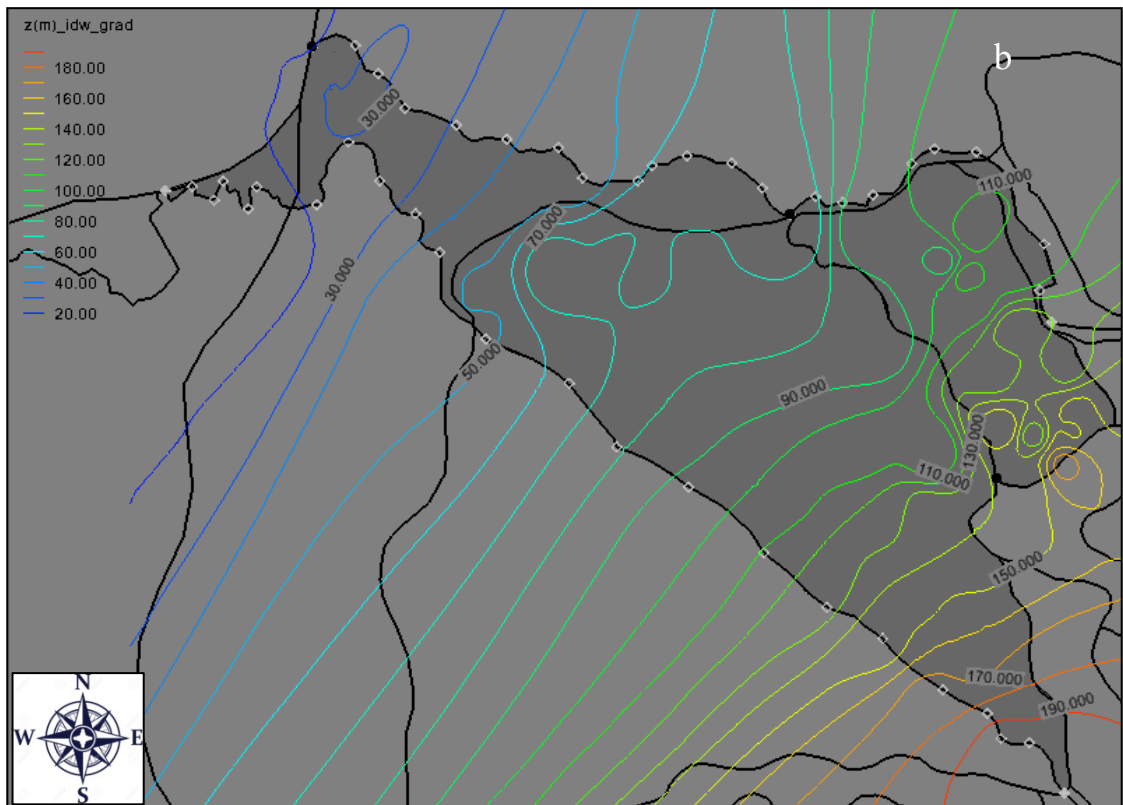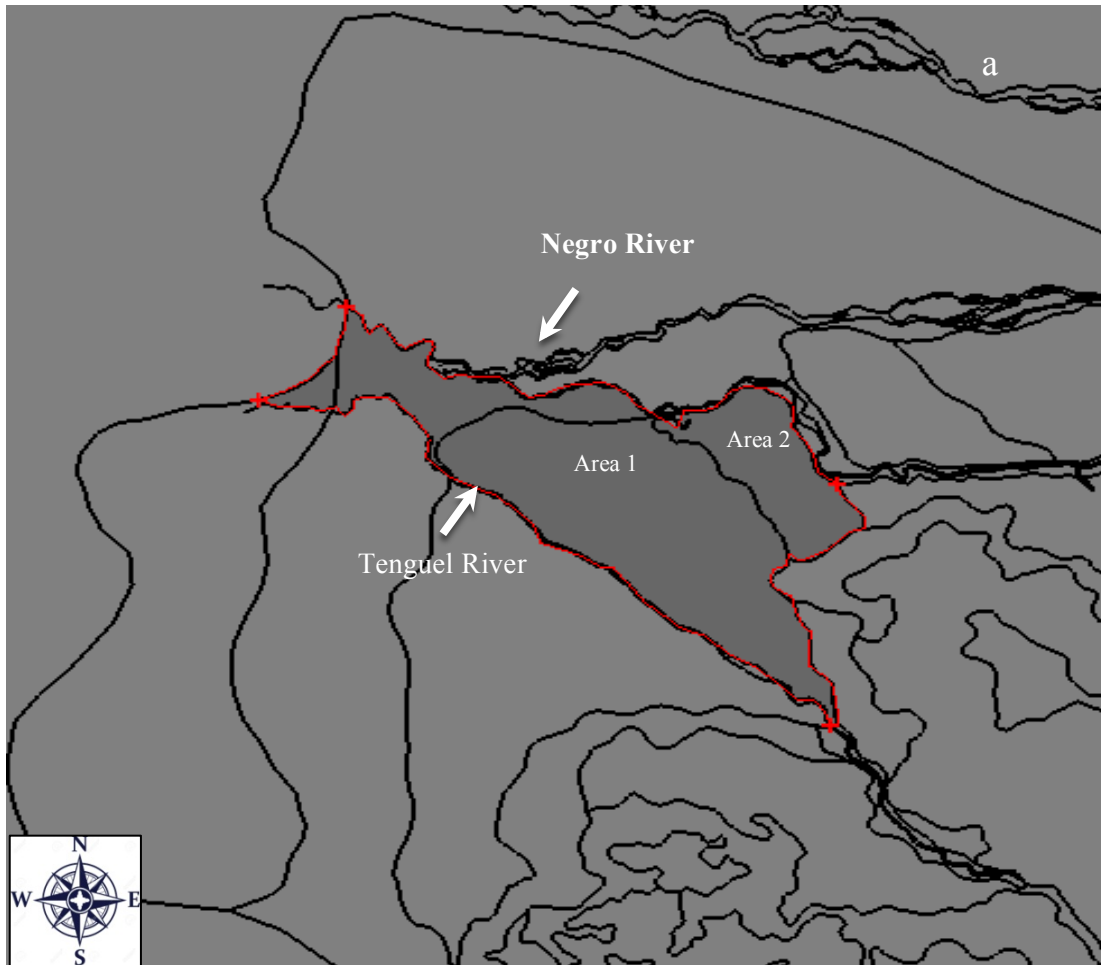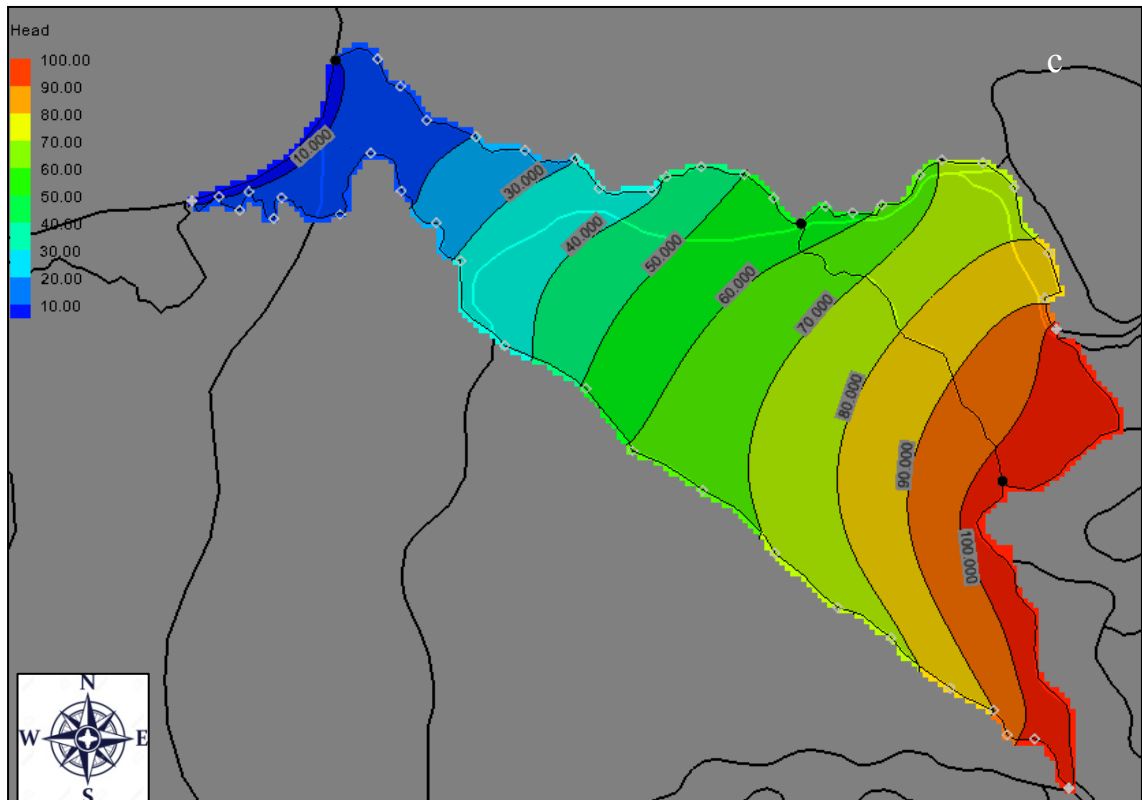
Figure 5.9 a)Ponce Enriquez district susceptibility study area. b) Level curves (piezometry) c) Groundwater flow model Ponce Enriquez district GMS 7.1- MODFLOW.

As can be seen in Figure 5.9 a, the study area is bordered by two important tributaries, the Negro River to the north and the Tenguel River to the south, which extend along the mining area, and constitute the natural limits of the area. The red line in the figure represents the boundary conditions surrounding the parishes of Buena Vista, La Esperanza, Cooperativa La Esperanza where the modeling will take place and in addition, the two lithological zones that are present in the study area are evidenced. Figure 5.9b shows the study area level curves obtained by the Sheppard method has values ranging from 190 m.a.s.l. to 20 m.a.s.l. and the Figure 5.9 c. shows the simulation results, that is the aquifer piezometric trend within the study area, which has an east-west direction.

This result will be used to simulate changes in concentrations of miscible contaminants, in groundwater. The fate and transport of mercury (Hg) produced by the small scale gold mine located in the modeling area will be discussed below.

5.6.4   MT3D Conceptual Model Approach.

The modular three-dimensional transport model named MT3D was originally developed by Zheng (1990) at S. S. Papadopulos & Associates, Inc., and subsequently documented for the Robert S. Kerr Environmental Research Laboratory of the United States Environmental Protection Agency. In the past several years, various versions of the MT3D code have been commonly used in contaminant transport modeling and remediation assessment studies. Nowadays the last version of MT3D works with, 1) a third-order total-variation-diminishing (TVD) scheme for solving the advection term that is mass conservative but does not introduce excessive numerical dispersion and artificial oscillation; 2) an efficient iterative solver based on generalized conjugate gradient methods to remove stability constraints on the transport time stepsize; 3) options for accommodating nonequilibrium sorption and dual- domain advection-diffusion mass transport; and 4) a multi-component program structure that can accommodate add-on reaction packages for modeling general biological and geochemical reactions. That it includes the three major classes of transport solution techniques in a single code, i.e., the standard finite difference method; the particle-tracking-based Eulerian-Lagrangian methods; and the higher-order finite-volume TVD method, offering a best approach for solving the most wide-ranging transport problems with desired efficiency and accuracy. This mass transport model was referred to as Modular 3-Dimensional Transport model Multi-Species (MT3DMS). (Zheng and Wang, 1999)

MT3DMS can be used to simulate changes in concentrations of miscible contaminants in groundwater considering advection, dispersion, diffusion and some basic chemical reactions, with various types of boundary conditions and external sources or sinks. The basic chemical reactions included in the model are equilibrium-controlled or rate-limited linear or non-linear sorption, and first-order irreversible or reversible kinetic reactions.

The partial differential equation describing the fate and transport of contaminants of species in three-dimensional, transient groundwater flow systems have been described extensively in section 2.7 (Model Transport). Furthermore in this section, it explained the Advection term of the transport equation (eq. 2.62) that describes the transport of

miscible contaminants at the same velocity as the groundwater and dispersion in porous media (eq. 2.69) that refers to the spreading of contaminants over a greater region than would be predicted solely from the average groundwater velocity vectors. In order to construct the transport model of a passive pollutant, it is necessary to establish the boundary and initial conditions and to assign the parameters of the dispersivity. The boundary conditions related to the concentration of a contaminant are of type:

- Dirichlet, condition of concentration assigned or of first type;

- Unassigned concentration gradient, Neumann condition or of second type;

- Mixed condition or Cauchy represents a combination of the above conditions.

Regarding the dispersion parameters, the longitudinal dispersivity α_L, the relationship between the horizontal transverse dispersivity to longitudinal dispersivity (TRPT)α_T / α_L, the ratio vertical transverse dispersivity to longitudinal dispersivity (TRPT) α_v / α_L and the coefficient of molecular diffusion, these must be specified in MT3D (Table 5.2).
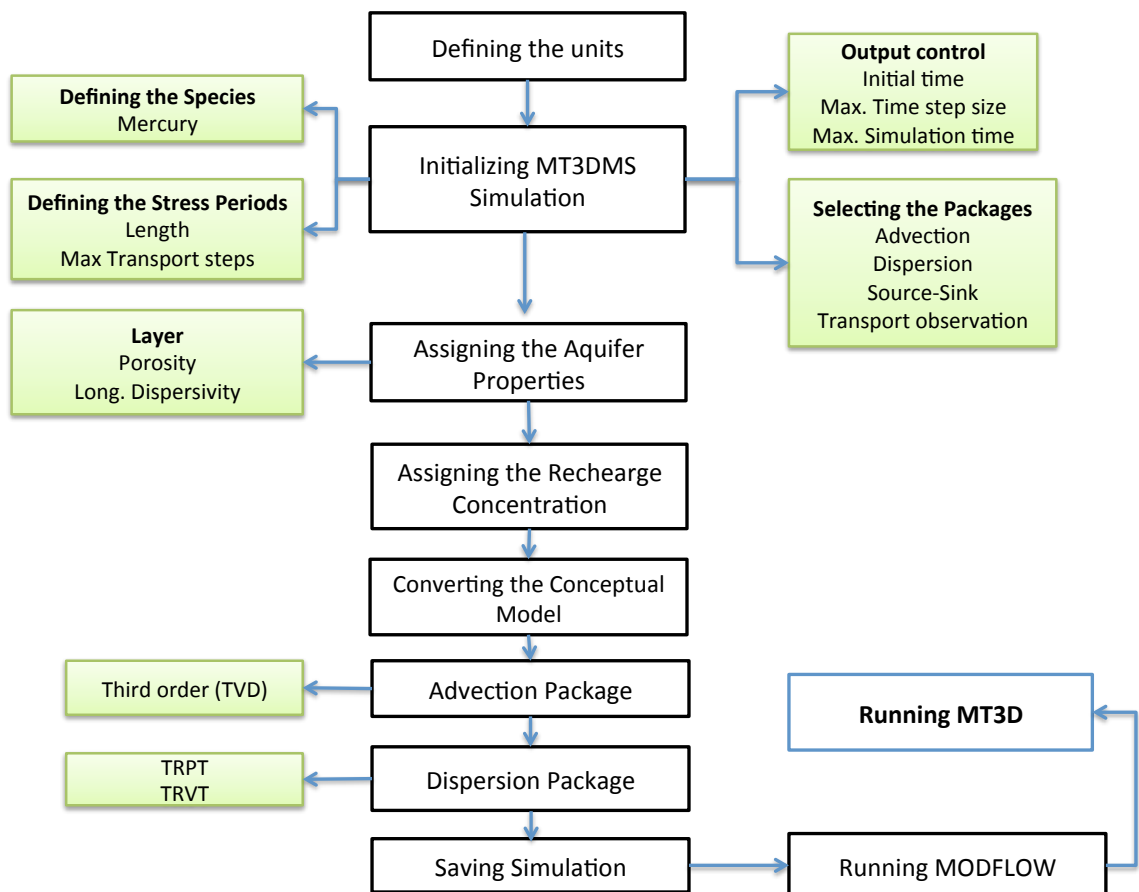

Figure 5.10 MT3D Conceptual Model Approach Process.

MT3DS simulation can be constructed using the grid approach where the data are entered on a cell-by-cell basics or using the conceptual model approach where the data are entered via points, arcs, and polygons.

5.6.5 Model of transport (Case study).

The study case exposed corresponds to one small-scale artisanal gold mine that used mercury amalgamation method. This mine worked for 10 years into the area Ponce Enriquez in this period of time, the mine carried out continuous discharges to the environmental of residues containing mercury. MT3D conceptual model approach was used, to analyze the long-term potential the mercury migration through of the aquifer applying advection and dispersion packages. The Modflow simulation performed above provides the flow field for the transport simulation in the MT3DMS environment.. MT3DMS is used in conjunction with Modflow in a two-step flow and transport simulation. Heads and cell-by-cell flux terms are computed by Modflow during the flow simulation and are written to a specially formatted file. This file is then read by MT3DMS and utilized as the flow field for the transport portion of the simulation. For the numerical model MT3D was imposed boundary condition Dirichlet-type in regard to the mercury concentration. The gold mine was located in the southeast of the area, at the coordinates UTM x = 643375; Y = 9667346, (Figure 5.11). The transport model of the mercury contaminant plume from the mine discharges, was carried out on the base of a continuous injection model, whereof a Hg concentration constant value was defined in the cells corresponding to the mine area using ICBUND button, that it is used to enter the values of the ICBUND array. The ICBUND array contains a value for each cell in the grid defining the type of the cell as either constant concentration, inactive, or variable concentration. A negative ICBUND value (-1) indicates that the cell has a constant concentration.

For the performed the simulation, a value of the initial concentration of mercury "Start concentration" equal to 0.01 mg / L of Hg (II) is considered. Another magnitude to be defined is the time (years) of the simulation, for which a value of 10 years was chosen to know the magnitude of the contaminant plume within this time period. Specifying as non-reactive species to Mercury.

The values and parameters necessary for the realization of the transport model are described in Table 5.2, which were obtained from researches as Innegem 2012, Trosti and Fallico 2012.
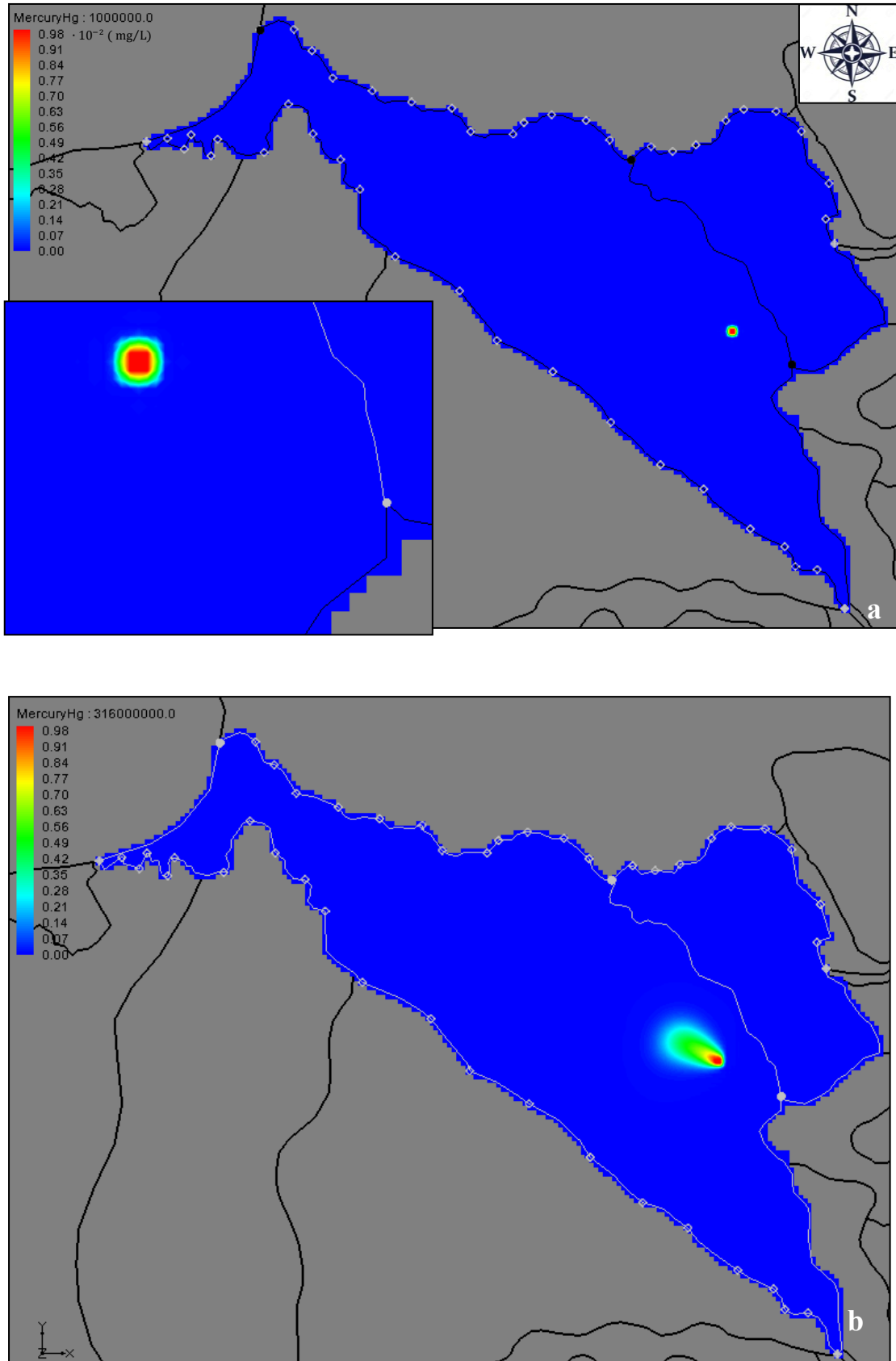
Figure 5.11 a) Ponce Enriquez area Mining zone. b) Three-dimensional transport modeling MT3DMS. Time 10 years.

Figure 5.11. Demonstrates the mobility of the species of Mercury within the whole dominium where the stress period was divided into several steps. Figure 5.11a. shows the gold mine location within the zone of high susceptibility, assigning to the cells a concentration of Hg constant (red cells) for a continuous immersion modeling. In Figure 5.11 b) we can be observed that the contaminant plume begins to transport with south-east north-west direction, evidenced by the range of colors, which represents the concentration of Hg present at a given time. In accordance with flow modeling, it presents an enlargement over time, where the longitudinal direction is greater than transversal motion, due to the mechanism of dispersion. Once the modeling of transport is completed, it is known how great is the contaminant plume into the aquifer, so that this information allows us to evaluate the suitability of the remediation techniques that can be installed in the study area.

5.7 PRB dimensioning procedure.

Batch and Column tests showed the important adsorption capacity that the Spanish broom holds with respect to Mercury in aqueous solutions. Thanks to this property and to the lignocellulosic structure of the fiber, which gives to the broom an interesting mechanical strength, the plant is suitable to be used in filtering systems. Therefore, its use as reactive material for a PRB production is considered.

In this section, the dimensioning of a PRB for the Ponce Enriquez district (Ecuador), will be discussed. The MT3D module will be used to estimate the Hg concentration entering the barrier. These data, together with the isotherm parameters obtained during the laboratory experiments, will be adopted to design the PRB, using the Double Thomas model developed in this thesis.

The gold mine located in the Ponce Enriquez district have caused groundwater contamination. Therefore considering the results of the simulation of MT3D for a time of 10 years with a continuous injection has been determined the position in which the PRB will be installed. In Figure 5.12 (a), shows the barrier location (points yellows), disposed approximately 1 Km downstream from the contamination source, because at this distance the mercury concentration is below the specified maximum limit 0.00018 mg L^{-1} for groundwater (TULSMA, 2012).
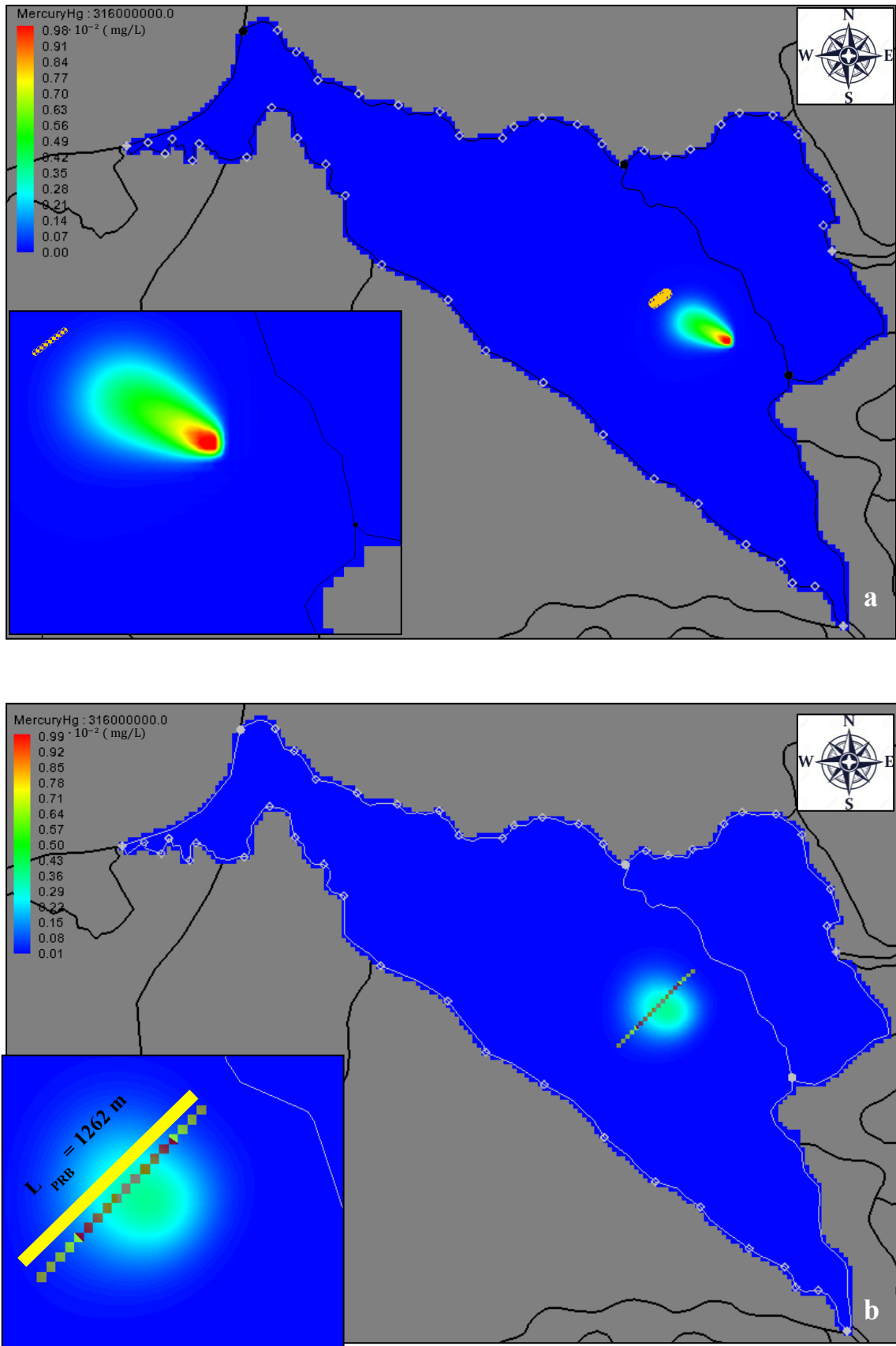
Figure 5.12 a) PRB localization (Area Ponce Enriquez). b) PRB length.

So taking into account that after 10 years of mining operations had been stopped, we have implemented a new transport simulation model, no continuous injection, to determine the evolution of the contamination plume until it reaches the barrier. Therefore, it was assigned a boundary condition of the Dirichlet-type concentration, and as initials concentrations within the aquifer, we have used the mercury concentrations obtained of MT3D to a time of 10 years to continuous injection.

Considering the displacement of the plume, it has been determined that the barrier must have a length of 1 262 m in order to capture all the mercury present in the aquifer. (Figure 5.12b).

5.7.1 Determination PRB's Thickness

The location of the PRB was determined in the eastern zone of the model coordinates UTM E 642370 N 9667647 ; E 642761 N 9667982 (Figure 512b). The characteristics of the area were described previously in section 5.3. The mercury concentrations within the aquifer vary following a Gaussian behavior, according to the results obtained by the MT3D no continuous injection, whereby the determination of the input concentration "C_0" the highest value of Hg (mg L^{-1}) displayed in the curve was considered. The PRB design involves the definition of two times, a time value t_1 to calculate the SB mass needed to remove the mercury present in the aquifer, and another time value t_2 to decide the PRB lifetime, i.e. when the concentration of Hg (II) inside of the aquifer is below the maximum limit prescribed by law.

Therefore, the value t_1 was obtained by means of approximation definite integral of the Breakthrough Curve (BTC) of the contaminating plume from MT3D no continuous injection simulation through trapezoidal rule. This value have a direct ratio with the amount adsorbent calculate required for the mercury removal within the aquifer, it is allowing us to optimize the amount of reactive material. Taking into account only the area that is within the concentration limit of 0.0018 mg / L Hg and through the equality between the BTC area and the rectangle area (A_{ret}) and considering C_0 as the maximum value of Hg concentration we obtain $A_{BTC} = A_{ret} = t \cdot C_{max}$ and expressing the variable t we yield (Figure 5.12):

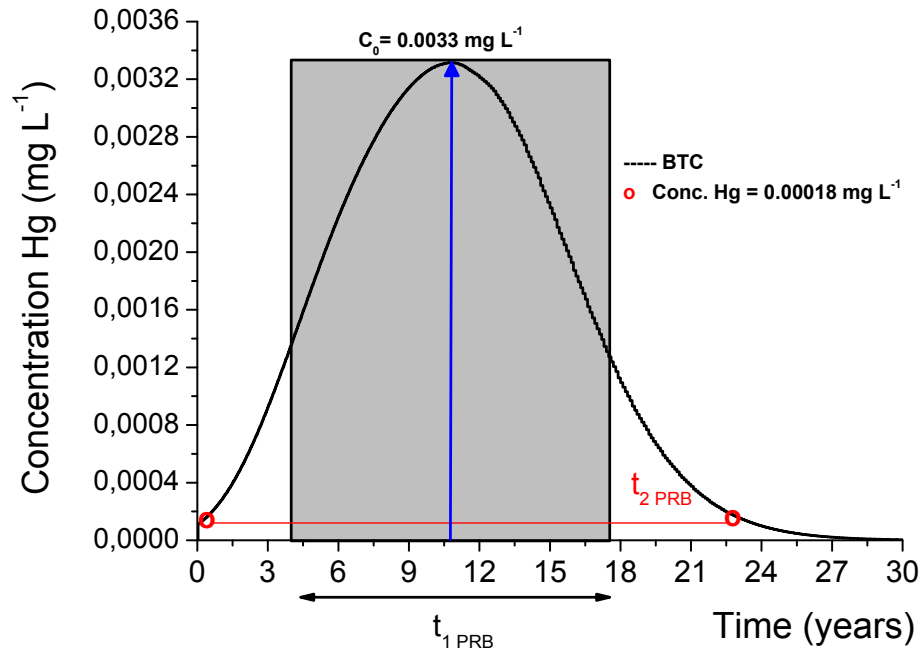$$t_1 = \frac{A_{BTC}}{C_{max}} = 12.14 \ \text{years} \qquad\qquad 5.1$$

Figure 5.13 Breakthrough Curve MT3D, Mercury concentration.

The hydraulic conductivity value is very important for the barrier design, since the PRB should not block or change the normal groundwater flow. The barrier must be designed to reach a hydraulic conductivity value equal or greater than the one characterizing the adjacent soil.

The SB porosity and permeability can vary, being a compressible material, according to the compaction force used for the realization of the filter. In Section 4.2, "Hydrodynamic characterization of Spanish broom", Density vs. Hydraulic Conductivity ratio was determined, obtaining a parabolic equation. This relation provides the proper reactive material density value to reach the aquifer hydraulic conductivity. The adsorbent material density calculation was performed using an hydraulic conductivity value higher than aquifer one to guarantee that the groundwater flow is not altered.

Once the material density has been calculated, the mass required for the groundwater mercury removal through a PRB will be determined.

The conditions and parameters necessary for the barrier thickness calculation are shown below: (Table 5.3)

Parameters	Value	Units
Groundwater Mercury concentration C_0	0.0033	mg L^{-1}
Limit Maximum Mercury (C_1)	0.00018	mg L^{-1}
Hydraulic Conductibility (K)	4 x10^{-5}	m s^{-1}
Density (ρ)	273	Kg m^{-3}
Double Thomas Constant (K_{TH2})	0.99 x 10^{-4}	mL min^{-1} mg^{-1}
Double Thomas Constant (K_{TH1})	0.98 x 10^{-4}	mL min^{-1} mg^{-1}
Active Surface Sites Fraction (f)	0.23	-
Maximum Adsorption Capacity (q_{01})	4.5	mg g^{-1}
Maximum Adsorption Capacity (q_{02})	11.22	mg g^{-1}
Length area (A_L)	1	m
Groundwater Flow (Q)	31.54	mL min^{-1}
Time$_1$ (T$_1$)	12.14	year
Bottom Area (D)	-10	m

Table 5.3. Parameters to Permeable Reactive Barrier design. Ponce Enriquez area. Case study.

In order to determine the barrier thickness, we must know the adsorbent mass required to remove the metallic ion. The mass (*m*) is calculated through the Double Thomas equation (eq. 4.3). The Wolfram Mathematicas 9.0, a computational engine, was used to find the optimal mass value.

$$C_t / C_0 = \frac{f}{1 + e^{-k_{Th\_1}C_0 t}\, e^{k_{Th\_1}q_{0\_1}m/Q}} + \frac{1-f}{1 + e^{-k_{Th\_2}C_0 t}\, e^{k_{Th\_2}q_{0\_2}m/Q}} \qquad (4.3)$$

The isotherm parameters, the groundwater Mercury concentration found in the site (C_0), and the maximum Mercury concentration value allowed by law (C_1) were entered.

Using the equation:
$$\rho = \frac{m}{V} \qquad 5.2$$

where, $V = A . S$ gives:

$$S = \frac{m}{\rho . A} \qquad 5.3$$

where S (m) is thickness, A (m^2) is the Cross-sectional area, ρ (Kg m^{-3}) adsorbent material density (SB) for a hydraulic conductivity = 4.5 x 10^{-5} ms^{-1} (Table 5.2.)
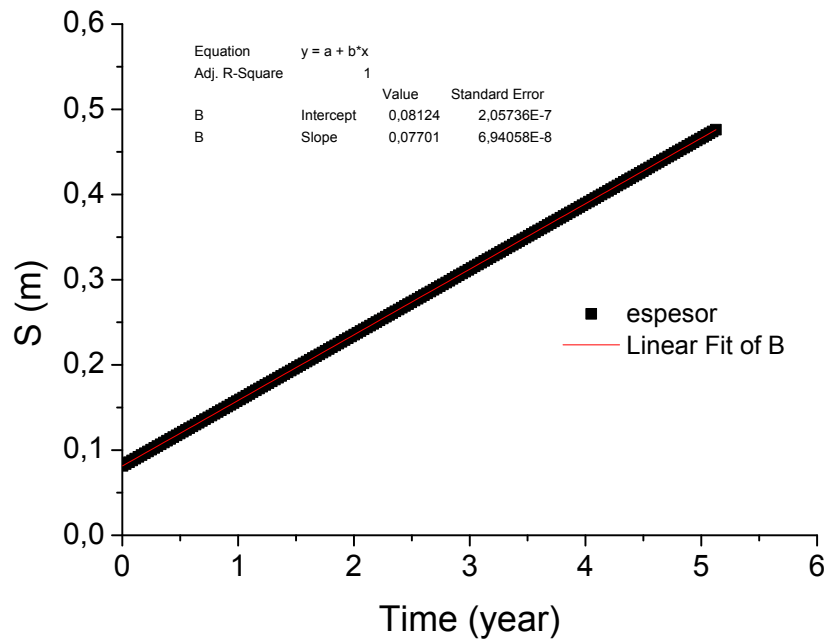
Figure 5.14 Linear Fitting Barrier Thickness vs Time.

Figure 5.14 shows a linear behavior S vs T. where S is directly proportional to T. Through the linear equation, the thickness (m) was calculated for the design of a reactive permeable barrier to 12.14 years giving a value of 0.86 m for a cross-sectional area of $1m^2$ using 0.23 Tons of SB to a flow of 31.54 mL s^{-1}.

It is worth noting that the lifetime, which must have the barrier is the 22.77 years that is the time it takes for all the contamination plume to cross the barrier, calculated by MT3D, that determined the time mercury permanence into the study area .

The estimated barrier thickness, can be realized just from a theoretical point of view. The natural fiber, with which the reagent material is made up, would not last actually for 22.14 years in these operating conditions. The biodegradability of the material rather suggests a durability not exceeding a ten year operating period. Giving that the required operating time is two times higher, we suggest that the barrier should have a thickness two times lower than the one obtained for a twenty two years period, and to replace the barrier reactor once every ten years. In this way the barrier will use the reagent within the limits of its durability and it will reach the same results obtained by theory. According to the results obtained, the amount of SB required for the PRB design in the Ponce Enriquez District depends on the depth of the barrier, as shown in Figure 5.15, we have a linear behavior of SB Tons vs. depth.
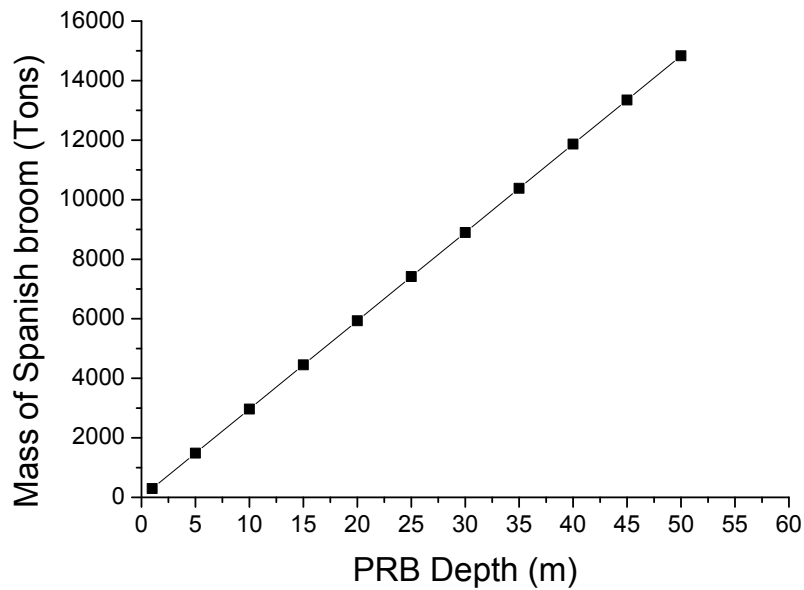
Figure 5.15 Linear Fitting PRB Depth vs Mass SB.

Considering that the PRB length is 1262 m and a depth of 10 m the total amount SB required is 2 900 Tons.

5.7.2 Design of Pump and Treat system (P&T).

In order to evaluate the best methodology for the mercury removal from the aquifer, a comparison between a permeable reactive (PRB) and a hydraulic (P&T) barrier was made. Conventional P&T systems are based on a theoretically very simple concept: contaminated ground water is extracted from the subsurface for treatment. The water portions extracted must be such as to ensure the interception of the whole contamination plume and treated by means of a groundwater treatment plant (GTP). For the P&T design, we have used the Modpath model in GMS. Modpath is a particle tracking code developed by the U.S. Geological Survey. It tracks the trajectory of a set of particles from defined starting locations using the Modflow solution. This tool is able to evaluate the necessary flow rate and the wells configuration in order to intercept the contaminated plume of the aquifer.
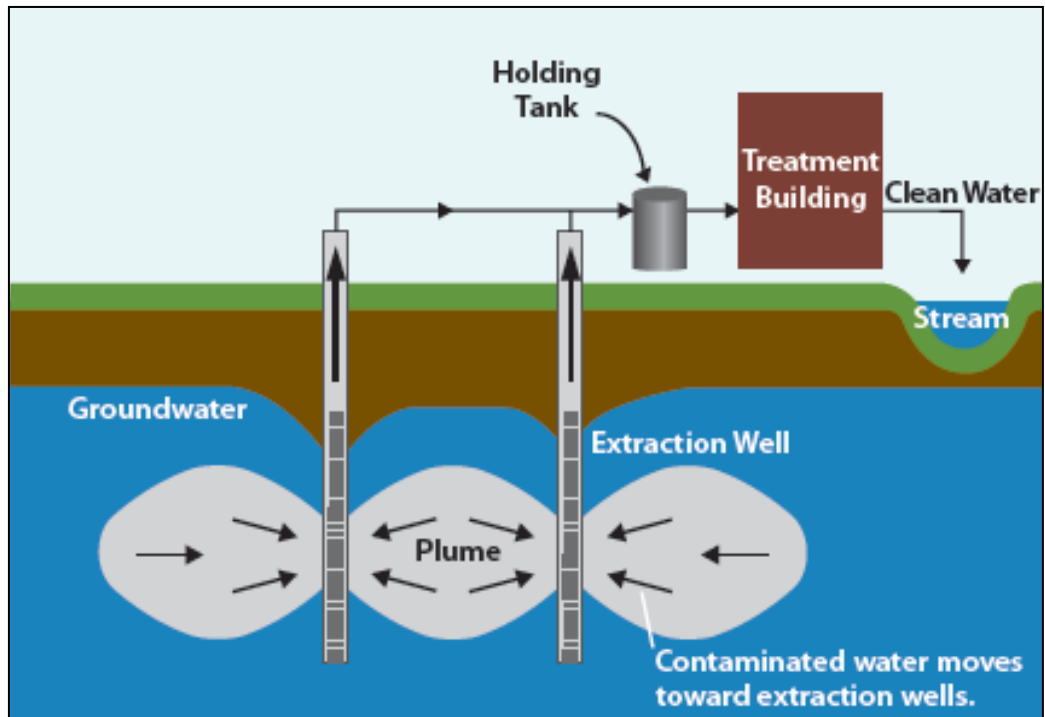
Figure 5.16. Pump and Treat system.

Considering the same boundary conditions of Modflow solution performed in the section 5.6.3 and following the procedure described in figure 5.8, adding the "well packet" of Modflow the model was launched again. The adding "well packet" allowed simulating injection or pumping wells, defining for each cell the extraction (negative) or injection (positive) rate. Taking into consideration the bottom of the aquifer, a value of "Top Screen" (z = -5) and a Flow rate value (3.5 L s^{-1}), were initially assigned.

The extraction wells location into the study area is approximately the same in which the PRB was located (Figure 5.12). In order to capture the entire contaminated plume, eight wells have been used. For each well have been defined the coordinates (x, y) in the UTM reference system WGS84 17 S. The distance between the pumping wells was set equal to 25 m, so that the hydraulic barrier extends for a length of 175 m.

Once the described conditions are assigned the Modflow simulation was carried out. The model solution shows a decrease of the piezometric levels of about six meters close to the wells, due to a total pumping rate of around 0.028 m^3 s^{-1}. The known Modflow solution, was used in Modpath to determine the path line of the contaminant plume, selecting the cells that correspond to the gold mine. The modeling results are displayed in Figure 5.17, where the piezometric levels variation in the extraction zone can be

clearly observed and the Modpath shows that the wells are able to capture all mercury flowing in the aquifer.
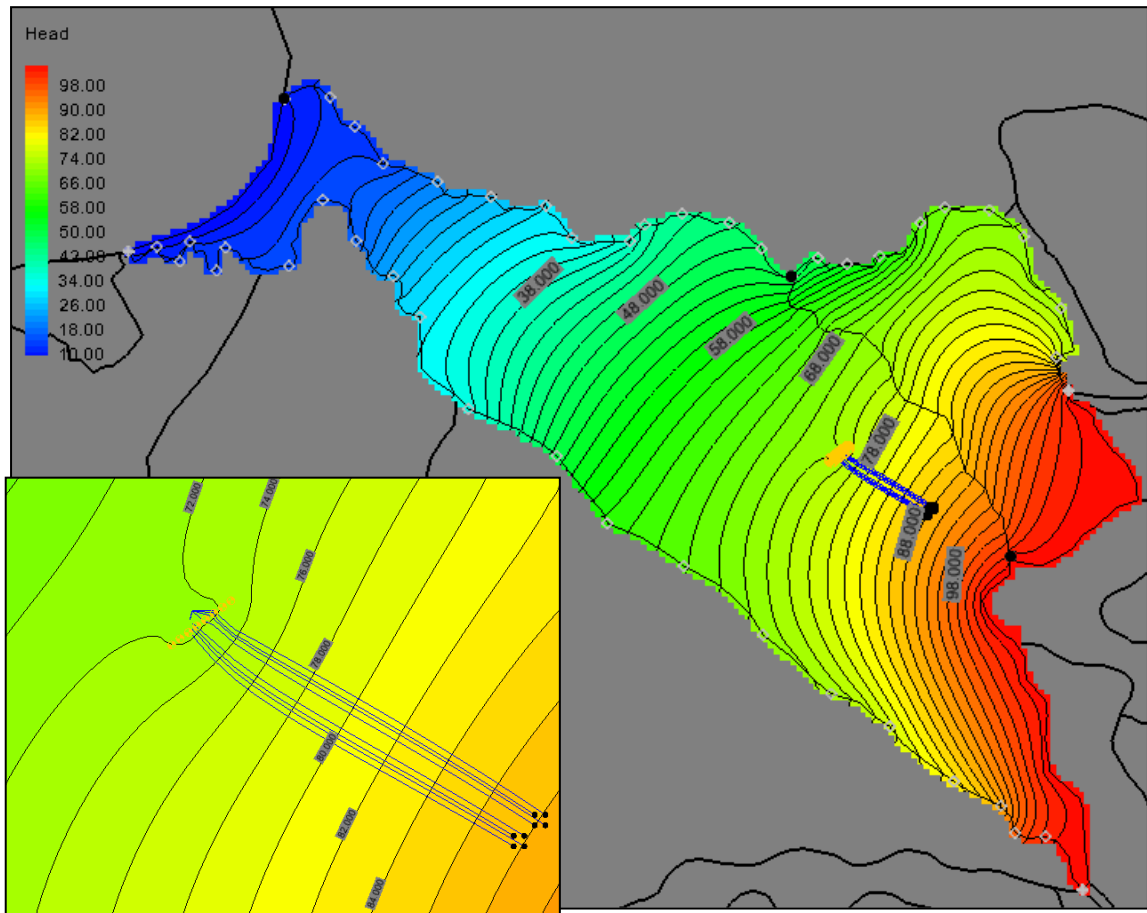

Figure 5.17. MODPATH solution Pump and Treat barrier.

5.7.3 Design Groundwater Treatment Plant (GTP),

We assume to send the groundwater pumped by the hydraulic barrier to a groundwater treatment plant. Adopting a Spanish Broom filter, even in this case, the required mass for GTP was determined applying the same procedure shown in paragraph 5.7.1.
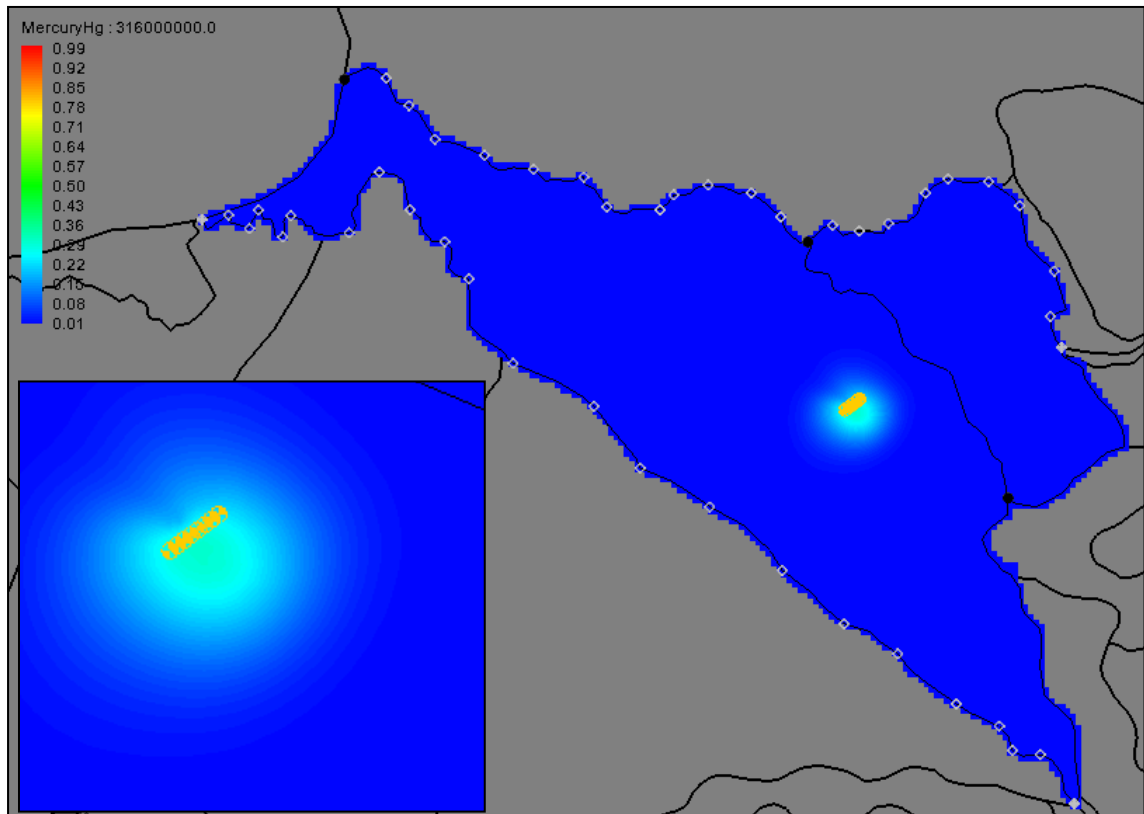
Figure 5.18 MT3D solution Pump and treat barrier.

Firstly, a new simulation of MT3D non-continuous with wells was performed (Figure 5.18.). Considering the Breakthrough Curve (BTC) (Figure 5.19) was calculated the time ($t_{1P\&T}$) and concentration maximum of the model. Applying the same procedure above described for PRB were obtained values, $t_{1P\&T} = 10.24$. and $C_{.max} = 0.0032$ mg L^{-1}. The initial mercury concentration C_0 to be used in equation (4.2) was calculated as a weighted average of Hg (II) concentrations in wells, and the Flow Rate with the sum of the flows of each well i.e. flow rate global. However, since the water after treatment are discharged into a surface water body, is considered as Limit Maximum Mercury (C_1), the mercury concentration value for surface water gave by TULSMA 2012.

Figure 5.19. BTC - MT3D solution Pump and Treat barrier.

The conditions and parameters necessary to calculate the Spanish broom mass are shown below: (Table 5.4)

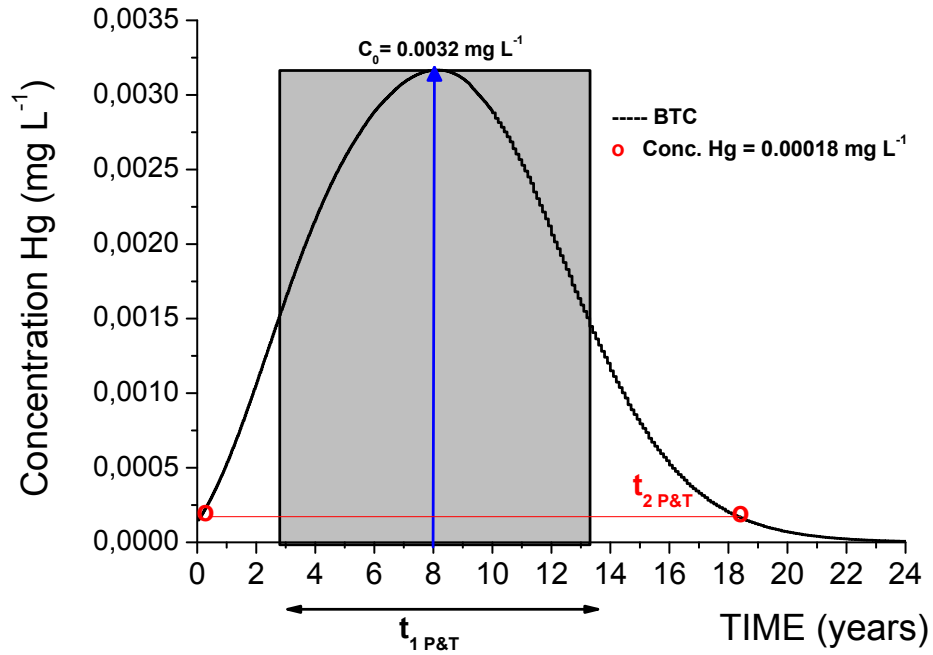| Parameters	Value	Units
Groundwater Mercury concentration C_0	0.00269	mg L^{-1}
Limit Maximum Mercury (C_1)	0.001	mg L^{-1}
Density (ρ)	273	Kg m^{-3}
Double Thomas Constant (K_{TH2})	0.99 x 10^{-4}	mL min^{-1} mg^{-1}
Double Thomas Constant (K_{TH1})	0.98 x 10^{-4}	mL min^{-1} mg^{-1}
Active Surface Sites Fraction (f)	0.23	-
Maximum Adsorption Capacity (q_{01})	4.5	mg g^{-1}
Maximum Adsorption Capacity (q_{02})	11.22	mg g^{-1}
Length area (A_L)	1	m
Groundwater Flow (Q)	1.68x10^{4}	mL min^{-1}
Time$_1$ ($T_{1\ P\&T}$)	10.24	year

Table 5.4. Parameters to Pump and Treat design. Ponce Enriquez area. Case study.

The SB mass necessary to remove the mercury from the water extracted through the designed hydraulic barrier is almost 3 475.458 tons, for a P&T lifetime of 18.26 years, that is the time required for that mercury concentration to goes down the maximum threshold value (TULSMA 2012).

This amount of SB will be managed through of GTP, which will contain 40 polypropylene impermeable tubular filters, with a length of 200 m and a diameter of 2

m, within each one will be disposed an amount of adsorbent material equal to 86.88 Tns. The water flow input for each tubular filter is 100.8 m^3 h^{-1}.

5.7.4 Numerical modeling evaluation of PRB and P&T barriers.

The PRB and P&T numerical modeling results were evaluated as systems for removing Hg (II) from the aquifer of the Camilo Ponce Enríque mining district, using the Spanish broom as an innovative and low-cost adsorbent.

The following table shows the main characteristics of each one methodology.

Parameters	PRB	P&T	Units
Groundwater Mercury concentration C_0	0.0033	0.00269	mg L^{-1}
Limit Maximum Mercury (C_1)	0.00018	0.001	mg L^{-1}
Length Barrier	1 262	175	m
Groundwater Flow (Q)	31.54	1.68×10^4	mL min^{-1}
Time$_1$ (T_1) (Double Thomas model)	12.14	10.24	year
Time$_2$ (T_2) (Lifetime)	22.14	18.26	year
Spanish broom (mass)	2 900	3 475.46	Tons.

Table 5.5. Parameters of Permeable Reactive Barrier and Pump and Treat.

It is worth noting that the barriers designed are for different types of treatment. PRB is a passive method for the aquifer remediation, a continuous barrier configuration places a permeable reagent in a trench perpendicular to groundwater flow main direction . It is simple to install and typically covers the entire width and depth of the contamination plume. (Day et al., 1999.)

The PRB is thought to be more cost effective to treat shallow aquifers in comparison to conventional P&T technologies; however long term cost data has not been collected for a full scale PRB. It is a cost-effective technique because the maintenance operations on the reactive material are minimal. P&T technique has a higher energy demand than the PRB because the PRB can use natural hydraulic gradients to drive the remediation. (Bronstein, 2005.)

Nevertheless, the P&T technique is able to estimate the initial contaminant mass, and continuously monitor the contaminant mass discharge, magnitudes and rates of mass removal, and assessment of contaminant persistence.

Taking into account the Spanish broom amount required for the different types of barriers, in Figure 5.18 it is observed that the design of a PRB at a depth less of 11.70 m (breakeven point) the adsorbent material amount required is smaller that the adsorbent

amount required by the P & T, however, as the depth of the PRB increases, the amount of SB increases considerably, so the P&T option, becomes more suitable.
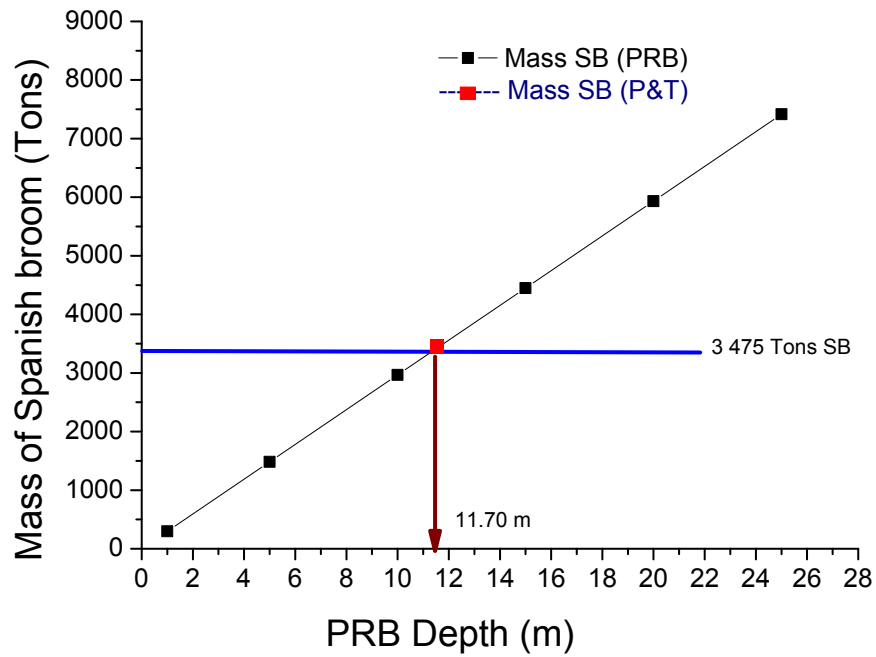

Figure 5.20. Confrontation Spanish broom (mass) PRB and P&T vs Depth (PRB) .

Finally, we can state that the choice of the most appropriate remedial technology must be based on many criteria, taking into account the economic aspects and the disadvantages and advantages of both techniques described previously.

Conclusions

In conclusion, here we have shown that the Spanish broom, due to its high diffusion in many areas of the world and its economic treatment process, can be used as adsorbent material for mercury removal from contaminated water with removal percentages as high as 86%.

The adsorption kinetics behavior followed a pseudo-second order law and intra-particle diffusion was involved in the adsorption process. Fitting of Langmuir isotherm data showed that the maximum adsorption capacity of 20,00 (mg/g) at pH 5.0 for adsorbent with 5 mm particle sizes and thermodynamic parameters suggest that the adsorption is a typical chemical process, spontaneous, and exothermic in nature.

Batch experiments revealed that the adsorption occurs due to the active carboxyl and hydroxyl binding sites available on its lignocellulosic surface. Interestingly, the adsorption dynamic study performed in column under different experimental conditions, revealed, for the first time, an unconventional breakthrough behavior displaying a double S-shape curve. This has been modeled by a Double-Thomas equation with the introduction of the active surface sites fraction (f), which discriminates the fraction of Hg(II) species adsorbed by the superficial active sites from that adsorbed by the inner ones (1-f). The parameter f is significantly affected by the contact time. In fact, the greater is the time in which the Hg(II) remains in contact with the adsorbent material, the greater is the efficiency of the filter because the inner sites come into play. This finding has therefore important implications for the design of filtering devices based on abosorbent materials. In general, this double mechanism, due to the intraparticle diffusion, suggests that this kind of filter is suitable for the remediation of aquifers contaminated by Hg(II), because in this context the flow rate and consequently the Peclet number, are very low.

The use of the Spanish Broom has, however, additional advantages with respect to other potential lignocellulosic adsorbent material: its high diffusion in many areas of the Earth, and the very simple and cheap pretreatment process (drying and milling).

The experimental results are very encouraging, indicating that the Spanish Broom could be a promising material for aquifer remediation, in those cases in which Hg pollution is observed.

This natural material, thanks to its mechanical properties, could be adopted, during the implementation of "on site" techniques, inside filtering devices included within pumping systems or, thanks to its extremely availability and affordability, by "in situ" techniques such as Permeable Reactive Barriers (PRB).

The mercury-polluted aquifer of Canton Ponce Enriquez was the case study adopted to apply the new methodology for the design of the Permeable Reactive Barriers. The groundwater flow (Modflow) and the pollutant transport (MT3DMS) modeling, was used to simulate the groundwater flow within the study area with respect to possible contamination of Hg, quantifying the extent of the pollutant plume and evaluating possible interventions of remediation.

The results obtained by the simulation of groundwater flow in stationary conditions showed that its direction is SE-NW and the hydraulic heads vary from 106 m asl to 8 m asl.

Due to a gold mine (i.e. the source of contamination) with an extractive activity of 10 years and a continuous discharge in aquifer of 0.010 Hg mg L^{-1}, the extent of the contaminant plume was determinate through the MT3D code. The PRB position was determined 1 km downstream from the gold mine, i.e. where the concentration of Hg (II) is below the maximum limit admitted, by means of the transport simulation. Due to a flow rate of 32.9 mL min^{-1}, a time period of 22.14 years is necessary to drive away the mercury from the site. To capture the entire contaminant plume, a continuous PRB of approximately 1 262 m is required. Using the Double Thomas model, developed in this thesis, the reagent mass required to break down Mercury concentration from a value of C_0 of 0.0033 mg L^{-1} to a value of C_t of 0.00018 mg L^{-1} is equal to 0.24 Tons of SB for each square meter of the transversal section of the barrier.

In order to compare the PRB performance, an alternative option for aquifer remediation (i.e. Pump & Treat) was carried out. By using the Modpath code, the modeling of a hydraulic barrier was performed, for which it was necessary to install eight wells with a total flow rate of 28 L s^{-1} in order to capture the entire contaminant plume. Once the water is extracted, it is sent to a groundwater treatment plant (GTP), which contains Spanish broom filters for the adsorption of Hg (II). The amount of SB required for the P&T is 3475 tons to reduce Hg concentration from 0.00269 mg L^{-1} to 0.001 mg L^{-1}. The treatment plant consists of 40 tubes with a diameter of 2 m and a length of 101.31 m for a P&T lifetime of around 18 years, that is the time required in order that Hg concentration could be admissible. Comparing the mass of SB necessary for these two

techniques, it was observed that until a depth of approximately 12 m it would be more convenient to apply a PRB.

A thorough understanding of the site characteristics is required to install a PRB or P&T, so the achieved design must still be studied in depth. PRBs typically take advantage of ambient flow conditions. Promoting active flow through siphoning or limited pumping may be desirable in some cases. The changes in groundwater flow and temperatures can affect the performance of the barriers, even though Thermodynamic Tests showed that the changes in temperature do not affect the adsorptive capacity of the Spanish Broom significantly.

Considering the encouraging results obtained in this study, new experiments involving the remediation of Hg contaminated aquifers using Spanish Brooms are requested in order to take in account of the actual operating situations in which this material must be used, which are, in most cases, water flowing conditions through or on the soil.

References

Adhoum, N., Monser, L., Bellakhal, N., Belgaied, J.E., 2004. Treatment of electroplating wastewater containing Cu2+, Zn2+ and Cr(VI) by electrocoagulation, J. Hazard. Mater., B112, 207–213.

Agrawal, A., K. K. Sahu, and B. D. Pandey, ''Removal of Zinc from Aqueous Solutions Using Sea Nodule Residue,'' Colloids Surf. A: Physicochem. Eng. Aspects, 237, 133 (2004).

Aksu, Z., Gönen, F., 2004. Biosorption of phenol by immobilized activated sludge in a continuous packed bed: prediction of breakthrough curves. Process Biochemistry, 39(5):599-613. [doi:10.1016/S0032-9592(03)00132-8]

Altundogan, H. S., ''Cr (VI) Removal from Aqueous Solution by Iron(III) Hydroxide-Loaded Sugar Beet Pulp,'' Process Biochem., 40, 1443 (2005).

Al-Damluji SF., 1976, Intoxication due to alkylmercury-treated seed-1971-72 outbreak in Iraq: clinical aspects, Bull World Health Organization 53, 65-81.

Alver, E., Metin, A.Ü., 2012. Anionic dye removal from aqueous solutions using modified zeolite: Adsorption kinetics and isotherm studies, Chem. Eng. J., 200–202, 59–67.

Alyüz, B., Veli, S., 2009. Kinetics and equilibrium studies for the removal of nickel and zinc from aqueous solutions by ion exchange resins, J. Hazard. Mater., 167, 482–488.

Amin S. M., Farjoud R., and Shabani A., Groundwater Contaminationy and Heavy Metals in Water Resources of Shiraz Area , Iran Agricultural Research, Vol. 30, No.1& 2, 2011

Atkins, P., De Paula, J., 2006 Physical Chemistry, Eighth ed., W. H. Freeman and Company, New York, 918-922.

Babel, S and Kurniawan, T.A. 2003. Low-cost adsorbents for heavy metals uptake from contaminated water: a review, J. Hazard. Mater, B97, 219-243.

Babel, S and Kurniawan, T.A. 2004, Cr (VI) removal from synthetic wastewater using coconut shell charcoal and commercial activated carbon modified with oxidizing agent and/or chitosan. Chemosphere, 54, 7, 951-967.

Backman B., BodišP. D., Lahermo S. Rapant T. Tarvainen, Application of a groundwater contamination index in Finland and Slovakia, Environmental Geology November 1998, Volume 36, Issue 1, pp 55–64.

Baes, C. F. and Mesmer R. E., 1976. The Hydrolysis of Cations. A Wiley-Interscience Publication.

Bag, S., Trikalitis, P. N., Chupas, P. J., Armatas, G. S. & Kanatzidis, M. G., 2007. Porous semiconducting gels and aerogels from chalcogenide clusters. Science 317, 490–493.

Bailey S. E., Trudy, J. O., Bricka, R. M., and Dean A., 1999. A review of potentially low-cost sorbent for heavy metals. Water Res., 33, 2469-2479.

Bakir, F., Rustam, H., Tikriti, S., Al-Damluji, S. F., H. Shihristani, H., 1980. Clinical and epidemiological aspects of methylmercury poisoning. Postgraduate Medical Journal , 56:1-10.

Barkay, T., Miller, S.M., , Summers., A. O., 2003. Bacterial mercury resistance from atoms to ecosystems, FEMS Microbiology Reviews 27, 355-384.

Barth S., Zimmermann S. (2008): Modeling ion motion in a miniaturized ion mobility spectrometer, COMSOL Conference, Hannover, Germany, November 2008.

Bear, J., 1972. Dynamics of Fluids in Porous Media, American Elsevier, New York.

Beneduci, A., Chidichimo, G., Dardo, G., Pontoni, G. 2011. Highly routinely reproducible alignment of ^{1}H-NMR spectral peaks of metabolites in huge sets of urines. Analytica Chimica Acta, 685, 186-195.

Bernhard, M., Buffoni, G., 1981. Mercury in the Mediterranean, An Overview. In: Proceedings of the International Conference on Environmental Pollution, September 21st–25th, Thessaloniki, Greece, pp. 458–484.

Bessbousse, H., Rhlalou T., Verchère J.-F., Lebrun, L., 2008, Sorption and filtration of hg(ii) ions from aqueous solutions with a membrane containing poly(ethyleneimine) as a complexing polymer, J. of Membrane Science, 325 (2):997-1006.

Betancur, M., Bonelli, P.R., Velásquez, J.A., Cukierman, A.L., 2009. Potentiality of lignin from the Kraft pulping process for removal of trace nickel from waste- water: effect of demineralization. Bioresour. Technol. 100, 1130-1137.

Bronstein, K. (2005). Permeable Reactive Barriers for Inorganic and Radionuclide Contamination. National Network of Environmental Manegment Studies Fellow.

Cantrell, K. J., Kaplan, D. I., Wietsma, T. W, 1995. Zero-valent iron for the in situ remediation of selected metals in groundwater: J. Hazard. Mater., 42, 201-212.

Casas A., Alonso M. V., Oliet M., Rojo E., and Rodríguez F., 2012. FTIR analysis of lignin regenerated from *Pinus radiate* and *Eucalyptus globulus* woods dissolved in imidazolium-based ionic liquids. J. Chem. Technol. Biotechnol., 87, 472-480.

Canga E. Hydro-geochemical processes affecting phosphorus retention in coarse granular drainage filters Hydraulic conductivity, solute transport and phosphate retention, Department of Agroecology, Science and Technology(2014).

Chiarle, S., Ratto, M., and Rovatti, M., 2000. Mercury removal from water by ion exchange resins adsorption. Water Res., 34, 2971-2978.

Chidichimo, G., Aloise, A., Beneduci, A., De Rango, A., Pingitore, G., Furgiuele, F., Valentino, P., 2015. Polyurethanes reinforced with Spartium Junceum fibers, Polym. Composites, doi: 10.1002/pc.23501.

Chu, M.A., 2010. Fixed bed sorption: Setting the record straight on the Bohart-Adams and Thomas models, J. of Hazard. Mat.,177,1006-1012.

D'Adamo, P., Ulivi, S., Beneduci, A., Pontoni G., Capasso G., Lanzara C., Andrighetto G., Hladnik U., Nunes V., Palacin M., and Gasparini P., 2010. Metabonomics and population studies: age-related amino acids excretion and inferring networks through the study of urine samples in two Italian isolated populations, Amino Acids, 38, 65-73.

Dagan, G., 1989. Flow and Transport in Porous Formations, Springer, Berlin, 465.

Day, S. R.; O'Hannesin, S. F.; Marsden, L. 1999. Geotechnical techniques for the construction of reactive barriers. J. Hazard. Mater., 67, 285–297.

De Marsily, G., 1986. Quantitative hydrogeology: groundwater hydrology for engineers. Academic Press, Orlando, FL.

Demirbas, A., 2008. Heavy metal adsorption onto agro-based waste materials: A review, J. Hazard. Mater., 157, 220–229.

Di Molfetta A., Sethi R. (2005). "*Barriere Reattive Permeabili*". Bonifica di siti contaminati. Caratterizzazione e tecnologie di risanamento. McGraw-Hill, ed. The McGraw-Hill Companies, S.r.l. Publishing Group Italia, cap. 26, pp.562-605.

Dimitrova S.V., Metal Sorption on Blast-Furnace Slag, Water Research. Vol. 30, 228-232.

El-Shafey, E.I., 2010. Removal of Zn(II) and Hg(II) from aqueous solution on a carbonaceous sorbent chemically prepared from rice husk. J. Hazard. Mater. 175(1-3): 319-327.

EPA, 1998, Permeable Reactive Barrier Technologies For Contaminant Remediation, . S. Environmental Protection Agency Cincinnati, Ohio 45268, 28-36.

Esalah, J.O., Weber, M.E., Vera, J.H., 2000. Removal of lead, cadmium and zinc from aqueous solutions by precipitation with sodium di-(n-octyl) phosphinate, Can. J. Chem. Eng., 78, 948–954.

Esteban, M., Casassas E. and Fernandez L., 1986. Formation constants of some mercury(II) complexes determined from their anodic polarographic signals. Talanta, 33, 843-846.

Ewell, Christopher (29 May 2015). "Aquaveo: Using Geospatial Modeling to Map Surface and Groundwater". Ubique: The American Geographical Society Newsletter. Archived from the original on 19 February 2016.

Feng, X., Fryxell, G. E., Wang, L.-Q., Kim, A. Y., Liu, J., Kemner, K. M., 1997. Functionalized monolayers on ordered mesoporous supports. Science, 276, 923–926.

Frega G., Troisi S., Straface S. , Idraulica Ambientale, Edizioni Librare, 2004.

Fu, F., Wang, Q., 2011. Removal Of Heavy Metal Ions From Wastewaters: A Review, J. of Environmental Management 92, 407-418.

Furia, E. and Sindona, G., 2012. Interaction of Iron(III) with 2-Hydroxybenzoic Acid in Aqueous Solutions. J. Chem. Eng. Data, 57, 195-199.

Furia, E., Falvo, M. and Porto, R., 2009. Solubility and Acidic Constants of l-Cystine in NaClO4 Aqueous Solutions at 25 °C. J. Chem. Eng. Data, 54(11), 3037-3042.

Furia, E., Napoli, A., Tagarelli, A, Sindona, G., 2013. Speciation of 2-Hydroxybenzoic Acid with Calcium(II), Magnesium(II), and Nickel(II) Cations in Self-Medium. J. Chem. Eng. Data, 58, 1349-1353.

Gabriele, B., Cerchiara, T., Salerno, G., Chidichimo, G., Vetere, M.V., Alampi, C., Gallucci, M.C., Conidi, C., Cassano, A., 2010. A new physical–chemical process for the efficient production of cellulose fibers from Spanish broom (Spartium junceum L.), Bioresour. Technol. 101, 724–729.

Gans, P., Sabatini, A. and Vacca, A., 1985. SUPERQUAD: An Improved General Program for Computation of Formation Constants from Potentiometric Data. J. Chem. Soc. Dalton, 6, 1195-1200.

Gao J, Tang LG. Cellulose science. Beijing: Science Press; 1996. and Tao YZ, Guan YT. 2003, Study of chemical composition of lignin and its application. J Cellul Sci Technol., 11(1), 42–55.

Ghasemi, M., Keshtkar, A.R., Dabbagh, R., Jaber Safdari, S., 2011. Biosorption of uranium (VI) from aqueous solu- tions by Ca-pretreated Cystoseira indicaalga: break-through curves studies and modeling. Journal of Hazardous Materials, 189(1-2):141-149 [doi:10.1016/j. jhazmat.2011.02.011]

Giles, C.H., Smith, D., Huitson, A., 1974. A general treatment and classification of the solute adsorption isotherm. I. Theoretical, J. Colloid Interf. Sci,, 47, 755–765.

Global Mercury Negotiations Commence, http://www.worldwatch.org/node/6024 (accessed 1/12/2016)

Gran, G., 1952. Determination of the equivalence point in potentiometric titrations. Part II. Analyst, 77, 661-671.

Guo, X., Zhang, S., Shan, X., 2008. Adsorption of metal ions on lignin, J. Hazard. Mater., 151, 134–142.

Gupta, V. K., Nayak, A., 2012. Cadmium removal and recovery from aqueous solutions by novel adsorbents prepared from orange peel and Fe_2O_3 nanoparticles. Chem. Eng. J., 180, 81-90.

Gupta, V. K., Nayak, A., Agarwal, S., 2015. Bioadsorbents for remediation of heavy metals: current status and their future prospects. Environ. Eng. Res., 20, 1-18.

Gupta, V. K., Srivastava, S. K., and Tyagi, R. 2000. Design parameters for the treatment of phenolic wastes by carbon columns (obtained From fertilizer waste material). Water Res. 34, 5, 1543-1550.

Gupta, V. K., Srivastava, S. K., Moham, D. and Sharma, S. 1997. Design parameters for fixed bed reactorsof activated carbon developed from fertilizer waste for the removal of some heavy metal ions. Waste Management, 17, 517-522.

Gupta, V. K., Suhas, Tyagi, I., Agarwal, S., Singh, R., Chaudhary, M., Harit, A., Kushwaha, S., 2016. Column operation studies for the removal of dyes and phenols using a low cost adsorbent. Global J. Environ. Sci. Manage., 2 (1), 1-10.

Haghseresht, F. and Lu, G., 1998. Adsorption characteristics of phenolic compounds onto coal-reject-derived adsorbents. Energy and Fuels, 12, 1100-1107.

Haileslassie T., , Gebremedhin, K., 2015. Hazards Of Heavy Metal Contamination In Ground Water, International J. Of Tech. Enhancements And Emerging Eng. Research, 3 Issue 2. 1-6

Hamdaoui, O., Naffrechoux, E., 2007. Modeling of adsorption isotherms of phenol and chlorophenols onto granular activated carbon. Part I. Two parameters models and equations allowing determination of thermodynamic parameters. J. Hazard. Mater., 147, 381-394.

Han, R., Ding, D., Xu, Y., Zou, W., Wang, Y., Li, Y., Zou, L., 2008. Use of rice husk for the adsorption of congo red from aqueous solution in column mode. Bioresource Technology, 99(8):2938-2946. [doi:10.1016/j.biortech. 2007.06.027]

Han,R., Zou,L., Zhao,Xu,F.,Li,Y.,and Wang,Y.,(2009), Removal of Methylene blue from aqueous solution by chaff in batch mode, Chemical Engineering Journal,149,123-131.

Henriksson, G., Lignin, in: M. Ek, G. Gellerstedt, G. Henriksonn (Eds.), Wood Chemistry and Technology, Walter de Gruyter GmbH and Co., Berlin, 2009, pp. 121-146.

Ho, Y.S,. 2006. Review of second-order models for adsorption systems, J. Hazard. Mater, 136, 681–689.

Ho, Y.S. and Wang C.C., 2008. Sorption equilibrium of mercury on ground-up tree fern. J. Hazard. Mater., 156, 398–404.

Ho, Y.S., McKay, G., 1999., Pseudo-second order model for sorption processes, J. Process. Biochem., 34, 51–465.

Holzbecher, E., and Kohfahl, C., 2009. The Use of COMSOL Multiphysics in Teaching Groundwater Flow and Transport, Int. J. of Engineering Education, 1-23.

INEC, 2010. Instituto Nacional de Estadística y Censos, Censo de Poblacion y Vivienda. Base de Datos Camilo Ponce Enriquez.

INIGEMM, (Instituto Nacional de Investigación Geológico Minero Metalúrgico), 2013, Assessment of the susceptibility to contamination of underground water resources, mining district of Zaruma – Portovelo, Ecuador, (Evaluación de la susceptibilidad, a la contaminación del recurso hídrico subterráneo del distrito minero Zaruma – Portovelo, Ecuador),, p. 239-241.

INIGEMM, (Instituto Nacional de Investigación Geológico Minero Metalúrgico), 2012, Assessment of the susceptibility to contamination of underground water resources, mining district of Camilo Ponce Enriquez – Ecuador, (Evaluación de la susceptibilidad, a la contaminación del recurso hídrico subterráneo del distrito minero Camilo Ponce Enriquez – Ecuador), p. 56-131.

Juang, R.S., Wu, F.C., Tseng, R.L., 2002. Characterization and use of activated carbons pre- pared from bagasse for liquid-phase adsorption, Colloids Surf. A: Physicochem. Eng. Aspects 201, 191–199.

Katović, D., Katović, A., & Krnčević, M. (2011). Spanish Broom (Spartium junceum L.)—History and Perspective. Journal of Natural Fibers, 8(2), 81–98. JOUR. http://doi.org/10.1080/15440478.2011.577277

Khachatourians, G. G., Arora, D.K., 2001. Applied Mycology and Biotechnology, Volume 1. Agriculture and Food Production, first ed., Elsevier Science B.V., Amsterdan, 325.

Khalil, M. M., Radalla, A. M., 1998. Binary and ternary complexes of inosine. Talanta, 46, 53–61.

Khoramzadeh, E., Nasernejad, B., Halladj, R., 2013. Mercury biosorption from aqueous solutions by Sugarcane Bagasse: J. Taiwan Inst. Chem. Eng., 44, 266–269.

Kitamura, S., Hirano, Y., Noguchi, Y., Kojima, T., Kakita, T., Kuwaki., H., 1959. Epidemiological studies regarding Minamata disease — second report, Kumamoto Igakkai Zasshi, 33 (suppl. 3), 569–571

Kohler, S.J., Cubillas, P., Rodriguez-Blanco, J.D., Bauer, C., Prieto, M., 2007. Removal of cadmium from wastewaters by aragonite shells and the influence of other divalent cations. Environ. Sci. Technol. 41, 112-118.

Kumar, K.V., 2006. Linear and non-linear regression analysis for the sorption kinetics of methylene blue onto activated carbon: J. Hazard. Mater., B137, 1538–1544.

Kumar, P.R., Chaudhari, S., Khilar, K.C., Mahajan, S.P., 2004. Removal of arsenic from water by electrocoagulation, Chemosphere, 55 (9), 1245–1252.

Kurniawan, T.A., Chang, G.Y.S., Lo, W., Babel, S., 2006. Comparisons of low-cost adsorbents for treating wastewaters laden with heavy metals, Science of the Total Environment 366, 409–426.

Lagergren, S., 1898. Zur theorie der sogenannten adsorption gelöster stoffe Kungliga Svenska Vetenskapsakademiens. Handlingar, 24 (4), 1–39.

Li, B., Zhang Y., Ma, D., Z., Shi, and Ma, S., 2014. Mercury nano-trap for effective and efficient removal of mercury(II) from aqueous solution. Nature Communication, 5:5537, DOI: 10.1038/ncomms6537.

Lia D., 2014. Utilizzo di materiali innovative per la rimozione di Mercurio dale acque sotterranee, Tesi di Laurea Ing. L'Ambiente ed il Territorio. Università dellla Calabria. 69-70.

Limousin, G., Gaudet, J.-P., Charlet, L., Szenknect, S., Barthe`s, V., Krimissa, M., 2007. Sorption isotherms: A review on physical bases, modeling and measurement, Appl. Geochem., 22, 249–275.

Lin, S.H., Peng, C.F., 1994. Treatment of textile wastewater by electrochemical method, Water Res., 28, 277–282.

Liu, J. Feng, X., Fryxell, G. E., Wang, Li-Q., Kim, A. Y. and Gong, M. 1998. Hybrid mesoporous materials with functionalized monolayers. Adv. Mater. 10, 161–165.

Liu, T., Wang, Z. L., Yan, X., Zhang, B., 2014. Removal of mercury (II) and chromium (VI) from wastewater using a new and effective composite: Pumice-supported nanoscale zero-valent iron, Chem. Eng. J., 245, 34–40.

Liu, Z.R., Zhou, L.M., Wei, P., Zeng, K., Wen, C.X., Lan, H.H., 2008a. Competitive adsorption of heavy metal ions on peat. J. China Univ. Min. Technol. 18, 255-260.

Lu, A.H., Zhong, S.J., Chen, J., Shi, J.X., Tang, J.L., Lu, X.Y., 2006. Removal of Cr(VI) and Cr(III) from aqueous solutions and industrial wastewaters by natural clino-pyrrhotite. Environ. Sci. Technol. 40, 3064-3069.

Lv J., Xue CY., Cao CY., Zhang Y., 2010. Lignin distribution in wood cell wall and its testing methods. J Beijing Univ. 32 (1), 136–41.

Lv, J., Luo, L., Zhang, J., Christie, P., Zhang, S., 2012. Adsorption of mercury on lignin: Combined surface complexation modeling and X-ray absorption spectroscopy studies, Environ. Pollut., 162, 255-261.

MacKay, G., Blair, H. S., Findon, A., 1989. Equilibrium studies for sorption of metal ions onto chitosan. Indian J. Chem., 28A, 356-360.

Mahajan, G., Sud, D., 2013. Application of ligno-cellulosic waste material for heavy metal ions removal from aqueous solution, J. Environ. Chem. Eng., 1, 1020–1027.

Manohar D.M., Krishnan K.A., Anirudhan T.S., 2002. Removal of mercury (II) from aqueous solutions and chloralkali industry wastewater using mercaptobenzimidazole clay. Water Res., (36) 1609-1619.

McCann, M.C. and Roberts, K. 1991. In: The Cytoskeletal Basis of Plant Growth and Form. Lloyd, C.W. London, Academic: 109-129

Medvidovic´ N.V., Peric´ J., and Trgo M., 2008 Testing of Breakthrough Curves for Removal of Lead Ions from Aqueous Solutions by Natural Zeolite-Clinoptilolite

According to the Clark Kinetic Equation. Separation Science and Technology, (43) 944–959, 2008

Menéndez-Díaz, J.A., Martín-Gullón, I., 2006. Chapter 1 Types of Carbon Adsorbents and their Production, Interface Science and Technology, 7, 1-47.

Mohan, D., Chander, S., 2006. Removal and recovery of metal ions from acid mine drainage using ligniteda low cost sorbent. J. Hazard. Mater. 137, 1545-1553.

Mondal, D.K., Nandi, B.K., Purkait, M.K., 2013. Removal of mercury (II) from aqueous solution using bamboo leaf powder: Equilibrium, thermodynamic and kinetic studies, J. Environ. Chem. Eng., 1, 891–898.

Motsi, T., Rowson, N.A., Simmons, M.J.H., 2009. Adsorption of heavy metals from acid mine drainage by natural zeolite. Int. J. Miner. Process 92, 42-48.

Mrozowski, J., Zielinski, J., 1983. Studies of zinc and lead removal from industrial wastes by electrocoagulation, Environ. Prot. Eng., 9. 77–85.

Murthy, Z.V.P., Parikh, P. A., Patel, N. B., 2013. Aplication of β – Zeolite, Zeolite Y, and Modernitte as absorbent for remove Mercury from aqueos solutions, J. Dispers. Sci. Technol., 34, 747–755.

Mustafa Y. A., Ebrahim S.E., 2010. Utilization Of Thomas Model To Predict The Breakthrough Curves For Adsorption And Ion Exchange, J. Eng. 4 (16), 6206 – 6223.

Nabi Shabnum, Toxic Effects of Mercury, Interdisciplinary Brain Research Centre (IBRC), Book on Line DOI 10.1007/978-81-322-1922-4, pag 19-68.

Naiya, T. K., Chowdhury, P., Bhattacharya, A.K., Das, S. K., 2009. Saw dust and neem bark as low-cost natural biosorbent for adsorptive removal of Zn(II) and Cd(II) ions from aqueous solutions, Chem. Eng. J., 148, 68–79.

Namasivayam, C., Kadirvelu, K., 1999. Uptake of mercury (II) from wastewater by activated carbon from an unwanted agricultural solid by-product: coirpith, Carbon 37, 79–84

Navi, S., 2014. Toxic effects of Mercury, Springer, New Delhi, 4-5.

Neuman, S.P., 1990. Universal scaling of hydraulic conductivities and dispersivities in geologic media. Water Resour. Res., 26, 1749–1758

Niu, Z., Fan, Q., Wang, W., Xu, J., Chen, L., Wu, W., 2009. Effect of pH, ionic strength and humic acid on the sorption of uranium(VI) to attapulgite, Applied Radiation and Isotopes 67, 1582–1590.

Nucon International Inc. 2017 , http://www.nucon-int.com/mercury-adsorbents, accesses 25-01-17.

Ostroski, I.C., Barros, M.A.S.D., Silvab, E.A., Dantas, J.H., Arroyo, P.A., Lima, O.C.M., 2009. A comparative study for the ion exchange of Fe(III) and Zn(II) on zeolite NaY. J. Hazard. Mater. 161, 1404-1412.

Oubagaranadin, J. U. K., Sathyamurthy, N., Murthy, Z. V. P., 2007, "Evaluation Of Fuller's Earth For The Adsorption Of Mercury From Aqueous Solutions: A Comparative Study With Activated Carbon", Journal Of Hazardous Materials, 142, 1-2, 165-174.

Patniak, P., 2003. Handbook of Inorganic Chemicals, First Ed, McGraw-Hill, New York , 559-580.

Pearson, R. G., 1963. Hard and soft acids and bases, J. Am. Chem. Soc., 85, 3533-3539.

Porto, R., De Tommaso, G. and Furia, E., 2005. The Second acidic constant of salicylic acid. Ann. Chim., 95, 551-558.

Porwal, S. K. Furia, E., Harris, M. E., Viswanathan R., Devireddy L., 2015. Synthetic, potentiometric and spectroscopic studies of chelation between Fe(III) and 2,5-DHBA supports salicylate-mode of siderophore binding interactions. J. Inorg. Biochem. 145, 1–10.

Pugliese L., Poulsen T., Straface S., 2013. "Gas Solute Dispersivity Ratio in Granular Porous Media as Related to Particle Size Distribution and Particle Shape". Water Air Soil Pollut., 224, (1691), 1-12.

Rao, M.M., Reddy, D.H.K.K., Venkateswarlu, P., Seshaiah, K., 2009. Removal of mercury from aqueous solutions using activated carbon prepared from agricultural by-product/waste, J. Environ. Management., 90 (2009) 634-643.

Ratcliffe H. E., Swanson G. M., Fischer L.J., 1996, Human Exposure to Mercury: A Critical Assessment of the Evidence of Adverse Health Effects, J. Toxicol Envirom Health, 49 (3), 221-270.

Reyes, I., Villarroel, M., Diez, M.C., Navia, R., 2009. Using lignimerin (a recovered organic material from Kraft cellulose mill wastewater) as sorbent for Cu and Zn retention from aqueous solutions. Bioresour. Technol. 100, 4676-4682.

Rodríguez-Lado L, Sun G, Berg M, Zhang Q, Xue H, Zheng Q, Johnson Ca., 2013. Groundwater Arsenic Contamination Throughout China, Science, 341(6148):866-8. Doi: 10.1126/Science.1237484

Rossotti F. J. C. and Rossotti H., 1965. Potentiometric titrations using Gran plots. A textbook omission. J. Chem. Edu., 42 (7), 375-378.

Sharma, Abhi, Anmol Sharma Anmol, Arya R.K., 2015. Removal of Mercury (II) From Aqueous Solution: A Review of Recent Work, Separation Science and Technology, Vol. 50 , Iss. 9.

Sheng, G.D., Wang, S.W., Hua, J., Lu, Y., Li, J.X., Dong, Y.H., Wang, X.K., 2009. Adsorption of Pb(II) on diatomite as affected via aqueous solution chemistry and temperature. Colloid Surf. 339, 159-166.

Shin, Y., Fryxell, G. E., Um, W., Parker, K., Mattigod, S. V. and Skaggs, R., 2007. Sulfur-functionalized mesoporous carbon. Adv. Funct. Mater. 17, 2897–2901.

Simon, F.-G., Meggyes T.,. Tuïnnermeier T., 2002. Advanced groundwater remediation, Federal Institute for Materials Research & Testing, Germany, T Meggyes, Federal Institute for Materials Research & Testing, Germanyand C McDonald, University of Leeds, Part 1. 6-20.

Smyth, D. A., Shikaze, S. G., Cherry, J. A., 1997. Hydraulic performance of permeable barriers for the in situ treatment of contaminated groundwater. Land Contamination and Reclamation 5(3), 131–137.

Snoeyink, V.L.; Summers, R.S., 1999. Adsorption of organic compounds. Water quality and treatment: a handbook of community water supplies. R. D. Letterman and A.W.W. Association, McGraw-Hill.

Storelli, M. M., 2000. "Fish for Human Consumption: Risk of Contamination by Mercury". Food additives and contaminants: 1007–1011. Retrieved 1 May 2014.

Straface S., (2015) Idrologia Sotterranea, flusso e trasporto nei mezzi porosi. Centro Editoriale e Librario Universita della Calabria, 2015. 55-85.

T J Brown, N E Idoine, E R Raycraft, R A Shaw, E A Deady, S F Hobbs, and T Bide, BRITISH GEOLOGICAL SURVEY. 2017. World mineral production 2011-15. (Keyworth, Nottingham: British Geological Survey.)

Taffarel, S.R., Rubio, J., 2009. On the removal of $Mn2þ$ ions by adsorption onto natural and activated Chilean zeolites. Miner. Eng. 22, 336-343.

Tao, Y. Z., Hardy, A., Drenth, J., Henzell, R. G., Franzmann, B. A., Jordan, D. R.,McIntyre, C. L., 2003. Identifications of two different mechanisms for sorghum midge resistance through QTL mapping. Theoretical and Applied Genetics, 107(1), 116–122. JOUR. http://doi.org/10.1007/s00122-003-1217-0.

The Hindustan Times, September 2-1999. Polluting India's groundwater. www.hindustantimes.com, accessed 13.01.17.

Thielke, M. W., Bultema, L. A., Brauer, D. D., Richter, B., Fischer, M. and Theato, P., 2016. Rapid Mercury(II) Removal by Electrospun Sulfur Copolymers. Polymers, 8, 266, 1-9.

Thiruvenkatachari, R., Vigneswaran, S., Naidu, R., 2008. Permeable reactive barrier for groundwater remediation, J. Indust. Eng. Chem. 14, 145–156.

Troisi S., Fallico C., 1992. "Metodi di stima delle grandezze e dei parametri che identificano i processi di trasporto di massa in mezzi porosi saturi". Tratto da La

salvaguardia delle acque sotterranee – Modelli di processi di trasporto di sostanze in mezzi porosi naturali, a cura di R. Giura, D. De Wrachien, S. Troisi, G. Gandolfi, C. Fallico, Ed. BIOS Cosenza.

Tunali, S., Ozcan, A.S., Ozcan, A., Gedikbey, T., 2006. Kinetics and equilibrium studies for the adsorption of acid red 57 from aqueous solutions onto calcined alunite, J. Hazard. Mater, 135, 141–148.

TULSMA, 2012. Texto Unificado Legislación Secundaria Medio Ambiente, Ministerio de Ambiente, Ecuador, Decreto Ejecutivo 3516. Libro VI, anexo 1 cap. 3.1, Criterios de calidad por usos..

U.S Geological Survey's (USGS) Water Science School, 2017. http://water.usgs.gov/edu/., PageLast Modified: Wednesday, 04-Jan-2017 07:25:45.

UNEP, 2013. Global Mercury Assessment 2013: Sources, Emissions, Releases and Environmental Transport. UNEP Chemicals Branch, Geneva, Switzerland.

Valls M, De Lorenzo V., 2002. Exploiting the genetic and biochemical capacities of bacteria for the remediation of heavy metal pollution. FEMS Microbiol. Rev., 26: 327-338.

Van-Nooten, T., Diels, L., Bastiaens, L., 2010. Design of a multibarrier for the treatment of landfill leachate contamination: laboratory column evaluation. In: Bastiaens, L. (Ed.), 4th International Symposium: Permeable reactive Barriers and Reactive Zones, Vito, Antwerp, Belgium, p. 34.

Vanholme, R., Demedts, B., Morreel, K., Ralph, J., Boerjan, W., Lignin Biosynthesis and Structure Plant Physiol. 2010 153: 895-905. First Published on May 14, 2010;doi:10.1104/pp.110.155119

Vazquez, I., J. Rodrı́guez-Iglesias, E. Maranon, L. Castrillon, and M. Alvarez, 2007. ''Removal of Residual Phenols from Coke Wastewater by Adsorption,'' J. Hazard. Mater., 147, 395.

Vidic R.D., Pohland F.G. (1996). "*Treatment walls*". Technology Evaluation Report TE 96-01, Ground Water Remediation Technologies Analysis Center, Pittsburgh (USA).

Viraraghavan, T., Kapoor, A., 1994, "Adsorption Of Mercury From Wastewater By Bentonite", Applied Clay Science, 9, 1, 31-49.

Visa, M., 2016., Synthesis and characterization of new zeolite materials obtained from fly ash for heavy metals removal in advanced wastewater treatment, Powder Technol., 294, 338–347.

Wang X., Andrews L., Riedel S., Kaupp M., 2007. Mercury is a Transition Metal: The first experimental evidence for HgF_4. Angew Chem Int Ed., Weinheim: Wiley, 46 8371-8375.

Wang, S., Peng, Y., 2010. Natural zeolites as effective adsorbents in water and wastewater treatment: review, Chem. Eng. J., 156, 11–24.

Wang, S., D. Z. Wang, L. J. Ji, Q. Gong, Y. F. Zhu, and J. Liang, 2007. ''Equilibrium and Kinetic Studies on Removal of NaCl from Aqueous Solutions by Electrosorption on Carbon Nanotube Electrodes,'' Sep. Purif. Technol., 58, 12.

Weber, W.J., Morris, C.J., 1962. Advances in water pollution research, in: Proceedings of the First International Conference on Water Pollution Research, vol. 2, Pergamon Press, Oxford, 231.

Wei JH., Song YR., 2001. Recent advances in study of lignin biosynthersis and manipulation. J. Intedr Plant Biol., 43 (8) 771-779.

Weisener C.G., Sale, K.S., Smyth, D.J.A., Blowes, D.W., 2005. Field Column Study Using Zerovalent Iron for Mercury Removal from Contaminated Groundwater, Environ. Sci. Technol., 39 (16), 6306–6312.

WHO, 1991, "Inorganic mercury: environmental health criteria 118," in International Programme on Chemical Safety.

Wilkin, R. T., Mc Neil, M. S., 2003. Laboratory evaluation of zero-valent iron to treat water impacted by acid mine drainage, Chemosphere 53, 715–725.

Worldwatch Institute, 2000, State of the World 2000, A Worldwatch Institute Report on Progress Toward a Sustainable Society, w.w. Norton & Company, New York-London, Chapter 3, 41-58.

Wu F.C., Tseng, R.L., Juang, R.S., 2009. Initial behavior of intraparticle diffusion model used in the description of adsorption kinetics, Chem. Eng. J., 153, 1–8.

Yee, K.-K. ; Reimer, N.; Liu, J.; Cheng, S.Y.; Yiu, S.M.; Weber, J.; Stock, N.; Xu, Z., 2013. Effective mercury sorption by thiol-laced metal_organic frameworks: in strong acid and the vapor phase. J. Am. Chem. Soc. 135, 7795–7798.

Yeh, C.-H., Lin, C.-W., & Wu, C.-H.,2010) A permeable reactive barrier for the bioremediation of BTEX-contaminated groundwater: Microbial community distribution and removal efficiencies. Journal of hazardous materials, 178(1-3), 74–80.

Zabihi, M., Haghighi Asl, A., Ahmadpour, A., 2010. Studies on adsorption of mercury from aqueous solution on activated carbons prepared from walnut shell, J. Hazard. Mater., 174, 251–256.

Zambrano J., Laborie, S., Viers, Ph., Rakib, M., Durand, G., 2002. Mercury removal from aqueous solutions by complexation–ultrafiltration, Desalination 144 201–206.

Zhan HY., 2005. Fiber chemistry and physics. Beijing: Science, 100.

Zhang, F.S., Nriagu, J.O., Itoh, H., 2005. Mercury removal from water using activated carbons derived from organic sewage sludge, Water Res., 39, 389–395.

Zhang, Y., M. Yang, and X. Huang, ''Arsenic(V) Removal with a Ce(IV)-Doped Iron Oxide Adsorbent,'' Chemosphere, 51, 945 (2003).

Zouboulis, A. I. and Kydros, K. A. 1993, Use of red mud for toxic metals removal: The case of nickel. J. Chem. Technol. Biotechnol., 58: 95–101. doi:10.1002/jctb.280580114

Acknowledgements.

Appendix 1.

River (data)	Head Stage (m)	Bot. Elevation (m)
1	11,09	10,09
2	11,69	10,69
3	11,79	10,79
4	12,17	11,17
5	12,49	11,49
6	12,74	11,74
7	13,14	12,14
8	13,24	12,24
9	13,26	12,26
10	13,87	12,87
11	14,51	13,51
12	15,28	14,28
13	16,08	15,08
14	20,30	19,30
15	25,27	24,27
16	25,73	24,73
17	30,02	29,02
18	30,68	29,68
19	31,05	30,05
20	34,11	33,11
21	35,97	34,97
22	40,97	39,97
23	42,97	41,97
24	45,04	44,04
25	47,93	46,93
26	48,38	47,38
27	50,01	49,01
28	50,80	49,80
29	55,56	54,56
30	58,42	57,42
31	60,99	59,99
32	65,13	64,13
33	65,50	64,50
34	67,75	66,75
35	68,60	67,60
36	70,28	69,28
37	70,47	69,47
38	70,84	69,84
39	72,36	71,36
40	75,06	74,06
41	75,32	74,32
42	80,60	79,60
43	85,05	84,05
44	95,41	94,41
45	110,00	109,00